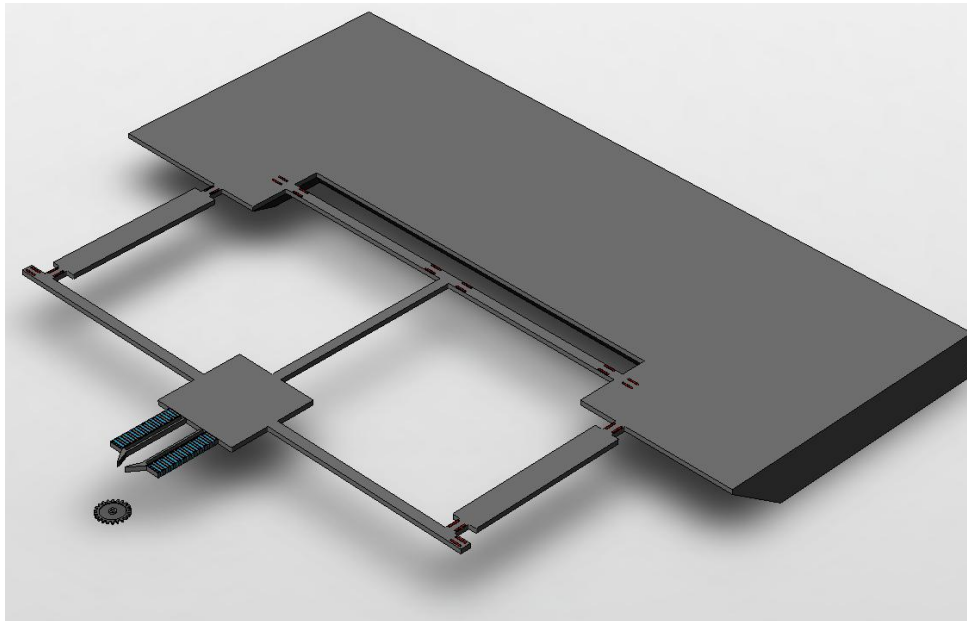


Department of Precision and Microsystems Engineering

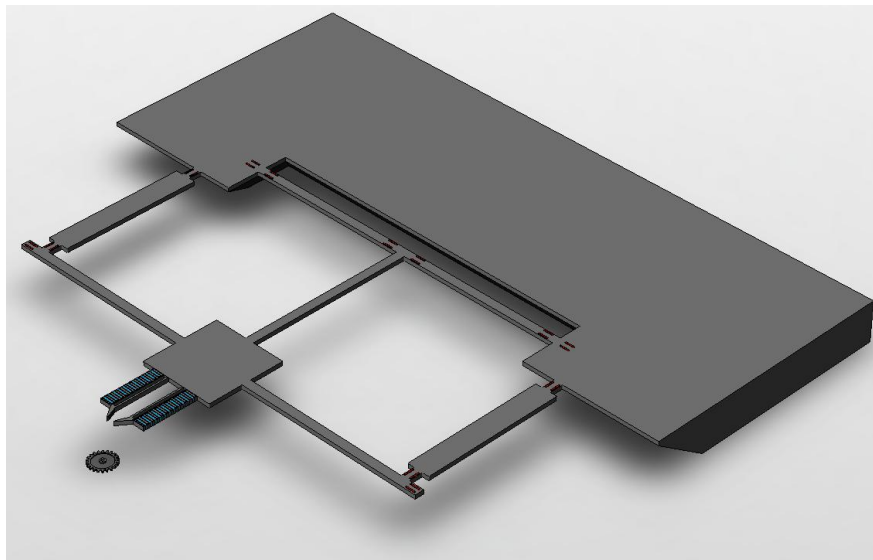


## **Development of a novel 6 DOF interaction force sensor for micro-gripper applications.**

Name:	J.M. Bank
Report no:	PT 10.022
Coach:	M. Porta, P. Estevez
Professor:	U. Staufer
Specialisation:	Production Technology
Type of report:	Master Thesis
Date:	June 18 <sup>th</sup> , 2010



# Development of a novel 6 DOF interaction force sensor for micro-gripper applications.



Author: Jesse Bank

Supervisor: Dr. M. Porta, Msc. P. Estevez

Professor: Prof. Dr. U. Staufer

Delft, June 18, 2010



# Summary

This thesis presents the design of the mechanical and electrical structure of a novel interaction force sensor, in which a micro-gripper can be easily integrated. Independent force/torque detection in six degrees of freedom (DOF), a wide force range (a few mN) and a high resolution (at  $\mu\text{N}$  and  $\mu\text{Nmm}$  level) are obtained. Piezoresistors are used for the detection of the interaction force due to the suitable force range and resolution. The interaction force sensor is fabricated with integrated circuit (IC) compatible processes.

In the micro-handling domain, micro-grippers are used for applications in micro-manipulation, life science and micro-surgery. In these fields, the micro-parts to handle have dimensions from a few  $\mu\text{m}$  to hundreds of  $\mu\text{m}$ . Typically, force sensing with  $\mu\text{N}$  and sub- $\mu\text{N}$  resolutions over a range of a few mN is needed. The lack of interaction force sensing, in current micro-grippers, limits the applications in these fields. Current external devices, able to detect the interaction force along multiple DOF, are difficult to be used in a micro-gripper due to assembly and calibration problems. Therefore there is the need for high resolution, six DOF interaction force monitoring integrated within micro-grippers.

In this thesis, a mechanical and electrical study is carried out for the development of the interaction force sensor according to typical requirements in micro-handling. Three different concepts are considered, all consisting of several beams with multiple integrated piezoresistors. Parameters such as dimensions and shape of the beams as well as the piezoresistor number and connections are taken into account in the design process. The different concepts are evaluated and compared based on their resolution, sensitivity, crosstalk, stiffness, dimensions, number of piezoresistors and the accessibility of the gripper.

The final design of the interaction force sensor has a dimension of  $3 \times 1.5 \times 0.03 \text{ mm}^3$  and it is capable of measuring six DOF independently, using 16 silicon integrated piezoresistors. Finite element models (FEM) show that resolutions between  $1.5 - 8.5 \mu\text{N}$  and  $2 - 10.5 \mu\text{Nmm}$  could be reached, for respectively force and torque measurement. Force/torques up to 30 mN and 37 mNmm can be measured.

A micro-gripper fabricated by IC compatible processes can be easily integrated in the interaction force sensor. However, the heat generation of the gripper has to be taken into account, since it causes thermal expansion (and therefore stresses) in the sensor. This effect influences the performance of the interaction force sensor in terms of crosstalk and resolution. The influence on the performance due to the heat generation of a thermal micro-gripper is studied.

The fabrication of the interaction force sensor is done at the Delft Institute for Microsystems and Nanoelectronics (DIMES). An experimental setup is also proposed to validate the theoretical performance of the fabricated interaction force sensor.



# Preface

This thesis is the result of my graduation project I started about 9 months ago and is part of the master Precision and Microsystems Engineering (PME) at the Delft University of Technology (DUT). It describes the design and mechanical and electrical design of an interaction force sensor, to be integrated in a micro-gripper.

This thesis is part of the development of a “smart and complete micro-gripper” performed within the Micro-Nano Engineering (MNE) research group in the PME department. The “smart and complete micro-gripper” must be able to detect the position of a grasped object, as well as the grasping force and the interaction force along the six DOF. This research is done in cooperation with Delft Institute of Microsystems and Nanoelectronics (DIMES) of the Delft University of Technology.

The interaction force sensor is developed to be used as a helpful tool for force sensing in micro-handling. Since the interaction force sensing is not well addressed in literature, it is tried to provide a useful piece of work, as a contribution to further research.

Delft, June 2<sup>nd</sup>, 2010

Jesse Bank



# Contents

<b>Summary</b>	<b>v</b>
<b>Preface</b>	<b>vii</b>
<b>Nomenclature and abbreviations</b>	<b>xi</b>
<b>1 Introduction</b>	<b>1</b>
1.1 Sensorized micro-handling .....	2
1.1.1 Fields of interest .....	2
1.1.2 Challenges in micro-handling .....	3
1.1.3 Force sensing in micro-handling.....	4
1.2 State of the art: Grasping force sensing .....	6
1.3 State of the art: Interaction force sensing .....	9
1.3.1 Interaction force sensing approach .....	9
1.3.2 Interaction force sensors .....	11
1.4 Global project description .....	13
1.5 Problem statement.....	14
1.6 Organization of this thesis .....	16
<b>2 Mechanical and electrical study of the interaction force sensor</b>	<b>19</b>
2.1 Sensor requirements.....	20
2.2 Concepts .....	22
2.2.1 Generation of concepts .....	22
2.2.2 Piezoresistor position .....	24
2.3 Mechanical and electrical design .....	25
2.3.1 Dimensions .....	26
2.3.2 Stiffness .....	28
2.3.3 Stress.....	28
2.3.4 Piezoresistor connections.....	29
2.3.5 Resolution and sensitivity .....	31
2.4 Selection of the concept .....	32
<b>3 Interaction force sensor design</b>	<b>35</b>
3.1 Mechanical structure.....	37
3.1.1 Test plate .....	37
3.1.2 Stress analysis.....	38
3.2 Electrical characterization .....	39
3.2.1 Piezoresistor layout .....	41
3.2.2 Sensitivity and crosstalk .....	41
3.2.3 Electrical noise.....	43
3.3 Thermal analysis.....	44
3.3.1 Heating of the interaction force sensor .....	45
3.3.2 Piezoresistor temperature dependency.....	47
3.3.3 Thermal-structural interaction.....	48

<b>4</b>	<b>Fabrication</b>	<b>51</b>
4.1	Fabrication issues .....	51
4.2	Fabrication process.....	53
<b>5</b>	<b>Experimental validation</b>	<b>55</b>
5.1	Experimental setup .....	55
5.1.1	Experimental layout .....	55
5.1.2	Data acquisition .....	56
5.2	Experimental approach .....	58
<b>6</b>	<b>Conclusions and recommendations</b>	<b>61</b>
6.1	Conclusions .....	61
6.2	Recommendations for further work.....	62
<b>A</b>	<b>Piezoresistor connection</b>	<b>63</b>
A.1	Wheatstone-bridge.....	63
A.2	Crosspoint Switch Array.....	65
<b>B</b>	<b>Force measurement analysis</b>	<b>67</b>
B.1	$F_x$ Measurement.....	68
B.2	$F_y$ Measurement.....	70
B.3	$F_z$ Measurement.....	72
B.4	$M_x$ Measurement.....	74
B.5	$M_y$ Measurement.....	76
B.6	$M_z$ Measurement.....	78
<b>C</b>	<b>Wafer design</b>	<b>81</b>
<b>D</b>	<b>Fabrication flowchart</b>	<b>85</b>
	<b>Acknowledgement</b>	<b>87</b>
	<b>Bibliography</b>	<b>89</b>

# Nomenclature and abbreviations

## Symbols

$c$	Charge carrier density	$[\text{cm}^{-3}]$
$E$	Modulus of Elasticity	$[\text{Pa}]$
$f$	Frequency	$[\text{Hz}]$
$F$	Force	$[\text{N}]$
$k_B$	Boltzmann constant	$[\text{J}\cdot\text{K}^{-1}]$
$K$	Stiffness	$[\text{N}\cdot\text{m}^{-1}]$
$l$	Length	$[\text{m}]$
$m$	Mass	$[\text{kg}]$
$M$	Moment/torque	$[\text{Nm}]$
$R$	Resistance	$[\Omega]$
$\Delta R$	Resistance change	$[\Omega]$
$S$	Power spectral density of the noise	$[\text{V}/\sqrt{\text{Hz}}]$
$[S]$	Sensitivity matrix	$[-]$
$[T]$	Transformation matrix with 1, -1 and 0	$[-]$
$t$	Thickness	$[\text{m}]$
$T$	Temperature	$[\text{K}]$
$\Delta T$	Temperature change	$[\text{K}]$
$U$	Voltage	$[\text{V}]$
$w$	Width	$[\text{m}]$

## Greek symbols

$\alpha_{\text{Si}}$	Temperature coefficient of resistance of Silicon	$[\text{K}^{-1}]$
$\delta$	Displacement	$[\text{m}]$
$\varepsilon$	Strain	$[-]$
$\mu$	Friction coefficient	$[-]$
$\pi$	Piezoresistive coefficient	$[\text{Pa}^{-1}]$
$\rho$	Doping-dependant electrical resistivity	$[\Omega\cdot\text{cm}]$
$\sigma$	Stress	$[\text{Pa}]$

## Abbreviations and acronyms

2D	Two-Dimensional
3D	Three-Dimensional
CSA	Crosspoint Switch Array
DIMES	Delft Institute for Microsystems and Nanoelectronics
DOF	Degree Of Freedom
DRIE	Deep Reactive Ion Etching
DUT	Delft University of Technology
FEM	Finite Element Model
IC	Integrated Circuit
KOH	Pottasium Hydroxide
LIA	Lock-In Amplifier
MEMS	Micro-Electromechanical System
MNE	Micro and Nano Engineering
PCB	Printed Circuit Board
PME	Precision and Microsystem Engineering
PVDF	Polyvinylide Fluoride
SNR	Signal to Noise Ratio
TCR	Temperature Coefficient of Resistance

---

# CHAPTER 1

## Introduction

In this chapter a short introduction is given to the subject of sensorized micro-handling. It starts with an introduction to sensorized micro-handling, its applications and challenges focusing on the need for force sensing. Afterwards grasping force sensing with the micro-grippers is discussed, followed by the approaches and types of sensors used for interaction force sensing. Then the global project is described of which this thesis is a part. Finally the problem statement is discussed, followed by the organization of this thesis.

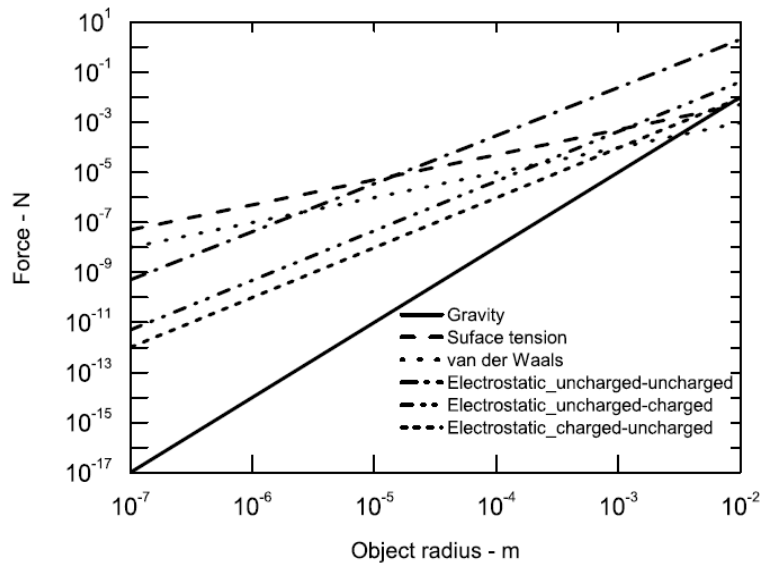


Figure 1.1: Gravitational force and attractive forces as a function of the object radius [1].

## 1.1 Sensorized micro-handling

In the last twenty years there is an ongoing interest in miniaturization of parts and micro-electromechanical systems (MEMS). These parts and systems need suitable instruments for their handling. The traditional tools used in the macro-domain cannot be used for the manipulation of such miniaturized parts, since their accuracy is not sufficient in terms of positioning and force control. As parts become smaller, so does the influence of the gravity, while the surface tension, van der Waals forces and electrostatic forces become dominant (Figure 1.1). The need for smaller tools, specifically designed for micro-handling is therefore desired. Nowadays, much research is being done in this field, where there is plenty of room for improvement.

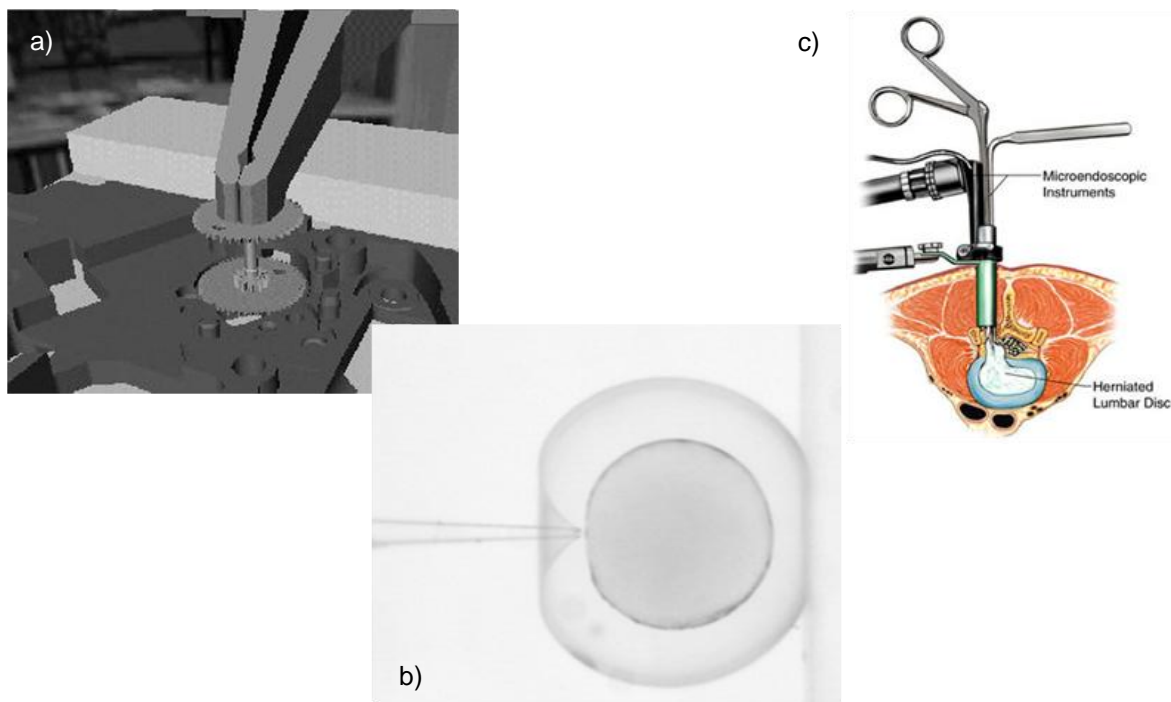


Figure 1.2: Fields of interest for sensorized micro-handling. a) micro-manipulation; assembling of hybrid products [2], b) life science; cell injection [3], c) minimal invasive surgery; spine surgery <sup>1</sup>.

### 1.1.1 Fields of interest

When considering manipulation in the micro-domain, the fields of interest are quite diverse. Typical fields are (Figure 1.2):

- **Micro-manipulation:** In hybrid products, multiple parts with different materials are assembled or aligned. High accuracy of force detection and dimensional control of fragile parts are key elements within micro-manipulation (Figure 1.2a).

<sup>1</sup> <http://www.neurosurgery.ufl.edu>

- **Life science:** Within the field of life science micro-manipulation is important when considering cell and tissue manipulation (Figure 1.2b). Cells and tissue are very fragile and in order to be used they must remain intact. Therefore delicate handling is required.
- **Surgery:** Surgery becomes more and more interesting since the introduction of minimally invasive surgery (Figure 1.2c). A surgical tool is inserted through an incision and since the tissue inside a body can be very delicate (e.g. eyes, brain), it is essential to execute the task with great accuracy.

Applications in these fields require great positioning accuracy and force control, since the parts and cells are very fragile. It is therefore important to handle these objects with care. The control of position and force of the micro-parts (often on  $\mu\text{m}$  and  $\mu\text{N}$  level) ensures the handling and assembly task to be carried out successfully.

### 1.1.2 Challenges in micro-handling

Within the micro-handling applications many challenges arise. Several challenges within sensorized micro-handling can be seen in Table 1.1. It shows the fields of interest with some of its major problems including requirements to solve these problems.

	Major problems	Need for	Applications
<b>Micro-manipulation</b>	<ul style="list-style-type: none"> <li>• Required high positional accuracy (<math>\mu\text{m}</math> range)</li> <li>• Loss of hand-eye contact</li> <li>• Limited vision, because of tiny spaces and limited depth of field</li> </ul>	<ul style="list-style-type: none"> <li>• High resolution force feedback systems (<math>\mu\text{N}</math>)</li> <li>• High dimensional control (<math>\mu\text{m}</math>)</li> <li>• Flexibility in micro-manipulators</li> <li>• Multi DOF sensing</li> </ul>	<ul style="list-style-type: none"> <li>• Hybrid products</li> <li>• Alignment issues</li> </ul>
<b>Life science</b>	<ul style="list-style-type: none"> <li>• Cell/tissue damaging</li> <li>• Loss of hand-eye contact</li> <li>• Required high positional accuracy</li> <li>• Required force control</li> </ul>	<ul style="list-style-type: none"> <li>• High resolution force feedback systems (<math>\mu\text{N}</math>)</li> <li>• High dimensional control (<math>\mu\text{m}</math>)</li> </ul>	<ul style="list-style-type: none"> <li>• Cell manipulation systems</li> <li>• Tissue characterization</li> </ul>
<b>Surgery</b>	<ul style="list-style-type: none"> <li>• Limited vision</li> <li>• Cell/tissue damaging</li> <li>• Required high positional accuracy</li> <li>• Limited space inside surgical tool</li> <li>• Limited freedom of movement</li> </ul>	<ul style="list-style-type: none"> <li>• High resolution force feedback systems (<math>\mu\text{N}</math>)</li> <li>• High dimensional control (<math>\mu\text{m}</math>)</li> <li>• Small tools (mm)</li> </ul>	<ul style="list-style-type: none"> <li>• Micro-surgical instruments for eyes and brains</li> <li>• Drug delivery systems</li> </ul>

Table 1.1: Micro-handling and its application, problems and needs.

From Table 1.1 it is clear that there is a need for small and flexible handling tools with force feedback and dimensional control. Such tools can be used for many tasks within the fields of interest. Typically, micro-grippers are used in micro-handling, since they handle multiple sizes, shapes and materials and are capable of performing various tasks.

The feedback system in micro-handling can be realized in different ways. Force and vision feedback are examples of feedback systems that are used in many cases. Vision feedback provides useful information to the user, but due to a lack of space in the micro-domain and the limited depth of field, it is often not possible to use a microscope. Therefore in many cases, it is not possible to use vision feedback. Force feedback on the other hand, allows the user to understand the forces that are present while performing a certain task. To get the required information, several force feedback systems are needed, since different types of forces are present during micro-handling.

### 1.1.3 Force sensing in micro-handling

From Table 1.1 follows that there is a need for position and force control in the micro-handling domain. When both types of control are combined, the position, orientation and force distribution on an object are known. However, when force control is considered, two types of forces on an object are of interest:

- **Grasping forces:** The force that is exerted in order to grasp an object is called the grasping force (Figure 1.3a). Using a micro-gripper to grasp a part with a high force might result in a damaged part, cell or tissue. The force can be exerted by means of different actuator principles (like piezoelectric, piezoresistive or capacitive actuators) and controlled by different sensors (based on the piezoelectric, piezoresistive, capacitive or optical principle).
- **Interaction forces:** The force that the environment exerts on the part is called the interaction force (Figure 1.3b). During certain tasks (like assembling or cell manipulation) forces are introduced on the grasped part. Inaccurate force control results in damaged parts and misaligned or defect devices. The control of the interaction force can be done in different ways (by using a piezoelectric, piezoresistive or capacitive based sensor).

It is important to highlight the difference between these forces, since the approach for detecting these forces is different. Moreover, even the sensing principle can be different for both the grasping and the interaction forces.

In order to grasp an object, a micro-gripper is actuated causing the gripper arms to move. The gripper arms close the gripper tip and grasp the object. Each gripper arm usually moves in one direction (the grasping direction). Grasping force control is therefore only needed for one direction. However, regarding the interaction forces, six degrees of freedom (DOF) are required to get all the possible information. Therefore, three forces (along the x, y and z-axis) and three moments (around the same axis) must be measured.

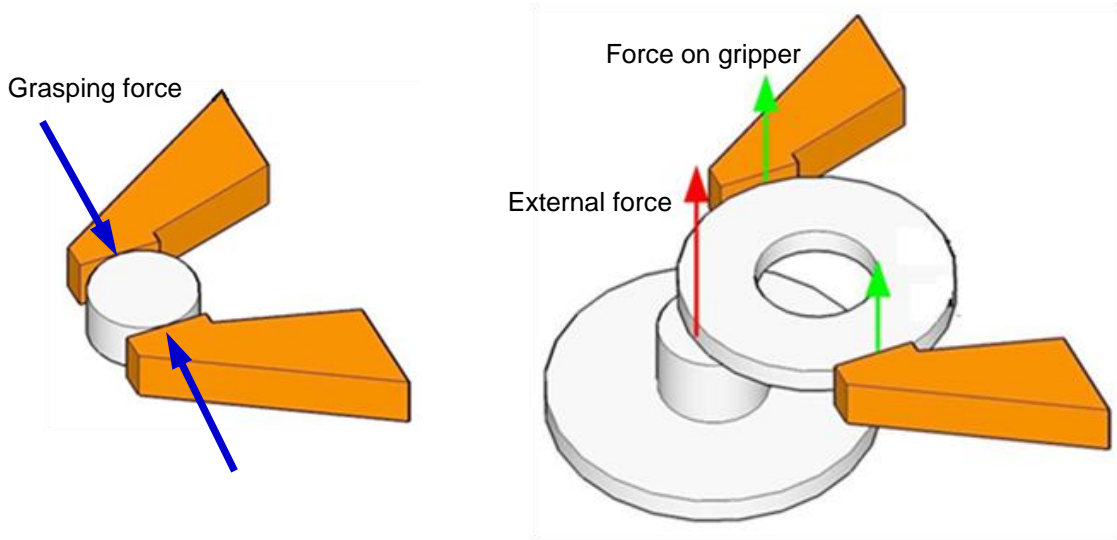


Figure 1.3: a) Grasping force, b) interaction force. [4]

Typical values for the grasping and interaction forces follow from the fields of interest in section 1.1.1 and can be found in literature.

For both the grasping and the interaction force, the force range is between the 0 and 10 mN. Micro-assembly uses parts up to a size for several hundreds of micrometers. For instance, an object with dimensions of  $\phi 100 \times 200 \mu\text{m}$  made of silicon (with a weight of 1.5 mN) is grasped with a force of 6 mN, when a friction coefficient of 0.25 is used between silicon and silicon [5] (see Equation (1.1)).

$$F_{\text{grasp}} = \frac{F_z}{\mu} \approx \frac{1.5 \text{ mN}}{0.25} = 6 \text{ mN} \quad (1.1)$$

During micro-assembly, low clearances result in similar ranges for the interaction force [6]. The same holds for alignment tasks of micro opto-electrical components such as optical fibers, which are fragile and easy to break. They typically break at the mN force range [7].

On the other hand the gripper must also be capable of holding fragile objects, which require handling with a resolution of  $5 \mu\text{N}$ . For example, during the assembly of small mirrors and lenses, it is needed to handle them with care. Assembling micro-mirrors requires handling with forces around  $2 \mu\text{N}$  [8].

In living cell manipulation, high resolution force control is essential as well, in order to prevent damaging the cells. During cell injection for instance, forces that occur differ from  $0.1 \mu\text{N}$  to 90 mN depending on the type of cell ([3], [9], [10]). A high resolution results in a wide variety of cell that can be handled. This means that the interaction force control and the grasping force control must be in the (sub)  $\mu\text{N}$  range.

## 1.2 State of the art: Grasping force sensing

Micro-grippers are of great interest in recent years and are used for applications as described in section 1.1.1. Gripper actuation and force sensing are usually based on different principles and can be handled separately. The choice regarding the actuation principle and grasping force measurement principle depends on the applications and the requirements.

For the measurement of the grasping forces, one approach is commonly found in the literature. Usually, the detection of the grasping force is inserted within the micro-gripper. Measuring principles like piezoelectric, piezoresistive and capacitive measurement systems are generally used. Optical measurement is used as well, although this principle is externally placed.

In the following section the most common sensor principles for the detection of the grasping force are given, including some examples of micro-grippers that are developed using such solutions.

### Piezoelectric force sensing micro-gripper with magnetic actuation

Piezoelectric materials are commonly used for gripper actuation and less often for grasping force sensing. In piezoelectric sensing a pressure change in a material produces an electric potential within the crystals. This principle is inverted when piezoelectric materials are used for gripper actuation.

One of the characteristics of piezoelectricity as sensing principle is that small deflections result in high voltage outputs. This means that high resolutions can be reached in force measurement. In Figure 1.4 a gripper is shown, which uses piezoelectricity for grasping force sensing (which is developed by [11]). The piezoelectric material used is Polyvinylidene fluoride (PVDF) polymer, because of its high linearity, wide bandwidth and high signal to noise ratio.

For the gripper actuation a moving coil is used to move the pushing shaft. Through elastic hinges the gripping arms are actuated. Objects up to a size of 300  $\mu\text{m}$  can be grasped with a grasping force up to 630 mN (with supply voltage of 8 V).

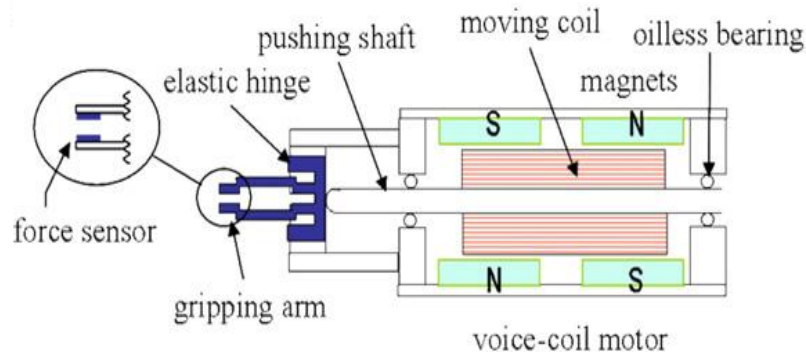


Figure 1.4: Force sensing micro-gripper with a grasping force sensor based on the piezoelectric principle [11].

### Piezoresistive force sensing micro-gripper with thermal actuation

Another possibility for measuring the grasping force in a micro-gripper is to use piezoresistors. There are two types of piezoresistive sensors: the conventional strain gauge and the silicon integrated piezoresistor. The silicon integrated piezoresistor is more sensitive and smaller compared to the conventional strain gauge. A force introduces stresses and strains in the material and due to a small change in length of the resistor, the resistivity changes (which is detected).

In the case of the gripper shown in Figure 1.5 (developed by [12]), the grasping force is measured with piezoresistors which are integrated in the silicon by doping. Two reference piezoresistors and two sensing piezoresistors are placed in a full-active Wheatstone-bridge for maximum sensitivity. This sensorized gripper is therefore capable of measuring a minimum detectable force of 770 nN. The bandwidth of the grasping force sensor is 29 Hz.

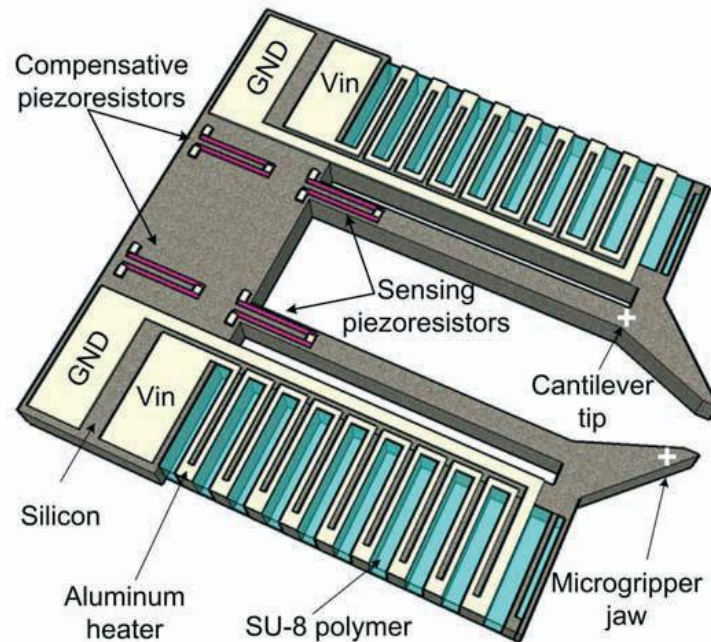


Figure 1.5: A micro-gripper with piezoresistors for detecting the grasping force, developed by [12].

The actuation principle used in this gripper is based on electrothermal expansion. A temperature change results in a change in length. In this case the electrothermal actuator consists of two beams with different materials and cross-sections. The change in length of each beam is different due to these differences and therefore the beams bend.

Polymers are used as electrothermal elements for one simple reason: they can produce a large displacement using relative low power. A polymer that is widely used for expansion is SU-8. The gripper developed by [12] uses SU-8 to produce a gripper with an opening range of 40  $\mu\text{m}$ , while having a gripper length of 490  $\mu\text{m}$ . The maximum operating temperature is 176  $^{\circ}\text{C}$  at an applied voltage of 4.5V and an opening range of 40  $\mu\text{m}$  is achieved. Forces up to 135 mN can be applied.

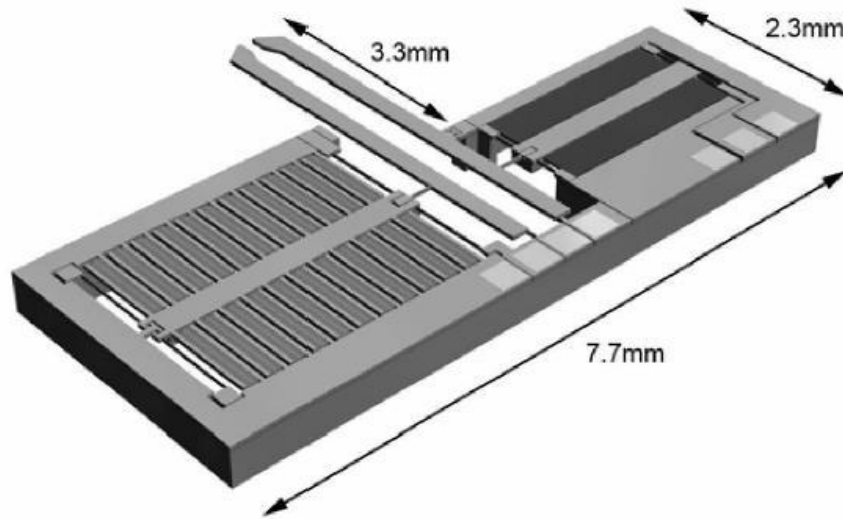


Figure 1.6: Capacitive based grasping force sensor integrated in gripper [13].

#### Capacitive based micro-gripper

The capacitive principle is based on distance change between a fixed electrode and a suspended one. When the distance between the two electrodes changes, the voltage outcome does change as well. In the capacitive principle the applied voltage is linear with the displacement.

The micro-gripper developed by [13], uses the capacitive principle for both the actuation and the sensing of the grasping force (Figure 1.6). One of the comb drives is used for the gripper actuation while the other one is used for grasping force control. An opening range of  $100\text{ }\mu\text{m}$  with an applied voltage of  $140\text{ V}$  is reached, which results in a maximum exerted force of  $380\text{ }\mu\text{N}$ .

High resolutions can be achieved using the capacitive principle for grasping force sensing. In this case a resolution of  $0.05\text{ }\mu\text{N}$  with a bandwidth of  $1000\text{ Hz}$  is achieved and even a resolution of  $0.01\text{ }\mu\text{N}$  with a bandwidth of  $30\text{ Hz}$  is reached. However, to reach such a high resolution, requires a large area.

#### Optical force sensing micro-gripper with piezoelectric actuation

One of the less used sensing principles in the micro-domain for grasping force sensing, is the optical principle. The reason is that it requires space for the light source (and path) as well as for the reflectors. However in [14] a micro-gripper is developed with a force sensor based on this principle (Figure 1.7). This gripper uses a laser to measure the deflection of the gripper arms. The reflective surface of the gripper arm is used and by measuring the phase delay of the laser, the deflection can be measured. High resolutions can be achieved, which in this case is in the order of  $2\text{ nN}$ . However, a high resolution usually means a small force range (which is limited by the stiffness of the cantilever). For this sensor the force range is not given.

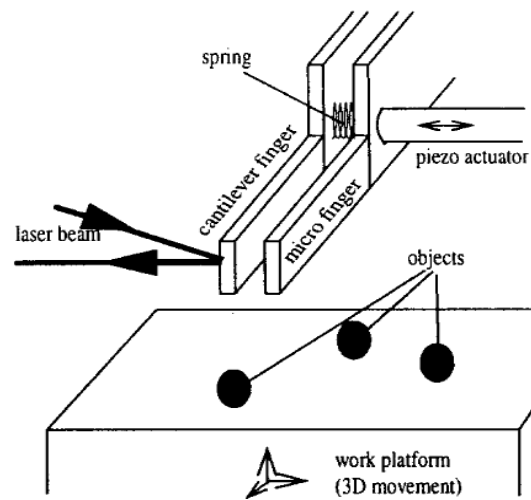


Figure 1.7: Grasping force principle based on optics [14].

## 1.3 State of the art: Interaction force sensing

For the detection of the interaction force there is no ideal approach or sensing principle. The choice for a certain approach or sensing principle is based on the applications and requirements.

### 1.3.1 Interaction force sensing approach

For detecting the interaction forces in micro-handling, there are three approaches that are considered in literature:

- **Monolithic approach:** The sensor is integrated in the gripper. No separated devices exist and the gripper and sensor are monolithically fabricated.
- **Hybrid approach:** The sensor is placed as the interface between the gripper and its support.
- **Sensorized environment:** The environment where the handling takes place is sensorized. The interaction force sensor and the gripper are completely decoupled.

#### The monolithic approach

The idea of this principle is to have a micro-gripper with an interaction force sensor integrated in it. Already a few grippers have been developed in the past with an integrated interaction force measurement system, for instance the one developed by [15]. This sensor is based on the capacitive principle with a thermal actuator for applying the grasping force and capacitive sensors for measuring the interaction forces (Figure 1.8). This interaction force sensor is only capable of measuring in one direction. Thanks to the large area with comb drives a resolution of 40 nN is reached for the interaction force.

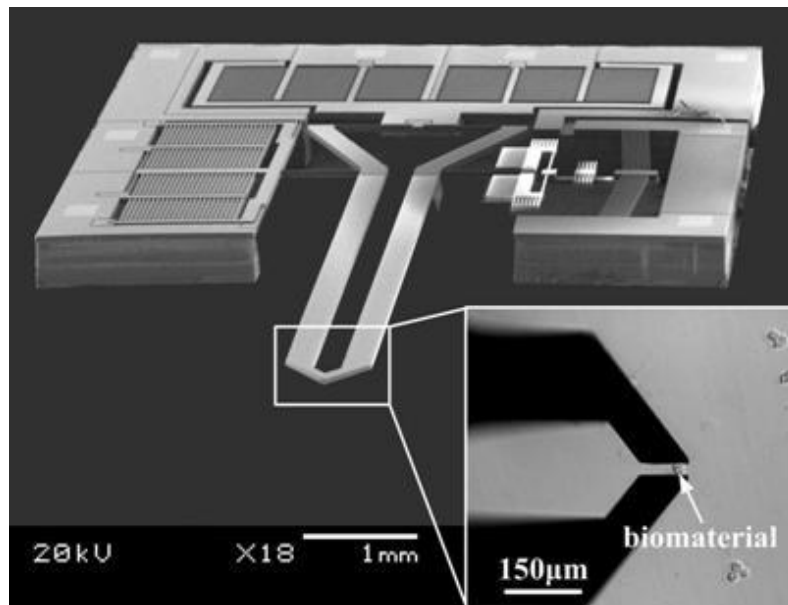


Figure 1.8: Gripper with integrated interaction force sensor, proposed by [15].

### The hybrid approach

In this approach the sensor is positioned between the gripper and its support, which means that the gripper itself is mounted on top of the interaction force sensor. In [16] a clear distinction is made between the instrument tip, the sensor (flexure beam plates) and support (Figure 1.9). This sensor is capable of measuring three DOF with a resolution of 0.5 mN and a force range of 1 N.

Another example is the sensor developed by [17], which developed an interaction force sensor capable of measuring three DOF. The force range of the sensor is 0.3 N with a resolution of 3 mN. This sensor is developed as a part of a minimally invasive surgery tool.

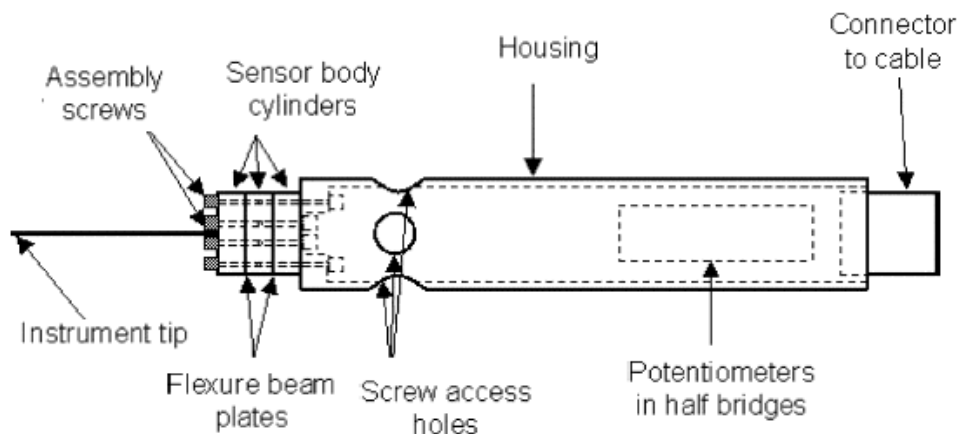


Figure 1.9: Interaction force sensor in the interface between tip and the support, proposed by [16].

### The sensorized environment

In the sensorized environment the sensor is not placed in (or connected to) the gripper, but it is decoupled from the gripper and placed somewhere else. For instance in [18] the force sensor is placed underneath the assembly table (Figure 1.10). Forces on the part are transferred to the table which is capable of measuring the interaction forces.

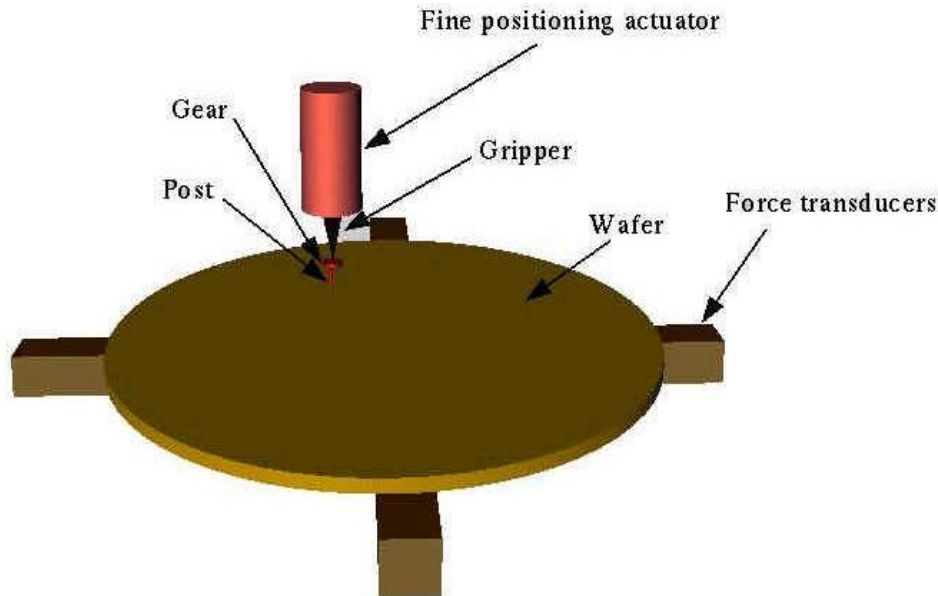


Figure 1.10: Gripper with sensorized environment, proposed by [18].

### 1.3.2 Interaction force sensors

In literature different principles are known for measuring interaction forces. The most common types of sensors that are used are piezoresistive, piezoelectric and capacitive sensors.

#### Piezoelectric sensor

Several examples exist of interaction force sensors using the piezoelectric principle to detect the forces in multiple directions. Such a sensor is shown in Figure 1.11. It uses PVDF as sensing material and due to a smart design it is able to measure three DOF independent from each other. High resolutions are reached (up to  $0.1 \mu\text{N}$ ), which results in a small force range as well ( $5 \mu\text{N}$ ). This sensor is developed for applications in the assembly of micro-mirrors and biomanipulation.

#### Piezoresistive sensor

The piezoresistive principle is widely used for detection of interaction forces. One of such a device is developed by [20] (Figure 1.12). Due to the two symmetry axis in the sensor (the x and y-axis) and a suitable arrangement of the piezoresistors, it is possible to detect six DOF independently. For force sensing 18 piezoresistors (embedded in the silicon) are used and a maximum crosstalk of 4% is reached.

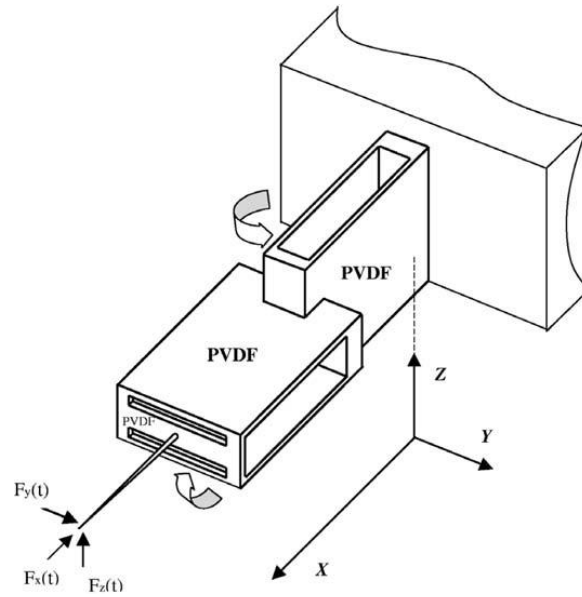


Figure 1.11: A piezoelectric sensor using PVDF, which is able to measure three DOF independently [19].

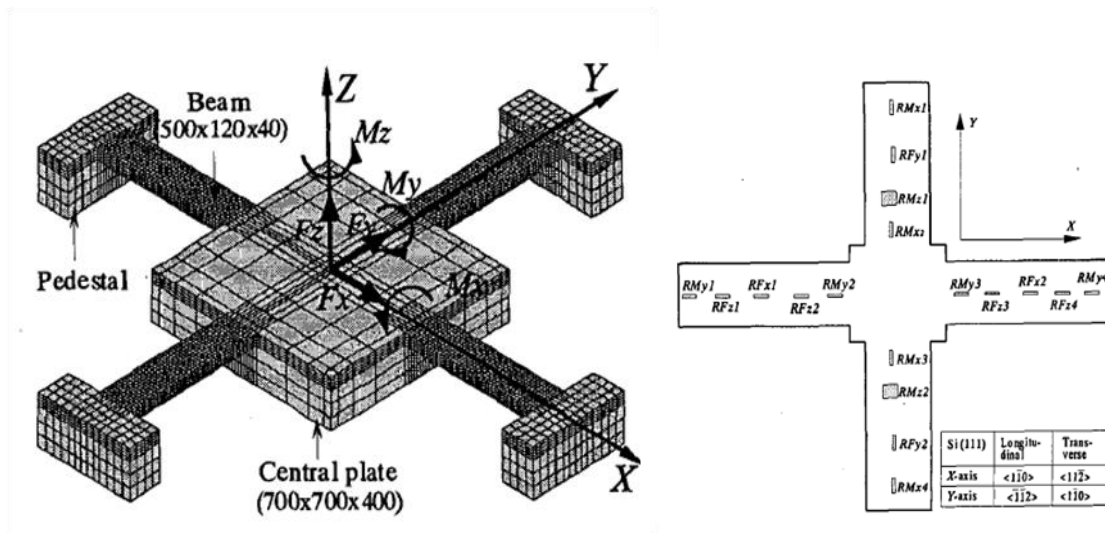


Figure 1.12: A piezoresistive sensor which is able to measure six DOF independently [20].

Due to the high stiffness of the sensor, a large force range is achieved. It has a force range of 0.1 N (in the z-direction) and 1 N (in the x and y-direction) and torque range of 300 N $\mu$ m (in the z-direction) and 30 N $\mu$ m (in the x and y-direction). However, due to the high axial stiffness in the sensor, the sensitivity and the resolution are low. Sensitivities up to 1.32 mV/mN and 3.88e-3 mV/mN $\mu$ m are achieved.

Several other examples exist (like [21] and [22]), where high resolutions are achieved. In the case of [21], resolutions of 3 and 10  $\mu$ N are reached. Three DOF can be detected independently by using 12 silicon integrated piezoresistors.

### Capacitive sensor

Multiple sensors have been developed using capacitive sensing. One particularly interesting case is a device developed by [15], which is able to detect two DOF. However, other devices exist, which are suitable for measuring six DOF. Such a sensor is developed by [23], using two different wafers that are glued together. High resolutions of 1.4  $\mu$ N are achieved with a force range of 1 mN at a readout frequency of 30 Hz. Each force can be measured independently. With an overall size of 10 x 9 x 0.5 mm<sup>3</sup> is relatively big.

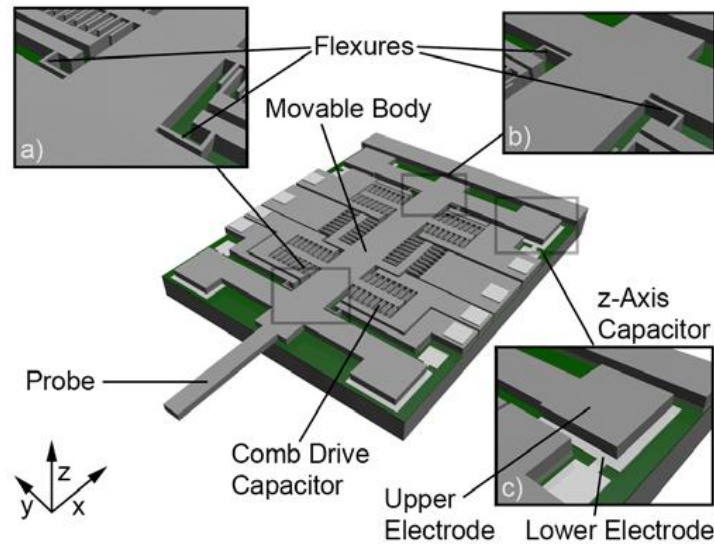


Figure 1.13: The first capacitive interaction force sensor that is capable of measuring six DOF [23].

## 1.4 Global project description

A research on the development of a “smart and complete micro-gripper” is performed within the Micro-Nano Engineering (MNE) research group at the Delft University of Technology (DUT). Actually, in the micro-handling domain there are many applications which require complete force detection and position control (see section 1.1). Therefore, this “smart and complete micro-gripper” must be able to detect the position of a grasped object, as well as the grasping force and the interaction force along the six DOF.

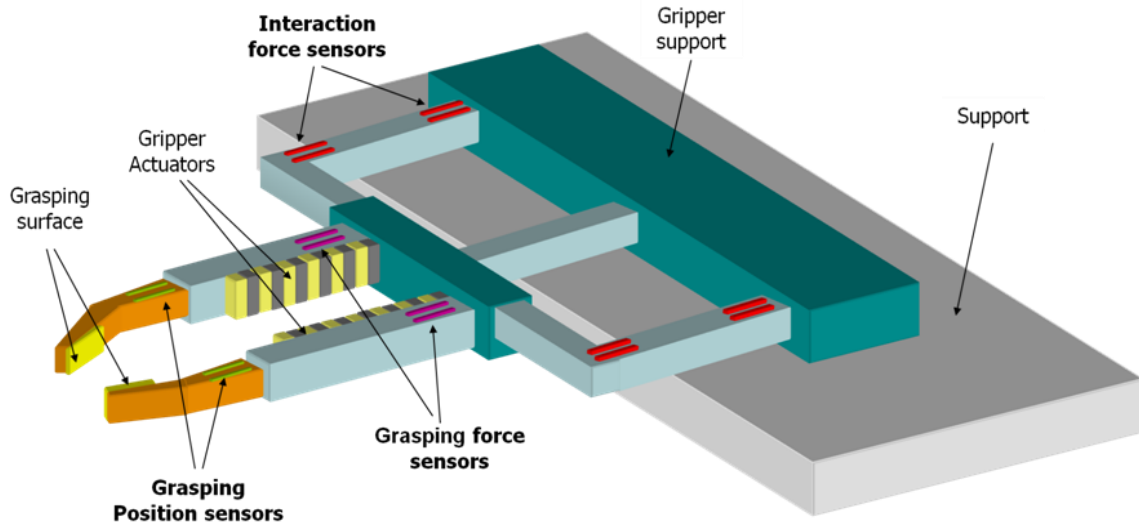


Figure 1.14: Schematic system layout of a “smart and complete micro-gripper”.

The detection of the grasping force (to be inserted in the “smart and complete micro-gripper”) is already well addressed in literature. Within the Delft University of Technology different micro-grippers with grasping force sensing capabilities have been developed. The gripper concept which is inserted in the “smart and complete micro-gripper”, is the one developed by [12].

Some efforts have also been done to provide the micro-gripper with the capability of detecting the position and orientation of the grasped object. Therefore the “smart and complete micro-gripper” is provided with a device for the position and orientation detection, developed by [4].

On the other hand, the detection of the interaction forces is not well addressed in literature. Only few devices are developed in the past for detection of interaction forces along multiple DOF. Measurement of the interaction force along six DOF usually results in narrow force ranges and/or low resolutions. Especially the combination of interaction forces sensing and micro-grippers is new in micro-handling.

Since many of these challenges still exist, the detection of the interaction forces is the focus of this research.

## 1.5 Problem statement

In order to provide the “smart and complete micro-gripper” with an interaction force sensing device, the drawbacks (discussed in section 1.4) need to be overcome.

The objectives of this thesis are:

- Development of an interaction force sensor ready to be integrated in a micro-gripper
- Development of an interaction force sensor capable of measuring the interaction force in six DOF (crosstalk <10%)
- Provide the interaction force sensor with high resolution ( $\mu\text{N}$ ) and large force range (mN), which is similar in multiple directions
- Low temperature dependency of the interaction force sensor

To realize these objectives, an approach and a sensing principle are selected for the development of the interaction force. In section 1.3.1 different interaction force sensing approaches are shown, followed by several interaction force sensing principles in section 1.3.2.

#### Interaction force sensing approach

In Table 1.2 an overview of the advantages and drawbacks is given of the different approaches.

	Advantages	Drawbacks
<b>Monolithic approach</b>	<ul style="list-style-type: none"> <li>• Plug and play (easy to be used)</li> <li>• No assembly needed</li> <li>• No calibration needed</li> </ul>	<ul style="list-style-type: none"> <li>• Hard to provide gripper with multiple, independent DOF detection</li> </ul>
<b>Hybrid approach</b>	<ul style="list-style-type: none"> <li>• Flexible</li> <li>• Parallel development of gripper and sensor</li> </ul>	<ul style="list-style-type: none"> <li>• Assembly of gripper and sensor is hard</li> <li>• Fabrication in two steps</li> <li>• Not simple to interchange grippers (no macro)</li> <li>• Calibration needed</li> </ul>
<b>Sensorized environment</b>	<ul style="list-style-type: none"> <li>• Parallel development of gripper and sensor</li> </ul>	<ul style="list-style-type: none"> <li>• No plug play (time consuming)</li> <li>• Calibration needed</li> </ul>

*Table 1.2: Comparison between different approaches for the interaction force sensor*

For the development of the interaction force sensor, the monolithic approach is the one followed. The gripper and sensor are monolithically fabricated and no separated devices exist. This has the advantage that no mounting errors due to misalignment of the gripper (with respect to the interaction force sensor) are introduced. In the hybrid approach, the assembly is done at a later stage, which could result in slightly misaligned gripper.

Since no assembly is required afterwards, this results in a ready to be used (plug-and-play) sensor. This is for instance, one of the major problems with the sensorized environment. The interaction can occur in different locations in the environment (relative to the sensor reference

frame), requiring re-calibrations or complex calculations. This is a time consuming process and therefore no plug-and-play approach. The selected approach has the advantage that the calibration of the device has to be done only once and therefore many different tasks can be performed with the same device.

The flexibility of the hybrid approach is one of the (possible) advantages compared to the monolithic approach. However, interchanging the gripper is not as straightforward as in the macro-domain due to the fragility of both the micro-gripper and the interaction force sensor. Usually the connection is permanent and therefore hard to replace with another gripper.

For those reasons, the monolithic approach is the approach that is followed during the development of the interaction force sensor.

### **Sensing principle**

The piezoresistive principle is chosen to base the interaction sensor on. The reason is that piezoresistors are very flexible. Since piezoresistors are reasonably small, they can be placed in many different ways. Therefore, different designs with independent force detection of six DOF can be realized. This is one of the main drawbacks of capacitive sensors. With capacitive sensing, it is hard to make the interaction force sensor capable of measuring six DOF. Large areas are needed for reaching high resolutions and since the space for the interaction force sensor is limited, the capacitive principle is not flexible.

Furthermore, piezoresistors are capable of reaching resolutions up to nN level and force ranges in the mN ([12] and [22]). For many applications in micro-handling this is enough. Piezoelectric sensors for instance, have the main drawback that the force range is limited. Due to the high sensitivity of the piezoelectric materials, high resolutions can be achieved. However, there is a trade-off between the resolution and range.

Another drawback of piezoelectric sensors is that the fabrication is complicated in integrated circuit (IC) compatible processes, due to complex processing. The technology for the production of piezoresistors on the other hand, can be easily integrated within the fabrication process. Since the technology is known within the Delft University of Technology (DUT), this experience can be used for the development of this sensor. Moreover, the fabrication processes are compatible with the processes of the micro-gripper developed by [12], which is used to validate the integration of a micro-gripper.

## **1.6 Organization of this thesis**

Realizing the objectives of the thesis requires several steps. Chapter 1 gives a brief overview of the applications and the challenges in the micro-handling domain. The detection of grasping and interaction force is explained and the challenges of the interaction force detection are discussed.

In Chapter 2 a set of requirements for the interaction force sensor is listed, followed by the introduction and explanation of three different concepts for the interaction force detection. These three concepts are studied by changing the mechanical and electrical layout. Afterwards the concept with the best performance in terms of resolution, sensitivity and crosstalk is selected.

The proposed interaction force sensor is then evaluated in Chapter 3 and adjustments to improve the performance are explained. The mechanical, electrical and thermal properties of the interaction force sensor are discussed and the influence of a micro-gripper is evaluated.

In Chapter 4 the fabrication issues and the fabrication process of the interaction force sensor are discussed. Afterwards (in Chapter 5) the experimental setup and the signal acquisition for the experimental validation of the interaction force sensor are discussed. The experiments to be done are explained.

Finally, in Chapter 6 the conclusions and some recommendations are given on which further research can be based.



# Mechanical and electrical study of the interaction force sensor

In this chapter the development of the mechanical structure and electrical layout of the interaction force sensor is discussed (see Figure 2.1). First the requirements of such a sensor are given after which the generation of the interaction force sensor designs is explained. Then the design process is extensively discussed. Finally, the concepts are compared in order to select the best option according to the specifications.

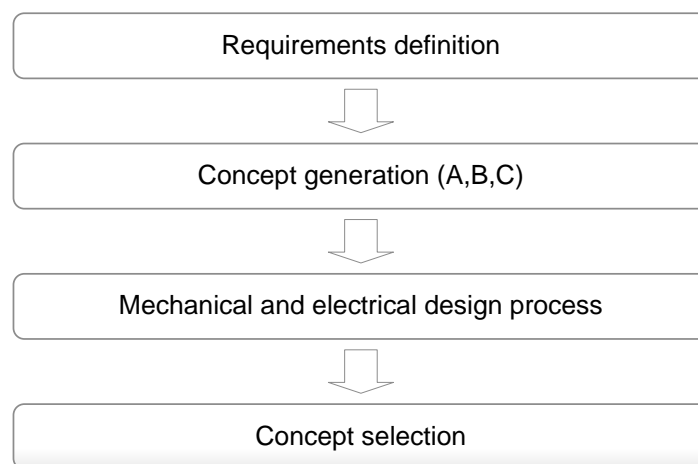


*Figure 2.1: The steps followed for the design of the interaction force sensor (Chapter 2).*

## 2.1 Sensor requirements

The requirements are derived from the applications in which the detection of the interaction force is required (see section 1.1). The requirements can be split up into three different parts: the general requirements, the force/torque requirements and additional performance requirements can be distinguished. The list of requirements of the interaction force sensor is given in Table 2.1.

Interaction force sensor		
Degrees of freedom (DOF)	6	-
Force resolution	10	$\mu\text{N}$
Force range	10	mN
Torque resolution	2	$\mu\text{Nmm}$
Torque range	2	mNmm
Maximum crosstalk	10	%
Minimum stiffness	50	N/m
Minimum resonant frequency	1000	Hz

Table 2.1: Requirements regarding the performance of the interaction force sensor

### General requirements

Silicon based technologies are used for the fabrication, because of their advantages: structures of sub- $\mu\text{m}$  scale can be fabricated, better sensitivity can be reached (compared to macro-scale sensors), integration of all the actuators and sensors in the same fabrication process. The major limitation of silicon based technology is that it is not possible to produce full 3D designs, but only “2.5D”. The limitations of this silicon based technology are considered and taken into account when designing the interaction force sensor.

The final device (including the gripper, grasping force sensor, grasping position sensor and the interaction force sensor) must be able to approach, grasp and move the objects around. Therefore, the accessibility of the gripper is one of the major concerns. At least one side of the interaction force sensor has to be accessible (on the side where the micro-gripper is inserted), allowing the gripper to perform its task.

### Force/torque requirements

As explained in section 1.1.3 it is necessary to detect six DOF to get all the information (three forces in the x, y and z-direction as well as the torques around the same axis). Ideally, the resolution and range of both the forces and the torques should be (almost) identical, for similar performance in all the directions.

The force range is defined by the highest forces that may occur during assembly tasks or cell handling. In literature a range of forces can be found for tasks in the micro-handling domain. For instance, during the assembly of micro-opto-electrical components such as optical fibers, typically, forces of several mN occur [7]. Optical fibers are fragile and easily break when high forces are applied. In other cases, such as the cell injection of salmon fish eggs, the force range that can be found is up to tens of mN [10].

The resolution to be achieved by the interaction force sensor is 10  $\mu\text{N}$  to prevent damaging of the parts or cells. In some cases (micro-mirror handling for instance) handling with forces of 2  $\mu\text{N}$  is required [8]. The same holds for tasks in cell manipulation; forces occur in the range from 0.1 to 600  $\mu\text{N}$  depending on the type of cell [3], [9]. A resolution of (at least) 10  $\mu\text{N}$  guarantees a good force control and therefore an intact cell or object. Moreover, a high resolution results in a wide range of cells to be handled. In micro-assembly, typically, forces up to 10  $\mu\text{N}$  are needed. In [6] the assembly and manipulation of micro-spheres is investigated. Forces up to tens of  $\mu\text{N}$  are necessary for successful collision detection and manipulation of the micro-spheres.

The size of the objects to be handled must be considered for obtaining the resolution and range of the torques, since a force on an object results in a torque to be measured. As a benchmark, an object with a diameter and length of 200  $\mu\text{m}$  is considered. When a force of 10  $\mu\text{N}$  is applied to the object, it results in a torque around the object of 2  $\mu\text{Nm}$ . For the torque range a similar calculation can be done, resulting in a torque range of 2  $\text{mNm}$ .

The independent detection of forces/torques by the interaction force sensor is needed for successful completion of its tasks. By measuring each force/torque independently, the direction in of the force/torque is obtained. This information is for instance used for determination of the final position of the object or the success rate of the task. Therefore, the maximum crosstalk that is allowed in the interaction force sensor is 10%.

#### Other performance requirements

A high positional accuracy is reached when the stiffness is high. If a force is applied and the device is moving around, it is unwanted for the structure to end up far from the desired point. For instance, when a peg is inserted in a hole, it is necessary to scan the surface in order to localize the hole. Therefore a minimum force of 10  $\mu\text{N}$  is applied in the z-direction to ensure there is contact between the part and the surface. The dimensional accuracy that is needed for preventing any missing information is 200 nm. This gives an absolute minimum of 50 N/m (see Equation (2.1)).

$$K_z = \frac{F_z}{\delta} \approx \frac{10 \mu\text{N}}{200 \text{ nm}} \approx 50 \text{ N/m} \quad (2.1)$$

The resonant frequency must be far from the operating frequency of the device. During “manual” use of the device, for instance, a human performs the operations. A human is capable of performing operations of 10 Hz [24]. During the automatic use of the sensor, operating frequencies are also limited to (around) 20 Hz. Therefore, the resonant frequency is set to be at least 1000 Hz.

$$f_1 = \frac{1}{2\pi} \cdot \sqrt{\frac{K}{m}} \quad (2.2)$$

Equation (2.2) can be used to calculate the minimum required stiffness to reach this resonant frequency. Considering that the interaction force sensor, a micro-gripper and a grasped object have a weight of approximately  $6 \cdot 10^{-8}$  kg, this results in a minimum required stiffness of 2.3 N/m. Since the minimum stiffness is already determined to be 50 N/m, this stiffness of 2.3 N/m is not considered.

## 2.2 Concepts

The need of accessibility from one side as well as the capability for independent detection of the six DOF has resulted in three structures shown in Figure 2.2. In these three concepts the silicon integrated piezoresistors are placed on top of the beams. The reason is, that it is a known fabrication technique (side implantation for instance still is an active research area [25]).

First the design considerations for the concepts are explained, followed by the discussion of the position of the piezoresistors.

### 2.2.1 Generation of concepts

The design rules for the generation of the three different concepts are explained in this section.

#### Accessibility

As explained in section 2.1 it is essential that the interaction force sensor is accessible from at least one side (for the gripper to approach, grasp and move the object). It is therefore not possible to design a completely symmetric sensor (as developed by [20]). Such symmetric sensors are easier in terms of crosstalk reduction and force separation. The structures shown in Figure 2.2 have only one symmetry axis (the y-axis) and therefore additional challenges for crosstalk minimization and separate force measurement are introduced.

In the beginning the gripper is considered as a black box for simplification. In a later phase the gripper is included, which introduces additional deflections, weight, stresses etc. The influence of the introduction of a micro-gripper is evaluated in Chapter 3.

#### Six DOF sensing design

It is important to design an interaction force sensor capable of detecting the interaction force along six DOF. The capability of independent detection of the six forces and torques is one of the major challenges in the design of the interaction force sensor.

In order to have independent force detection, each force or torque (exerted on the sensor) must result in a specific deformation and stress distribution. This stress distribution must be unique; meaning that each specific stress distribution belongs to only one force or torque. This unique stress distribution is detected by the piezoresistors. The piezoresistors are subjected to compressive stress, tensile stress or no stress at all. Due to this stress change, the resistivity of the piezoresistors (and thus the output voltage) changes as well. The combination of resistance change (in Wheatstone-bridges) needs to be unique for each force in order to separate the forces/torques from each other.

#### Fabrication issues

The embedded piezoresistors have various properties which are depending on the crystallographic orientation (Figure 2.3). The wafer orientation, the type of wafer, the piezoresistor orientation and the type of piezoresistor have great influence on the performance of the piezoresistors.

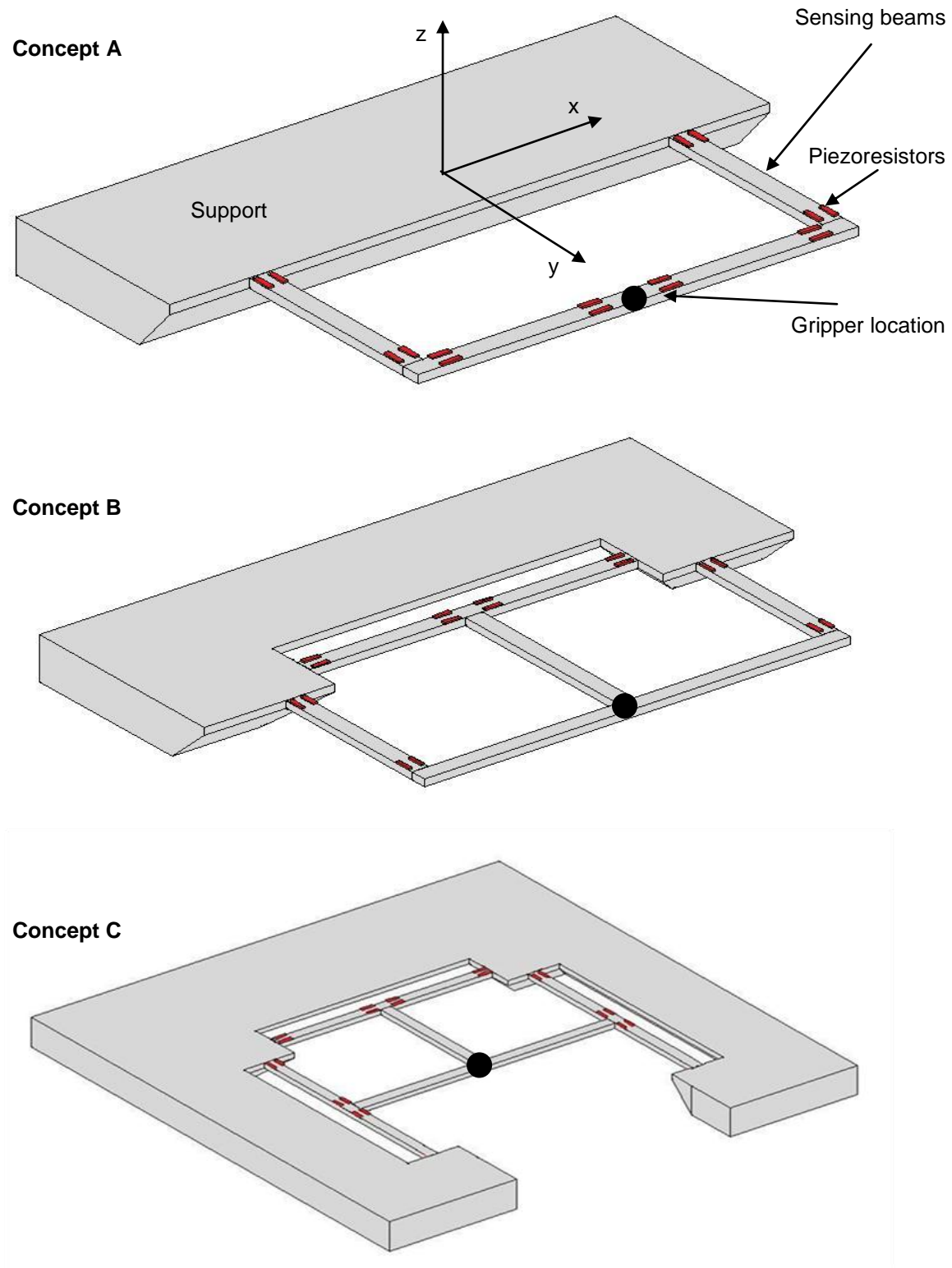


Figure 2.2: Generated concepts, where the black dot represents the point where the force is applied (the gripper is placed at this location later on) and the red squares represent the position of the piezoresistors.

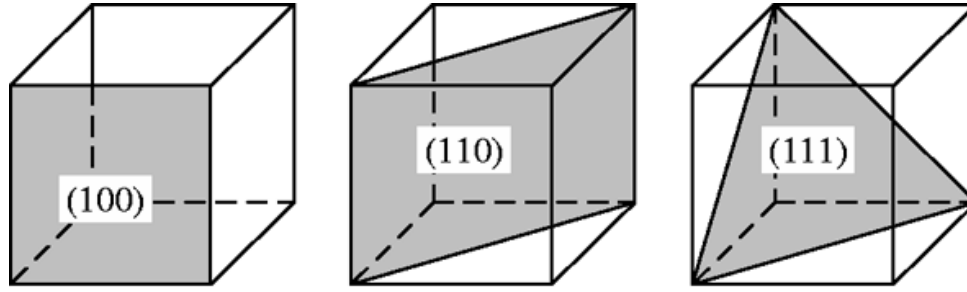


Figure 2.3: Crystal planes in single crystalline silicon.

Especially the piezoresistive coefficient is very sensitive. Although multiple options exist, it is decided to base the interaction force sensor on a p-type, (100) wafer, with integrated p-type piezoresistors along the [110] direction. The reason for this is that the sensitivity of the piezoresistive coefficient is much larger than in the other configurations. The only drawback of this choice is that the piezoresistors must be placed in the x- or y-direction (see Figure 2.2), which limits the design freedom of the sensor.

The general equations and graphical representations used for obtaining the piezoresistive coefficient are given by [26], [27], [28].

### 2.2.2 Piezoresistor position

The number and position of the piezoresistors is important for the performance of the sensor, because it must make the independent detection of the forces possible. It is therefore important to know where to place the piezoresistors and the number of piezoresistors that is needed.

For the best performance of the interaction force sensor (in terms of resolution, sensitivity and crosstalk), the piezoresistors must be placed in areas where the stresses are high. In general the stresses in the beams are the highest at the top of the beam, at the edge and at both (fixed) ends of the beam.

In each of the concepts shown in Figure 2.2 there are many stress concentration regions for placing the piezoresistors. However, the number of resistors needs to be kept to a minimum for a simpler detection and an easier separation of the forces. Furthermore, reducing the number of piezoresistors reduces the number of connections. Especially concept B and C have many stress concentration regions. Several of the piezoresistors are eliminated after severe research and applying the following guidelines for removing the piezoresistors:

- When a piezoresistor is completely symmetric with another piezoresistor, it does not add any additional information. So this piezoresistor can be removed.
- When a force is applied and the stress within the piezoresistor is relatively low (compared to the other piezoresistors), this piezoresistor can be removed.
- Piezoresistors can be included for reducing the crosstalk. If this is not the case, the piezoresistor can be removed.

## 2.3 Mechanical and electrical design

To improve the performance of each of the three concepts, many parameters can be studied, such as the dimensions and shape of the beams as well as the number and combination of piezoresistors. These parameters are included in the design process shown in Figure 2.4. Multiple concepts (with different sets of parameters) satisfy the requirements given in section 2.1.

To define the best solution, it is necessary to evaluate the concepts in terms of:

- Minimum resolution
- Maximum sensitivity
- Minimum crosstalk
- Stiffness
- Accessibility
- Number of piezoresistors
- Overall dimensions

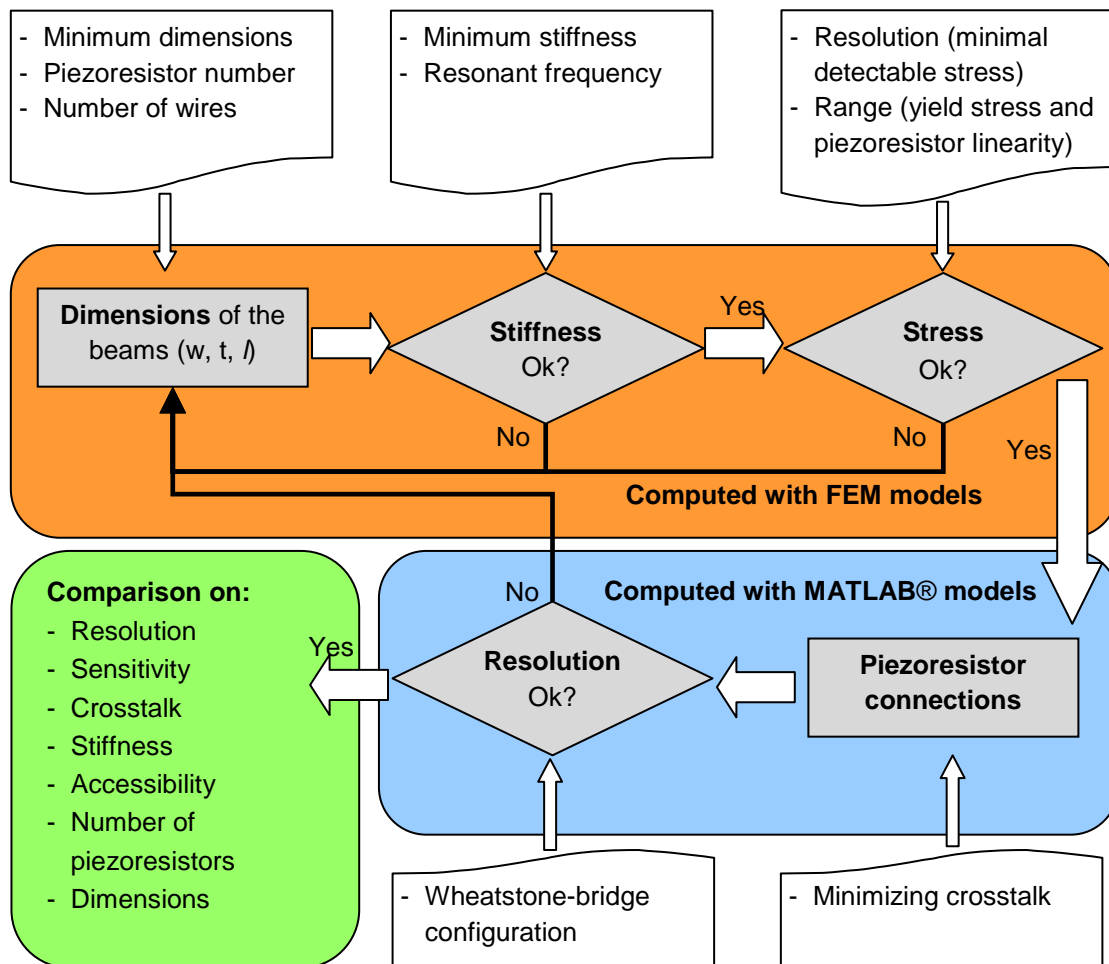


Figure 2.4: The mechanical and electrical design process.

The starting point of this process is the selection of the dimensions (length, width and thickness) of the beams. With these dimensions a Finite Element Model (FEM) is built with COMSOL® and it is checked if the model satisfies the stiffness and stress conditions. This is done for each of the six DOF. If the conditions for stiffness and stress are satisfied, the piezoresistor layout is optimized in terms of crosstalk using MATLAB®. This assures the forces can be separated. As a final step, the resolution and sensitivity are checked.

For each concept there is a configuration (with certain dimensions, piezoresistor connections, etc.), which is the best in terms of stiffness, resolution, sensitivity and crosstalk. However, the accessibility, the number of piezoresistors and the overall size of the sensor are considered as well for the best concept.

Each block of this design process contains some considerations for improving the final concept. This is explained in the next sections.

### 2.3.1 Dimensions

The dimensions of the beams have major influence on the performance of the interaction force sensor. By changing the dimensions of the beams, the resolution, the sensitivity, the crosstalk and the stiffness are affected.

There are three different parameters to be considered: the width, the thickness and the length of the beams. The dimensional limitations of the beams are shown in Table 2.2.

	concept A		concept B		concept C	
	Min.	Max.	Min.	Max.	Min.	Max.
<b>Width</b>	100 $\mu\text{m}$	-	65 $\mu\text{m}$	-	50 $\mu\text{m}$	-
<b>Thickness</b>	10 $\mu\text{m}$	50 $\mu\text{m}$	10 $\mu\text{m}$	50 $\mu\text{m}$	10 $\mu\text{m}$	50 $\mu\text{m}$
<b>Length</b>	-	-	-	-	-	-

Table 2.2: Boundary conditions regarding the dimensions of the beams.

#### Width

Regarding the width of the beams, there is a minimum width to take into account. An outer limit for the width of the beams, however, does not exist.

The minimum width is defined by number of wires of the final “smart and complete micro-gripper” (shown in Figure 1.14). Actually, the wires for the gripper actuation, the object position control, the grasping force sensor and the interaction force sensor have to pass through the beams to apply a voltage to the actuators of the micro-gripper and to bring the signal of the piezoresistors outside. Additional wires are necessary for the grounding and bias voltage of the piezoresistors.

A minimum gap width between the wires is needed to prevent fabrication and short circuit problems. Additional space is required for the interconnection between the wires and the piezoresistors. The space that is needed for a wire and a connection can be seen in Figure 2.5.

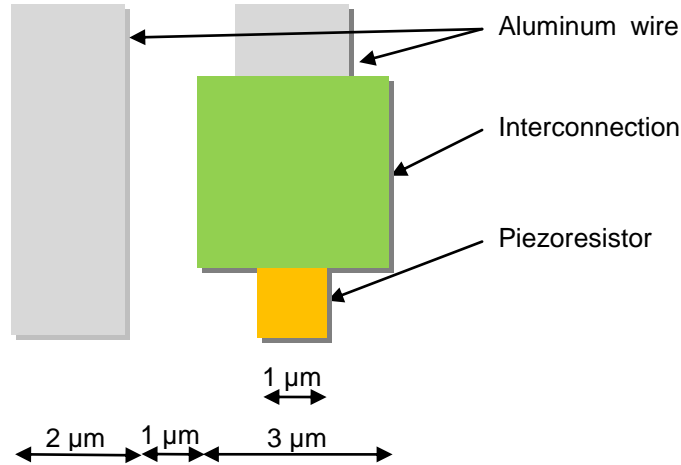


Figure 2.5: Required space for the wires and interconnections.

The number of wires that has to pass on top of the beams depends on the concept and the number of piezoresistors. The calculation that is being used to determine the minimum width is given in Table 2.3. For this calculation it is necessary to organize the wires in an optimal way, by defining which wire passes through which beam. It is considered that the concepts are symmetrical around the y-axis and therefore only half of the wires is considered in this calculation (for actuation and sensing of one gripper arm).

Number of piezoresistors	x 2 wires	
Wires for grounding/bias voltage		+ 2 wires
Wires for the gripper		+ 6 wires
Wires for the sensing tip		+ 8 wires
<hr/>		
Space required in between wires	x 3 μm	
Space required for bondpads (3 x 3 μm)		+ 4 μm
<hr/>		
<b>Total minimum width</b>		

Table 2.3: Calculation for the minimal width of a beam.

### Thickness

For the thickness there is only one constraint. The thickness of the beams has to be the same as the thickness of the gripper, since they are monolithically fabricated. The micro-gripper (developed by [12], which is selected to validate the integration of interaction force sensor) has a thickness of 30 μm. This is slightly variable, according to the requirements for opening range and gripping force.

### Length

Regarding the length there are no constraints to be taken into account. The length is an easy tool to adjust the stiffness and stress of the interaction force sensor. For more information on stiffness and stress see section 2.3.2 and 2.3.3. Once the requirements are satisfied, the length is kept to a minimum in order to keep the dimensions of the interaction force sensor as little as possible.

### 2.3.2 Stiffness

A low stiffness in the interaction force sensor has a negative impact on the position accuracy, and therefore must be taken into account. However, by decreasing the stiffness the stresses in the beams increase and therefore a higher resolution can be achieved.

FEM models are used to verify in that the stiffness is at least 50 N/m. For the definition of the stiffness, only the stiffness in the x, y and z-directions is taken into account. Torsional stiffnesses require knowledge about the angles during deformation and since there is no limitation of the angles, this is not considered.

Ideally the stiffness in the direction of the three forces (and three torques) is the same, so the force range and resolution are close to each other. However this is not possible since the concepts are not identical in the x, y and z-direction.

### 2.3.3 Stress

Since the piezoresistors measure stresses on the surface of the beams, it is necessary to consider the limits that can be measured.

#### Measuring principle

As described in section 2.2.1 a p-type, (100) wafer is used, where the piezoresistors are placed in the [110] direction. The piezoresistive coefficient is then given by Equation (2.3).

$$\begin{aligned}\pi_{l,110} &= \frac{1}{2} \cdot (\pi_{11} + \pi_{12} + \pi_{44}) \\ \pi_{t,110} &= \frac{1}{2} \cdot (\pi_{11} + \pi_{12} - \pi_{44})\end{aligned}\tag{2.3}$$

where the  $\pi$  are the piezoresistive coefficients in the different stress directions, due to the crystallographic orientation of the silicon. For the piezoresistive coefficients for p-type silicon a range of values can be found. In this thesis, the values reported by [26] are assumed.

Parameters	Value	Unit
$\pi_{11}$	$6.6 \cdot 10^{-11}$	$\text{Pa}^{-1}$
$\pi_{12}$	$-1.1 \cdot 10^{-11}$	$\text{Pa}^{-1}$
$\pi_{44}$	$138.1 \cdot 10^{-11}$	$\text{Pa}^{-1}$

Table 2.4: Piezoresistive coefficients for p-type silicon by [26].

Using the values shown in Table 2.4 results in a piezoresistive coefficient of  $7.18 \cdot 10^{-10} \text{ Pa}^{-1}$  ( $\pi_{l,110}$ ) and  $-6.66 \cdot 10^{-10} \text{ Pa}^{-1}$  ( $\pi_{t,110}$ ).

The resistivity change is then calculated using the change in local stress, given by:

$$\frac{\Delta R}{R} = (\pi_l \cdot \sigma_l + \pi_t \cdot \sigma_t)\tag{2.4}$$

where  $\sigma_l$  is the stress in the longitudinal direction and  $\sigma_t$  is the stress in the transverse direction. Since the beams are long compared to its deflection, the stress  $\sigma_t$  can be neglected [26].

#### Minimum and maximum detectable stress

The aim in terms of resolution is to develop a sensor which has a minimum detectable force of 10  $\mu\text{N}$  and minimum detectable torque of 2  $\mu\text{Nmm}$ . This is only possible if the stresses that occur (when this minimum detectable force is applied) can be detected. Therefore it is necessary to calculate the minimal detectable stress. The stress that can be measured by one piezoresistor is depending on the voltage noise as well as the input voltage and the piezoresistive coefficient.

When two piezoresistors are placed in a half-active Wheatstone-bridge (see Appendix A.1) the voltage output (which is the difference between the two legs) is given by Equation (2.5). Combining Equation (2.5) and Equation (2.4), results in the minimum detectable stress in Equation (2.6).

$$U_{\text{noise}} = (U_{\text{out } 1} - U_{\text{out } 2}) \approx \frac{1}{2} \frac{\Delta R}{R} U_{cc} \quad (2.5)$$

$$\sigma_{l,110} = \frac{2\sqrt{2} \cdot U_{\text{noise}}}{\pi_{l,110} \cdot U_{cc}} \quad (2.6)$$

Using an input voltage of 1 V and a noise voltage of 10  $\mu\text{V}$  (as observed for a similar setup in previous works by [12]), the calculated minimum detectable stress is 40 kPa. If this stress is not reached within each of the piezoresistors, the force cannot be measured.

The maximum detectable stress is defined by the linearity of the piezoresistors. When considering a single piezoresistor, a piezoresistive change of 10% corresponds to a stress of 140 MPa. However, experiments must verify if the piezoresistive change of 10% is still linear. Other research points out, that resistivity changes up to 16% are known to be linear within 7% of the force range [12].

#### Yield stress

The range of the interaction forces sensor is limited by the yield stress of the silicon and the piezoresistive linearity. The yield stress of silicon is 7 GPa [29], which should be taken into account. Beyond this point, the sensor deforms plastically and therefore it is damaged afterwards. However, the yield stress is higher than the maximum detectable stress and therefore not the limiting factor.

### 2.3.4 Piezoresistor connections

By combining the piezoresistors in a smart way, the output voltage can be maximized (maximum sensitivity) and the forces can be detected independently (minimized crosstalk). It is therefore necessary to consider the piezoresistor layout in more detail.

In order to be able to measure six DOF independently from each other, several piezoresistors must be combined into Wheatstone-bridges (see Appendix A.1). To do this, a strain matrix  $[\epsilon]$  is obtained using COMSOL®, such as given in Equation (2.7).

$$[\varepsilon_{(6 \times n)}] = \begin{bmatrix} \varepsilon_{1,Fx} & \varepsilon_{1,Fy} & \varepsilon_{1,Fz} & \varepsilon_{1,Mx} & \varepsilon_{1,My} & \varepsilon_{1,Mz} \\ \varepsilon_{2,Fx} & \varepsilon_{2,Fy} & \varepsilon_{2,Fz} & \varepsilon_{2,Mx} & \varepsilon_{2,My} & \varepsilon_{2,Mz} \\ \vdots & \vdots & \vdots & \vdots & \vdots & \vdots \\ \varepsilon_{n,Fx} & \varepsilon_{n,Fy} & \varepsilon_{n,Fz} & \varepsilon_{n,Mx} & \varepsilon_{n,My} & \varepsilon_{n,Mz} \end{bmatrix} \quad (2.7)$$

Each of the  $n$  piezoresistors (16 to 20 depending on the concept) changes in value due to the fact that a force is applied. The six different forces and torques are applied one by one and the strain in each piezoresistor is obtained. This results in one column of strains for each force and the six forces combined form the strain-matrix  $[\varepsilon]$ .

The  $6 \times n$  strain-matrix  $[\varepsilon]$  (shown in Equation (2.7)) has to be reduced to a  $6 \times 6$  matrix by performing the calculation shown in Equation (2.8).

$$[S] = [T] \cdot \left( [\varepsilon] \cdot \frac{1}{F} \right) \Rightarrow \quad (2.8)$$

$$\begin{bmatrix} S_{11} & S_{12} & \dots & S_{16} \\ S_{21} & & & \vdots \\ \vdots & & & \vdots \\ S_{61} & \dots & \dots & S_{66} \end{bmatrix} = \begin{bmatrix} T_{Fx,1} & T_{Fx,2} & \dots & T_{Fx,n} \\ T_{Fy,1} & & & \vdots \\ \vdots & & & \vdots \\ T_{Mz,1} & \dots & \dots & T_{Mz,n} \end{bmatrix} \cdot \left( \begin{bmatrix} \varepsilon_{1,Fx} & \varepsilon_{1,Fy} & \dots & \varepsilon_{1,Mz} \\ \varepsilon_{2,Fx} & & & \vdots \\ \vdots & & & \vdots \\ \varepsilon_{n,Fx} & \dots & \dots & \varepsilon_{n,Mz} \end{bmatrix} \cdot \frac{1}{F} \right)$$

The first step is to make the strain-matrix  $[\varepsilon]$  force independent, by dividing the strain-matrix by the force. This ensures that the combination of piezoresistors is always the same, independent from the force that is applied.

The second step is multiplying the matrix  $[\varepsilon/F]$  by a transformation matrix  $[T]$ . Each row in matrix  $[T]$  represents the way the piezoresistors are placed in Wheatstone-bridges, for measuring a single force (row 1 is for measuring  $F_x$ , etc). The matrix  $[T]$  consists of 1, -1 and 0, because each piezoresistor might be added, subtracted or not be used in a Wheatstone-bridge. This matrix  $[T]$  is obtained by using MATLAB®.

By multiplying the matrix  $[\varepsilon/F]$  and the transformation matrix  $[T]$ , it results in a diagonal sensitivity matrix  $[S]$ , which can be used for independent detection of the six forces and torques. This  $[S]$ -matrix relates the forces and torques to the voltages that are measured. The constant  $C$  depends on the number and type of Wheatstone-bridges, the piezoresistive coefficient, Young's modulus and the input voltage (see section 3.2.2). Ideally each voltage output represents only one force. In that case, the  $[S]$ -matrix is perfectly diagonal (Equation (2.9)), meaning that the terms on the diagonal are non-zero, while the terms outside the diagonal are zero.

However, the terms outside the diagonal are not completely zero, due to the fact that the forces cannot be measured completely independent.

$$[U] = C \cdot [S]_{diag} \cdot [F] \Rightarrow \quad (2.9)$$

$$\begin{bmatrix} U_1 \\ U_2 \\ \vdots \\ U_6 \end{bmatrix} = C \cdot \begin{bmatrix} S_{11} & 0 & \dots & 0 \\ 0 & \ddots & & \vdots \\ \vdots & & \ddots & \vdots \\ 0 & \dots & \dots & S_{66} \end{bmatrix} \cdot \begin{bmatrix} F_x \\ F_y \\ \vdots \\ M_z \end{bmatrix}$$

By changing the piezoresistor layout of the Wheatstone-bridges, the matrix  $[T]$  changes and so is the sensitivity matrix  $[S]$ . Even if it is not always possible to find a Wheatstone-bridge layout that

achieves a perfect diagonal sensitivity matrix, the matrix  $[T]$  can be tuned to get as close as possible to that result.

$$[U] = C \cdot [S] \cdot [F] \Rightarrow$$

$$\begin{bmatrix} U_1 \\ U_2 \\ \vdots \\ U_6 \end{bmatrix} = C \cdot \begin{bmatrix} S_{11} & S_{12} & \cdots & S_{16} \\ S_{21} & & & \vdots \\ \vdots & & & \vdots \\ S_{61} & \cdots & \cdots & S_{66} \end{bmatrix} \cdot \begin{bmatrix} F_x \\ F_y \\ \vdots \\ M_z \end{bmatrix} \quad (2.10)$$

Considering Equation (2.10) it can be seen that for each row  $i$ , the term  $S_{i,i}$  needs to be significantly larger than all the other  $S_{i,j}$  in the same row (where  $i \neq j$ ). The relation between the diagonal terms  $S_{i,i}$  and the other terms in the same row is the crosstalk. So the bigger the difference in magnitude between the terms  $S_{i,i}$  and  $\sum S_{i,j}$ , the lower the crosstalk.

However, when combining piezoresistors in order to minimize the crosstalk, they always have to be combined into pairs. This is an important boundary condition, because in this way the piezoresistors can be arranged in Wheatstone-bridges. Since the outcome of a Wheatstone-bridge is not affected by the temperature (in several configurations, see Appendix A.1), this is of great importance.

Finding the optimal piezoresistor layout in terms of crosstalk is about optimizing the matrix  $[T]$ . This matrix is an important parameter to control the performance of the interaction force sensor.

### 2.3.5 Resolution and sensitivity

The resolution of the three concepts depends on the dimensions of the beams and the piezoresistor layout (as defined in section 2.3.4). After the optimization regarding the crosstalk is done, it should be checked if the sensitivity is high enough to be measured (the minimum detectable voltage should be high enough). In order to do this, the sensitivity matrix has to be evaluated including the Wheatstone-bridges that are needed. The first step is to calculate the resistance change according to Equation (2.4), using the minimum detectable stress of 40 kPa and the piezoresistive coefficient of  $7.18 \cdot 10^{-10} \text{ Pa}^{-1}$ . With these values the resistance change is only 0.003%.

When a bias voltage of 1V is applied, the output voltage for a half-active Wheatstone-bridge is 20  $\mu\text{V}$ . For a full-active Wheatstone-bridge, it is 40  $\mu\text{V}$ . As long as these values are higher than the voltage of the noise (roughly 10  $\mu\text{V}$ , see section 2.3.3), it is possible to measure this value.

Combining multiple of these Wheatstone-bridges causes the voltages to add up, increasing the output voltage even more. Each Wheatstone-bridge has a different influence on the total outcome, depending on the stress that is present within the piezoresistors. In the end the output voltage is given by Equations (2.11) (half-active Wheatstone-bridge) and (2.12) (full-active Wheatstone-bridge).

$$U_{H-WB} = \frac{1}{2} \cdot \pi_{l,110} \cdot \sigma_l \cdot U_{cc}$$

$$U_{F-WB} = \pi_{l,110} \cdot \sigma_l \cdot U_{cc} \quad (2.11)$$

$$U_{out} = U_1 + U_2 + U_3 + \cdots \quad (2.12)$$

This output voltage should be higher than the noise introduced by the voltage. In that case the stresses can be measured and the resolution given by the requirements can be reached.

## 2.4 Selection of the concept

The design process described in section 2.3 results in several different sets of dimensions for concept B and C, which all fulfil the requirements reported in section 2.1. The stiffness, sensitivity and crosstalk for each of these sets of dimensions are different and therefore multiple sets of dimensions are evaluated. The performance of each concept is shown in Table 2.5 and based on these results the choice for the final concept is made.



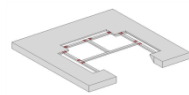
		concept A	concept B			concept C	
							
			set B <sub>1</sub>	set B <sub>2</sub>	set B <sub>3</sub>	set C <sub>1</sub>	set C <sub>2</sub>
Dimensions (μm)	l	1400	1000	1200	1400	1000	1300
	w	100	65	65	65	50	50
	t	30	25	30	35	20	30
Number of piezoresistors		16	16	16	16	20	20
Stiffness (N/m)	x	2133	1889	1367	1032	1703	1212
	y	2425	3160	2288	1722	1275	913
	z	54	59	61	62	61	93
Resolution (μN / μNmm)	F <sub>x</sub>	8.0	6.5	6.0	6.0	5.0	5.5
	F <sub>y</sub>	7.5	7.5	7.5	7.0	4.5	4.5
	F <sub>z</sub>	2.5	1.0	1.5	1.5	2.5	3.0
	M <sub>x</sub>	2.5	1.0	1.5	2.0	2.0	3.0
	M <sub>y</sub>	3.0	1.5	1.5	3.0	3.0	4.0
	M <sub>z</sub>	7.0	10.5	11.0	12.0	5.5	7.5
Sensitivity (N <sup>-1</sup> / (Nmm) <sup>-1</sup> )	F <sub>x</sub>	0.070	0.370	0.368	0.189	0.371	0.297
	F <sub>y</sub>	0.233	0.371	0.146	0.324	0.434	0.470
	F <sub>z</sub>	0.834	1.582	1.364	1.175	2.100	0.623
	M <sub>x</sub>	0.391	0.535	0.683	0.278	2.358	1.011
	M <sub>y</sub>	1.275	0.334	0.672	0.867	1.409	0.777
	M <sub>z</sub>	0.150	0.223	0.186	0.160	0.183	0.210
Crosstalk (%)	F <sub>x</sub>	16.895	10.191	7.597	8.797	4.5586	4.1171
	F <sub>y</sub>	3.974	5.585	10.693	12.924	0.8528	1.8405
	F <sub>z</sub>	1.336	1.088	3.371	2.150	1.6007	1.9457
	M <sub>x</sub>	14.267	3.428	5.439	9.475	1.3815	1.8061
	M <sub>y</sub>	0.673	1.237	1.356	1.522	0.2522	0.7930
	M <sub>z</sub>	9.809	24.916	9.288	14.989	8.3457	11.7723

Table 2.5: Performance of the concepts A, B and C after using the design process.

### Performance of the concepts

The performance of each concept depends on the dimensions of the beams and the piezoresistor configuration. The possibilities shown in Table 2.5 fulfil the requirements. It is difficult to do a quantitative comparison based on the reached performances. The performance in terms of sensitivity and crosstalk not only depends on the dimensions of the beams, but also on the DOF that is considered. Therefore, this table can only be used as a global indication of the performance for each set of dimensions.

The important parameters for the selection of the best concept are the resolution, the sensitivity, the crosstalk, the number of piezoresistors and the accessibility of the gripper. The first three parameters (i.e. the resolution, the sensitivity and the crosstalk) specify the performance of the interaction force sensor. The number of piezoresistors on the other hand, needs to be kept to a minimum, to reduce the number of connections. Furthermore, since the open side of the interaction force device has to be provided with a gripper, the mechanical 'boundaries' of the sensor need to be considered. Therefore, the interaction force sensor must be accessible on the side where the gripper is inserted in order to allow the gripper to perform the tasks.

The stiffness and the overall dimensions of the concepts are taken into account as well, but are considered less important.

### Chosen concept

Concept B is selected as the concept for the interaction force sensor. There are several reasons to support this choice, based on the parameters described before.

The structure of each of the concepts differs in terms of accessibility. Concept A and B have large open regions, making it better accessible when provided with a micro-gripper. Concept C does not have as much space for the gripper to operate as concept A and B and therefore it would have more difficulties performing its tasks.

Furthermore, concept A and B use only 16 piezoresistors, while concept C needs 20 piezoresistors. This results in a better performance of concept C. However, the number of connections of concept C is higher, which requires larger (overall) dimensions of the sensor. Another drawback of using 20 piezoresistors in concept C is that the connection of the piezoresistors is difficult. Since no obvious piezoresistor pairs exist, the arrangement of piezoresistors in half and full-active Wheatstone-bridges is more complicated. This is due to the complicated stress distribution in concept C.

The comparison of the performance of the different concepts shows that the performance of concept A is not as good as concept B, while concept C has a slightly better performance. For instance, the crosstalk of concept A is high in the  $F_x$ ,  $M_x$  and  $M_z$  direction, while the crosstalk of concept C is below 10% (except for one direction). The crosstalk of concept B is reasonable, however, depending on the dimensions of the beams. Furthermore, if the resolution is compared, it can be seen that the resolution of concept C is more uniform in every DOF. The resolution of concept B is better in the  $F_z$ ,  $M_x$  and  $M_y$  direction, but the resolution of concept A is slightly less compared to the resolution of concept B and C. The comparison of the sensitivity shows similar results, where the sensitivity of concept A is slightly less compared to the sensitivity of concept B and C.

Overall, concept B has a good performance in terms of crosstalk, sensitivity and resolution, without any extreme values like concept A. Although the performance of concept C is slightly better, concept B is preferred because it has only 16 piezoresistors that form logical pairs to be arranged in Wheatstone-bridges. Furthermore, accessibility of concept B is better

The different sets of dimensions of concept B have different performances as well. It is decided to choose concept B with dimensions  $1200 \times 65 \times 30 \mu\text{m}^3$  as the best concept for the interaction force sensor. The reason for this, is that the crosstalk is slightly better when the thickness is  $30 \mu\text{m}$ . Furthermore, when the interaction force sensor has a thickness of  $30 \mu\text{m}$  the micro-gripper developed by [12] can be integrated for validation of the interaction force sensor.

The proposed interaction force sensor is further analyzed in Chapter 3. The mechanical, electrical and thermal properties of the interaction force sensor are discussed and the influence of a micro-gripper is evaluated.

# Interaction force sensor design

In this chapter the selected concept from the previous chapter is evaluated. The mechanical structure is further improved and its thermal and electrical performance is analyzed. This final design is obtained using the structure shown in Figure 3.1.

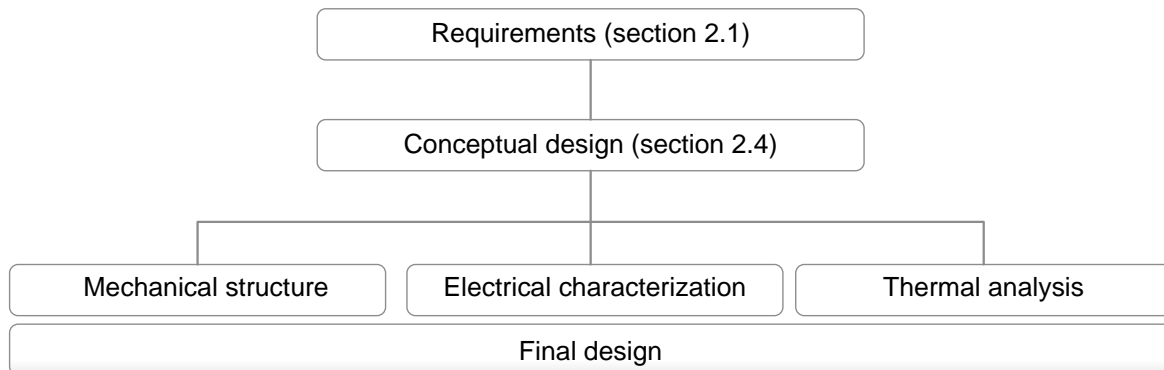


*Figure 3.1: Steps followed to design the interaction force sensor (Chapter 3).*

The final design is shown in Figure 3.2 (with dimensions in Table 3.1), which has several modifications compared to the design shown in Chapter 2 due to additional considerations. These considerations (regarding the mechanical structure, electrical connections and temperature influences) are further explained in the next sections.

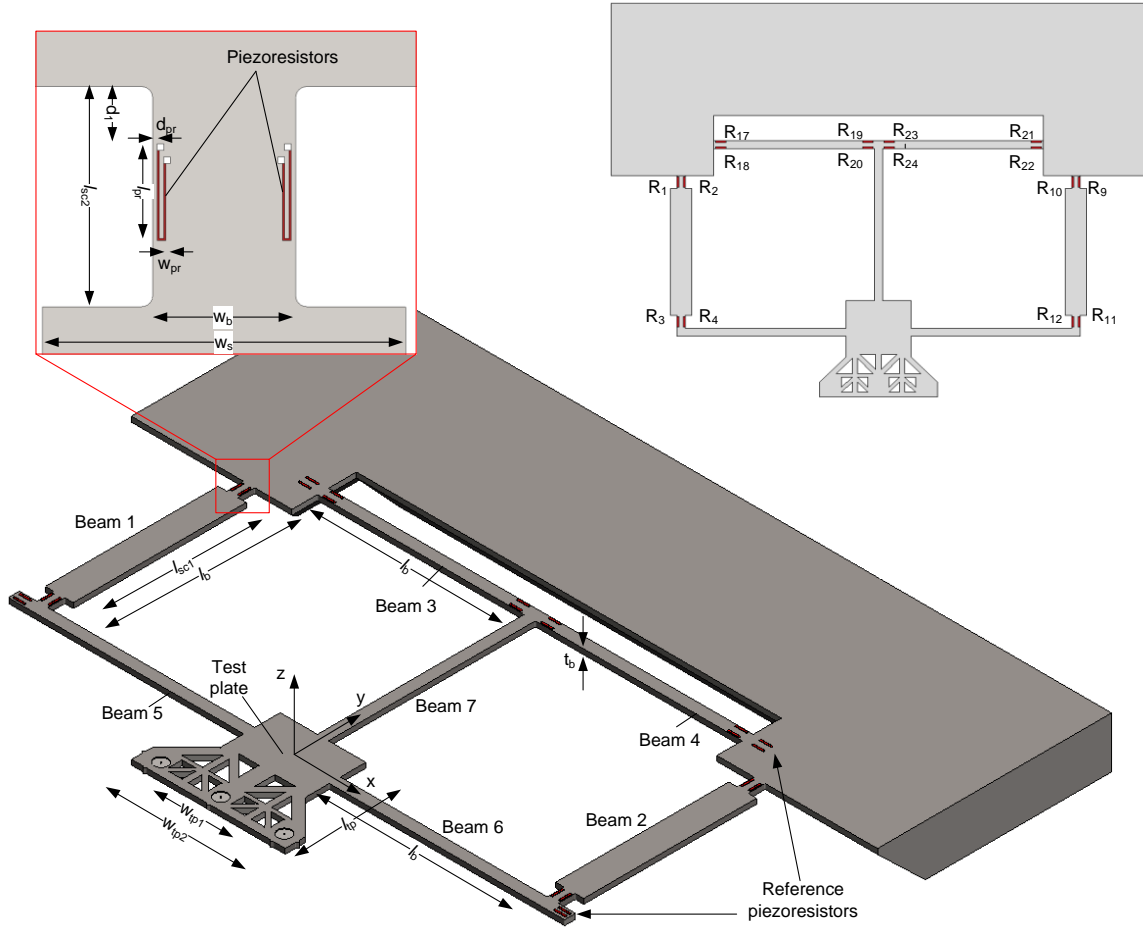


Figure 3.2: Final layout of the interaction force sensor, with dimensions and piezoresistor positions.

Parameter	Symbol	Value
Length of beam	$l_b$	1220 $\mu\text{m}$
Width of beam	$w_b$	65 $\mu\text{m}$
Thickness of beam	$t_b$	30 $\mu\text{m}$
Length of stress concentration (1)	$l_{sc1}$	1020 $\mu\text{m}$
Length of stress concentration (2)	$l_{sc2}$	100 $\mu\text{m}$
Width of stress concentration	$w_s$	165 $\mu\text{m}$
Length of piezoresistor (overall)	$l_{pr,o}$	80 $\mu\text{m}$
Length of piezoresistor	$l_{pr}$	40 $\mu\text{m}$
Width of piezoresistor	$w_{pr}$	1 $\mu\text{m}$
Distance between piezoresistor and edge	$d_{pr}$	2 $\mu\text{m}$
Distance between piezoresistor and bulk (beam 1 and 2)	$d_1$	35 $\mu\text{m}$
Distance between piezoresistor and bulk (beam 3 and 4)	$d_2$	50 $\mu\text{m}$
Width of the test plate (1)	$w_{tp1}$	500 $\mu\text{m}$
Width of the test plate (2)	$w_{tp2}$	900 $\mu\text{m}$
Length of the test plate	$l_{tp}$	700 $\mu\text{m}$

Table 3.1: Dimensions of the final design.

### 3.1 Mechanical structure

In the final structure a test plate can be seen as well as two beams with increased width (beams 1 and 2 in Figure 3.2). The reasons for these modifications are explained in the following two sections (3.1.1 and 3.1.2).

In Table 3.2 the mechanical properties of the interaction force sensor are given. These values belong to the structure shown in Figure 3.2.

Parameter	Value	Unit
<b>Stiffness (x-direction)</b>	1930.5	N/m
<b>Stiffness (y-direction)</b>	2419.1	N/m
<b>Stiffness (z-direction)</b>	59.6	N/m
<b>Mass (including test plate)</b>	76	µg
<b>1<sup>st</sup> resonant frequency (z-direction)</b>	4456.5	Hz

Table 3.2: Mechanical properties of the interaction force sensor.

#### 3.1.1 Test plate

To test the performance of the interaction force sensor in measuring the six DOF independently, it is important to apply precise forces in precise locations. A test plate is introduced (Figure 3.3) to be able to apply these forces. A calibrated force probe is used to apply the forces and validate the sensor experimentally (see Chapter 5).

In the analysis in Chapter 2 the forces and torques are applied at the “black dot” location. However, in reality the forces and torques are applied at the tip of the gripper. Applying a single force at the test plate, results in a combination of forces and torques at the centre of the interaction force sensor (the “black dot” location). The forces and the locations where they are applied can be seen in Figure 3.3.

During testing a mix of forces is present within the centre point of the interaction force sensor. This relation (between the applied force at a certain location of the test plate and the forces/torques present in the centre point of the sensor) is given by the matrix shown in Equation (3.1). To separate the forces from each other it is essential that this matrix is invertible.

$$\begin{bmatrix} F_x \\ F_y \\ F_z \\ M_x \\ M_y \\ M_z \end{bmatrix} = \begin{bmatrix} 0 & 0 & 0 & 1 & 0 & 0 \\ 0 & 0 & 0 & 0 & 1 & 1 \\ -1 & -1 & -1 & 0 & 0 & 0 \\ 0 & -l_y & -l_x & 0 & 0 & 0 \\ 0 & 0 & -l_x & 0 & 0 & 0 \\ 0 & 0 & 0 & l_y & 0 & l_x \end{bmatrix} \cdot \begin{bmatrix} F_1 \\ F_2 \\ F_3 \\ F_4 \\ F_5 \\ F_6 \end{bmatrix} \quad (3.1)$$

Since the matrix in Equation (3.1) is invertible, it can be used for translating the measured forces at the centre point of the interaction force sensor, to the actual forces acting on the sensing plate.

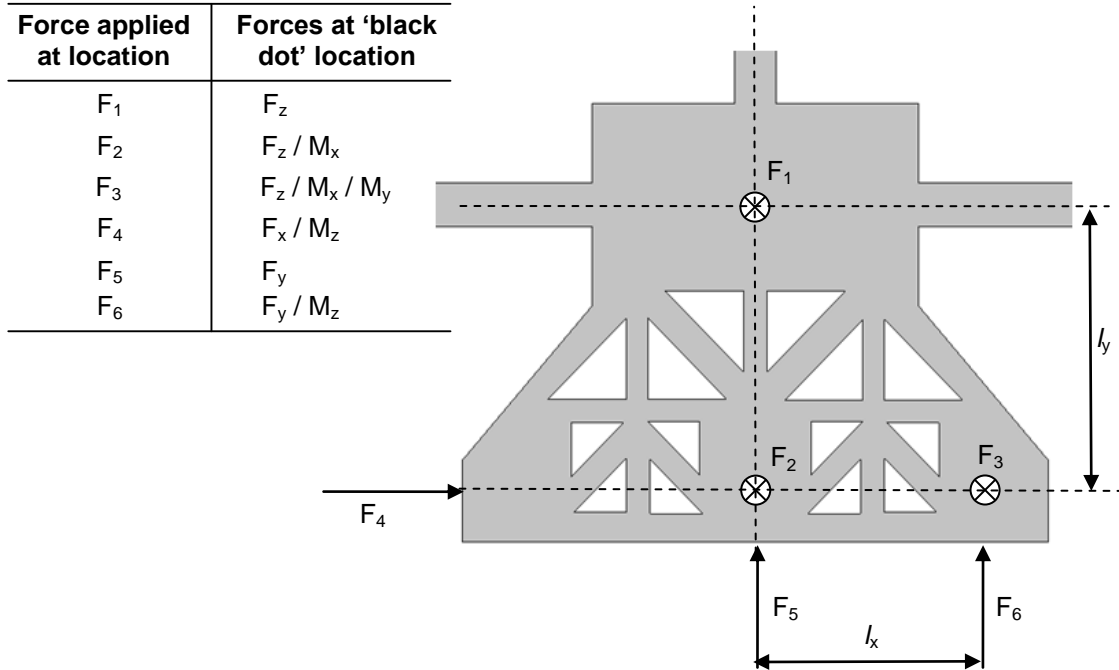


Figure 3.3: Test plate for applying the forces during experimentation.

Verification of this translation is only possible when the exact position of the applied force is known. However, the tip of the force probe is square, introducing uncertainties in the position of the applied force. To know the exact location of the applied force, two solutions are introduced to ensure that there is a point contact between the force probe and the test plate:

- Two types of mechanical structures are introduced, to provide a contact point between the force probe and the test plate (see section 4.1).
- The force probe is placed on a goniometer (an angular stage) to tilt the force probe. Then the test plate can be approached with one edge (or one point, if double tilted) of the force probe (see section 5.1.1).

### 3.1.2 Stress analysis

To improve the performance of the interaction force sensor, further optimization is needed in terms of stress. This results in better sensitivity and resolution as well as a lower crosstalk. Improving the stress is done, by improving the stress distribution and the piezoresistor positioning.

#### Stress concentration beams

Changing the shape of the beams has influence on the stresses as well as the stiffness of the interaction force sensor. In Figure 3.2 it can be seen that two beams in the interaction force sensor have a different width compared to the other beams. This is the result of the analysis done with COMSOL®. The performance of the sensor (in terms of sensitivity, crosstalk and stiffness) is evaluated, while considering different shapes, sizes and the number of beams with stress concentration.

Usually in stress concentration beams, the stresses are increased by decreasing the cross-section of the beams. However in the interaction force sensor, there is still a minimum width to be considered (see section 2.3.1). Therefore, the width of other parts of the beam (where no piezoresistors are placed) can be increased.

The changing of the width of the beams has two important advantages:

- The stress concentration beams has influence on the performance of the sensor. Due to the introduction of stress concentration beams the distribution of the force over the beams changes and therefore the stress distribution. A different stress distribution means (minor) changes in the piezoresistor layout, which improves the sensitivity and crosstalk.
- The stiffness of the sensor is increased by increasing the width of the stress concentration beams. Therefore the positioning accuracy of the interaction force sensor is improved.

### Piezoresistor positioning

For further optimization of the interaction force sensor, it is essential to look at the stresses inside the beams. This information is used for optimizing the position of the piezoresistors.

It can be seen in Appendix B that the stresses in the proximity of the sharp (but rounded) corners are not linear. It is therefore essential to place the piezoresistors away from these corners to avoid any non linear influences and other stress components.

The stress distribution along the sensing beams is used to find the optimal position for the piezoresistors. In Appendix B the stresses along the sensing beams can be seen, when different forces are applied. It is clear that the stresses in the 'stress concentration regions' are much higher than in the other part of the beam. Furthermore, the influence of the corners on the stress is evident, which can be seen due to the peaks near the corners. In order to reduce these influences, the length of the stress concentration beams is carefully chosen. In addition to that, the piezoresistors are positioned in the middle of this part to reduce the corner influences even more.

## 3.2 Electrical characterization

To evaluate the performance of the interaction force sensor in terms of resolution, range, sensitivity and crosstalk, the same computation is done as is explained in Chapter 2. However, several modifications (as discussed in section 3.1) are introduced to the mechanical structure and furthermore the piezoresistor configuration is considered. In Table 3.3 the performance of the interaction force sensor can be seen.

	$F_x$	$F_y$	$F_z$	$M_x$	$M_y$	$M_z$
<b>Minimum detectable force (<math>\mu\text{N}</math> and <math>\mu\text{Nmm}</math>)</b>	4.0	8.5	1.5	2.5	2.0	10.5
<b>Force range (mN and mNmm)</b>	14.5	30.5	4.0	4.5	7.0	37.5
<b>Sensitivity (V/N and V/Nmm)</b>	11.3	8.0	51.8	23.9	30.8	5.9
<b>Crosstalk (%)</b>	3.2	2.7	1.4	2.8	0.9	4.7

Table 3.3: Interaction force sensor performance.

	Wheatstone-bridges					
	$F_x$	$F_y$	$F_z$	$M_x$	$M_y$	$M_z$
$R_1$	$WB_{Fx,1}$	$-WB_{Fy,1}$	$WB_{Fz,1}$		$WB_{My,1}$	
$R_2$	$-WB_{Fx,1}$	$WB_{Fy,1}$	$WB_{Fz,1}$		$WB_{My,1}$	
$R_3$			$WB_{Fz,2}$	$WB_{Mx,1}$	$-WB_{My,2}$	$WB_{Mz,1}$
$R_4$			$WB_{Fz,2}$	$WB_{Mx,1}$	$-WB_{My,2}$	$WB_{Mz,1}$
$R_9$	$-WB_{Fx,1}$	$-WB_{Fy,1}$	$WB_{Fz,3}$		$-WB_{My,1}$	
$R_{10}$	$WB_{Fx,1}$	$WB_{Fy,1}$	$WB_{Fz,3}$		$-WB_{My,1}$	
$R_{11}$			$WB_{Fz,4}$	$WB_{Mx,2}$	$WB_{My,2}$	$-WB_{Mz,1}$
$R_{12}$			$WB_{Fz,4}$	$WB_{Mx,2}$	$WB_{My,2}$	$WB_{Mz,1}$
$R_{17}$		$-WB_{Fy,2}$	$WB_{Fz,5}$	$-WB_{Mx,3}$		$WB_{Mz,2}$
$R_{18}$		$WB_{Fy,2}$	$WB_{Fz,5}$	$-WB_{Mx,3}$		$-WB_{Mz,2}$
$R_{19}$	$-WB_{Fx,2}$	$WB_{Fy,3}$	$-WB_{Fz,5}$		$-WB_{My,3}$	$-WB_{Mz,3}$
$R_{20}$	$WB_{Fx,2}$	$-WB_{Fy,3}$	$-WB_{Fz,5}$		$-WB_{My,3}$	$WB_{Mz,3}$
$R_{21}$	$-WB_{Fx,3}$	$-WB_{Fy,2}$	$WB_{Fz,6}$	$-WB_{Mx,4}$		$-WB_{Mz,2}$
$R_{22}$	$WB_{Fx,3}$	$WB_{Fy,2}$	$WB_{Fz,6}$	$-WB_{Mx,4}$		$WB_{Mz,2}$
$R_{23}$		$WB_{Fy,3}$	$-WB_{Fz,6}$		$WB_{My,3}$	$WB_{Mz,3}$
$R_{24}$		$-WB_{Fy,3}$	$-WB_{Fz,6}$		$WB_{My,3}$	$-WB_{Mz,3}$

Table 3.4: Representation of the 22 independent Wheatstone-bridges used for measuring a certain force. Each Wheatstone-bridge has a different colour and name.

	Stress (Pa)					
	$F_x$	$F_y$	$F_z$	$M_x$	$M_y$	$M_z$
$R_1$	1.385.939	- 75.915	5.234.756	4.479.121	3.137.528	-204.252
$R_2$	- 1.361.206	55.890	5.204.028	4.461.120	3.136.479	168.933
$R_3$	-426.899	490.402	723.629	2.200.547	- 499.466	532.296
$R_4$	429.596	-500.562	712.135	2.262.162	- 533.377	- 554.767
$R_9$	- 1.382.683	- 75.959	5.227.582	4.475.159	- 3.137.163	203.868
$R_{10}$	1.358.868	56.149	5.210.348	4.462.025	- 3.137.584	-168.575
$R_{11}$	427.617	490.528	688.284	2.180.966	505.018	- 532.622
$R_{12}$	-429.913	-501.407	672.557	2.242.458	540.308	555.176
$R_{17}$	130.381	-666.842	599.179	- 1.102.583	364.853	103.482
$R_{18}$	-118.752	662.881	627.673	- 1.095.530	365.975	- 88.992
$R_{19}$	-273.001	664.400	-582.355	1.078.034	- 770.590	- 208.989
$R_{20}$	275.650	- 662.019	-623.812	1.089.243	- 813.084	216.855
$R_{21}$	-130.779	- 667.580	617.813	- 1.096.473	-364.270	- 103.337
$R_{22}$	118.857	662.531	627.607	- 1.097.014	-367.061	88.282
$R_{23}$	272.592	664.759	- 553.110	1.083.565	773.916	208.228
$R_{24}$	-277.115	- 661.507	- 617.800	1.081.664	806.102	- 217.166

Table 3.5: Average stresses within the piezoresistors when  $F = 100 \mu\text{N}$  or  $M = 100 \mu\text{Nmm}$  is applied. The logical pairs can be seen in combination with the Wheatstone-bridges in Table 3.4.

### 3.2.1 Piezoresistor layout

For measuring each force, several different full and half-active Wheatstone bridges are necessary. Table 3.6 indicates how many piezoresistors are needed for measuring a certain force including the number of Wheatstone-bridges needed for doing this.

	$F_x$	$F_y$	$F_z$	$M_x$	$M_y$	$M_z$
<b>Number of piezoresistors used</b>	8	12	16	8	12	12
<b>Number of half-active bridges</b>	2	0	4	4	0	0
<b>Number of full active bridges</b>	1	3	2	0	3	3

Table 3.6: Number of Wheatstone bridges which are used.

The way the piezoresistors are placed in Wheatstone-bridges, is defined by the matrix [T] (see section 2.3.4). The [T] matrix has to be interpreted in terms of (logical) Wheatstone-bridges and connection diagrams. Only the connections with symmetrical piezoresistors and equal (compressive and/or tensile) stresses are considered.

In Table 3.4 the Wheatstone-bridges used for measuring a certain force can be seen. Each Wheatstone-bridge is represented by a different colour and name. The colours correspond to the electrical schemes shown in Appendix B, which also shows the position of the piezoresistors. Table 3.4 has to be considered column by column, since this specifies the Wheatstone-bridges necessary for measuring a certain force or torque. For measuring  $F_x$  for instance, it is necessary to look at the first column of the table, etc.

In Table 3.5 the stresses within the piezoresistors can be seen when a force of 100  $\mu\text{N}$  or a torque of 100  $\mu\text{Nmm}$  is applied. Gray and strikethrough values are not being used for measuring a certain force. Combining this information with Table 3.4 shows the logical pairs. Moreover, it can be seen how the Wheatstone-bridges cancels out the stresses caused by other forces/torques, when evaluated row by row.

Each piezoresistor takes part in measuring more than one component of force or torque in different configurations. This means that each piezoresistor is part of different full and/or half-active Wheatstone-bridges. Therefore, switching systems are needed to arrange the different piezoresistors in the different bridges. Even if simultaneous measurement is not possible, a switching frequency of 50 kHz is reached (the switching speed of the Crosspoint Switch Array, see section 5.1.2) and then the six components of force can be measured many times per second.

### 3.2.2 Sensitivity and crosstalk

The sensitivity matrix of the interaction force sensor is given in Matrix (3.2), which follows from the strain-matrix [ε] (see section 2.3.4).

$$[S] = \begin{bmatrix} \mathbf{0.3700} & 0.0003 & -0.0005 & 0.0007 & -0.0026 & -0.0075 \\ -0.0002 & \mathbf{0.3280} & 0.0067 & -0.0014 & 0.0003 & -0.0000 \\ 0.0001 & -0.0020 & \mathbf{1.3482} & 0.0157 & -0.0007 & 0.0001 \\ 0.0000 & -0.0007 & 0.0200 & \mathbf{0.7810} & 0.0007 & 0.0000 \\ -0.0021 & -0.0000 & -0.0029 & -0.0023 & \mathbf{1.0463} & -0.0025 \\ -0.0069 & -0.0000 & 0.0016 & 0.0005 & -0.0004 & \mathbf{0.2006} \end{bmatrix} \quad (3.2)$$

The sensitivity matrix  $[S]$  is very useful since the voltage outcome follows directly from the matrix. It has therefore to be multiplied by the piezoresistive coefficient  $\pi_{l,110}$ , the input voltage  $V_{cc}$ , the modulus of elasticity  $E$  and a factor for the Wheatstone-bridges (see Equation (3.3)). The factor of 0.25 is due to the presence of the Wheatstone-bridges. The voltage output of a Wheatstone-bridge (see Appendix A.1) depends on the number of sensing resistors. A factor of 0.5 is introduced in a half-active and a factor 1 for a full-active Wheatstone-bridge. By comparing the factors of all the Wheatstone-bridges combined, to the number of piezoresistors used for constructing matrix  $[T]$  (see section 2.3.4), it turns out that the matrix  $[S]$  is off by a factor of four and therefore the factor 0.25 is introduced.

$$\begin{bmatrix} U_{F_x} \\ U_{F_y} \\ U_{F_z} \\ U_{M_x} \\ U_{M_y} \\ U_{M_z} \end{bmatrix} = \frac{1}{4} \cdot \pi_{l,110} \cdot U_{cc} \cdot E \cdot [S] \cdot \begin{bmatrix} F_x \\ F_y \\ F_z \\ M_x \\ M_y \\ M_z \end{bmatrix} \quad (3.3)$$

Using the voltage outcome and the applied force, the sensitivity of the device can be calculated using Equation (3.4).

$$Sensitivity = \frac{U_{out}}{F} = \frac{1}{4} \cdot \pi_{l,110} \cdot U_{cc} \cdot E \cdot [S] \quad (3.4)$$

The graphical representation of the sensitivity can be seen in Figure 3.4, where the force-voltage relation is shown. The slope of the graph represents the sensitivity.

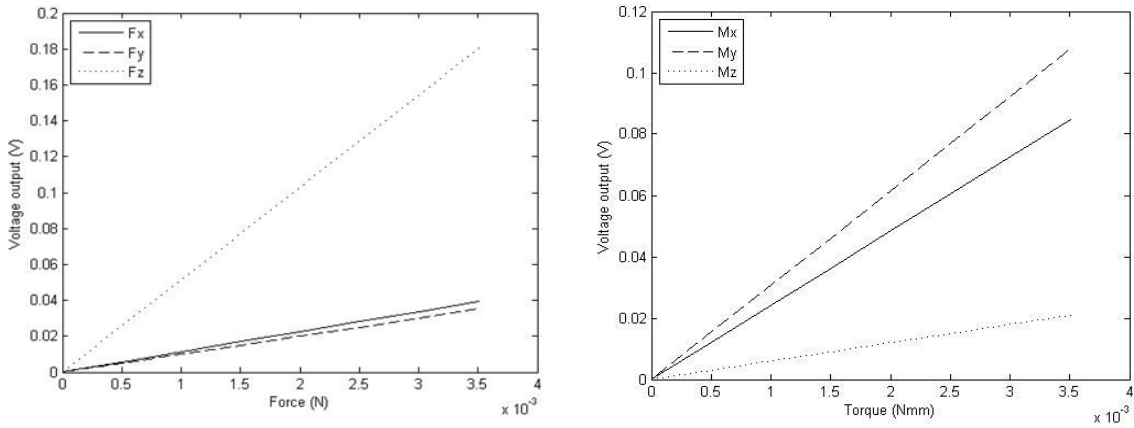


Figure 3.4: Force/torque input vs. Voltage output.

For obtaining the crosstalk an identical computation is done as explained in section 2.3.4. The crosstalk that is present within the interaction force sensor is given by Equation (3.5). Considering Matrix (3.2), the crosstalk in each row  $i$ , is determined by the term  $S_{i,i}$  (on the diagonal) that needs to be significantly larger than all the other  $S_{i,j}$  (outside the diagonal) in the same row (where  $i \neq j$ ).

$$\text{Crosstalk (row } i) = \frac{S_{i,i}}{\sum_{j=1}^6 S_{i,j} - S_{i,i}} \quad (3.5)$$

The crosstalk of the interaction force sensor is shown in Table 3.3.

### 3.2.3 Electrical noise

The two dominant factors of noise for piezoresistive cantilevers are the thermal noise (Johnson noise) and 1/f noise (see Figure 3.5 by [30]). The thermal noise comes from thermal agitation of the charge carriers. It is a 'white noise' which is independent from the applied voltage (power spectral density independent from the frequency), but only depending on the resistivity and the temperature.

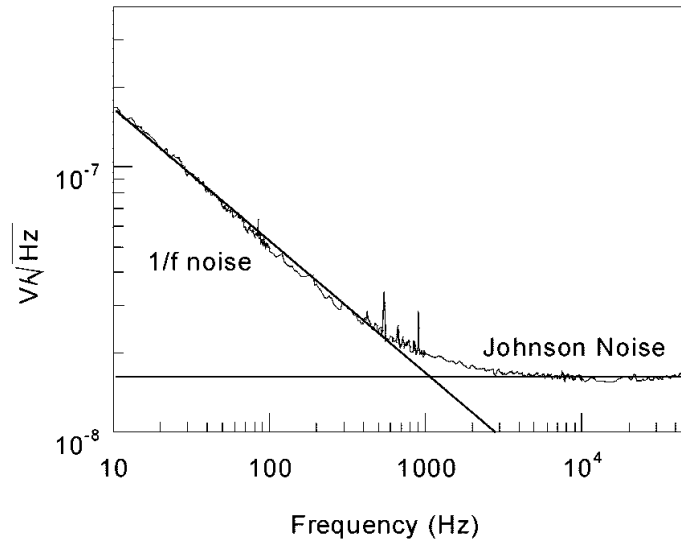


Figure 3.5: Sources of noise in piezoresistive cantilevers [30].

The power spectral density (units  $[V^2/\text{Hz}]$ ) of the thermal noise is given by Equation (3.6), where  $k_B$  is the Boltzmann constant.

$$S_T = 4 \cdot k_B \cdot T \cdot R \quad (3.6)$$

The 1/f noise on the other hand becomes lower at increasing frequency. The cause of this noise is not well understood and still an active area of research. The 1/f noise is given by Equation (3.7).

$$S_f = \frac{\alpha \cdot U_{in}^2}{c_i \cdot l_{pr} \cdot w_{pr} \cdot t_{pr} \cdot f} \quad (3.7)$$

where,  $f$  is the frequency,  $c_i$  the charge carrier density and  $\alpha$  a dimensionless constant ([31]).

In the case of the interaction force sensor, the piezoresistors are mounted in Wheatstone-bridges. The total noise of a Wheatstone-bridge is the sum of the noise of four piezoresistors. For the total voltage noise, the spectrum needs to be integrated across the bandwidth of interest ( $f_{\min}$ ,  $f_{\max}$ ). Equation (3.8) shows the electrical noise of a Wheatstone-bridge.

$$U_{noise} = 2 \cdot \sqrt{4k_B T R (f_{\max} - f_{\min}) + \frac{\alpha U_{in}^2}{c_i l_{pr} w_{pr} t_{pr} f} \cdot \ln\left(\frac{f_{\max}}{f_{\min}}\right)} \quad (3.8)$$

Depending on the specifications (size piezoresistor, doping concentration, bandwidth, temperature and input voltage), the noise voltage is usually in the range of tens of  $\mu V$ . If a full-active Wheatstone-bridge is used, the voltage noise is the same. However the measured signal is twice as high, causing the signal to noise ratio (SNR) to increase with a factor two as well.

Using multiple Wheatstone-bridges causes the voltage noise to add up. However, since the signal adds up as well, the signal to noise ratio changes according to the output signal of the Wheatstone-bridge.

### 3.3 Thermal analysis

The influence of an increasing temperature on the performance of the interaction force sensor has to be investigated. Therefore, the micro-gripper (developed by [12]) is integrated in the interaction force sensor to validate the performance of the interaction force sensor. When this micro-gripper is inserted, three sources of heat can be distinguished within the interaction force sensor:

- Heat generation in the piezoresistors
- Heat generation in the wires for the actuator
- Heat generation in the thermal actuators of the gripper

The performance of the interaction force sensor is affected by the increasing temperature inside the sensor. This effect can be split up into:

- Piezoresistor temperature dependency
  - The changing piezoresistive coefficient ( $\pi_{l,110}$ )
  - The resistivity change due to the temperature coefficient of resistance (TCR)
- Thermal expansion of the sensor

In section 3.3.1 the three sources of heat generation are considered and the influence of each source on the total heat generation is investigated. Then the influence on the performance is considered in section 3.3.2, which is focused on the piezoresistive coefficient and the resistivity change. Finally in section 3.3.3 the thermal expansion of the interaction force sensor is considered and the influence on the performance is investigated.

### 3.3.1 Heating of the interaction force sensor

#### Heat generation in the piezoresistors

Considering the zero-stress resistivity in Equation (3.9) which is given by [26], the power consumption in a piezoresistor can be calculated using Joule's law combined with Ohm's law.

$$\frac{1}{R_0} = \int_0^{t_{pr}} \frac{w_{pr}}{l_{pr} \cdot \rho(t)} dt \quad (3.9)$$

Using a doping-dependant electrical resistivity ( $\rho(t)$ ), the zero-stress resistivity is estimated to be 50 k $\Omega$ . With a supply voltage of 1V, this results in a heat generation of 0.02 mW for one single piezoresistor. This heat generation is limited and since the heat generation is the same in every piezoresistor, this heat generation does not have to be taken into account.

#### Heat generation in the wires for the actuator

The wires connecting the gripper to the computer generate are heated as well. Especially the wires on the beams of the interaction force sensor increase in temperature due to the small cross-section of these wires. The resistance of these wires is (roughly) 330  $\Omega$  per wire (compared to 205  $\Omega$  for the aluminum heater in the gripper). This means that the heat generation in the each wire is 150 mW. This is large, however, the influence of this heat generation is not significant in the thermal analysis, since the heat is distributed evenly over the beam and the heat dissipation is large.

#### Heat generation in the thermal actuators of the gripper

The gripper selected to be integrated in the interaction force sensor, uses 120 mW of power for closing the gripper tip completely. The maximum working temperature is about 450 K [12]. In the original gripper the actuators are separated from the rest of the device with a trench for insulation. However in the new configuration this is not possible, due to the electrical connections. The actuators are not isolated and therefore the temperature influence is bigger than the original configuration.

Three types of temperature transfer exist: radiation, convection and conduction. Heat loss caused by conduction is the most dominant type of heat loss. As long as the temperature is below 500 K, the heat loss due to radiation and convection can be neglected in electrothermal gripper calculations [32].

A 3D model is build with COMSOL® (including surrounding air) to see the influence of the actuator heating with a temperature of 450K. The 3D model can be seen in Figure 3.6 and the thermal profile of each sensing beam in Figure 3.7. The model a simplified version of the developed gripper, and the heat transfer through different layers (SU-8, Aluminum and Silicon) is not taken into account. Therefore a maximum temperature of 450 K is applied (instead of a heating of 120 mW), since this temperature is needed to close the gripper. For this calculation a constant bulk temperature is assumed as well as constant material properties at room temperature. The silicon bulk structure is assumed to have a temperature of 293.15 K at the edges. As mentioned, the convection and radiation are neglected.

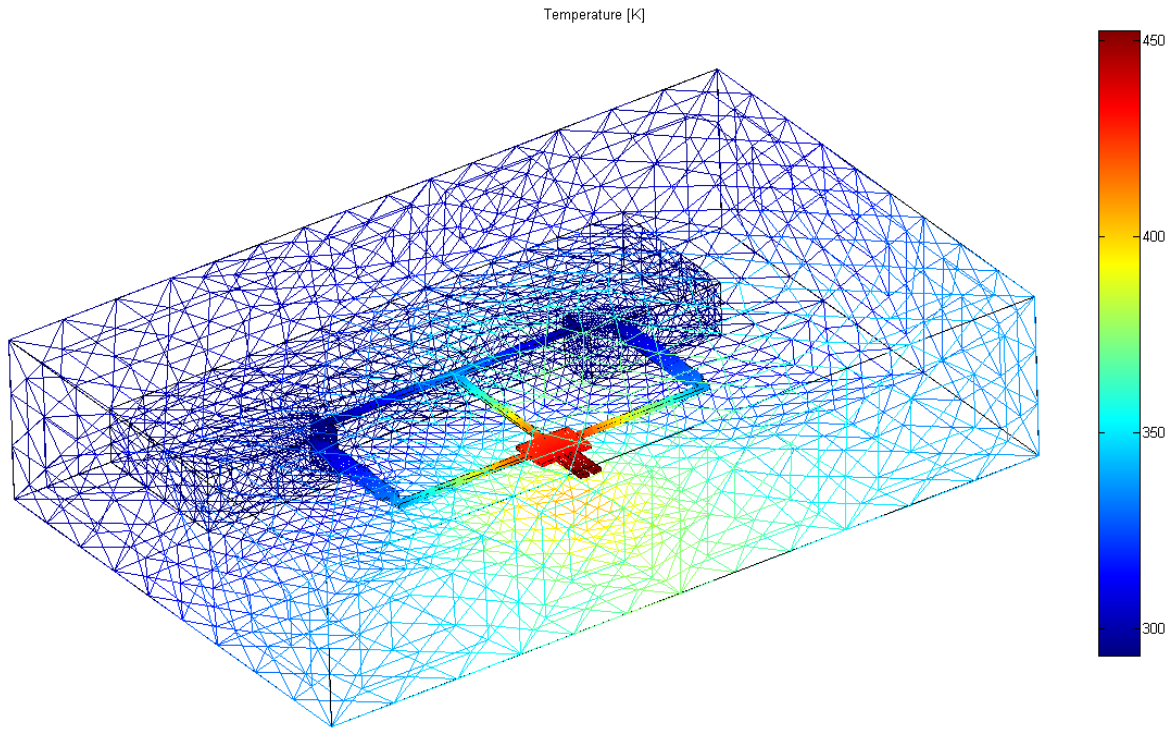


Figure 3.6: 3D thermal model of the interaction force sensor modelled with air.

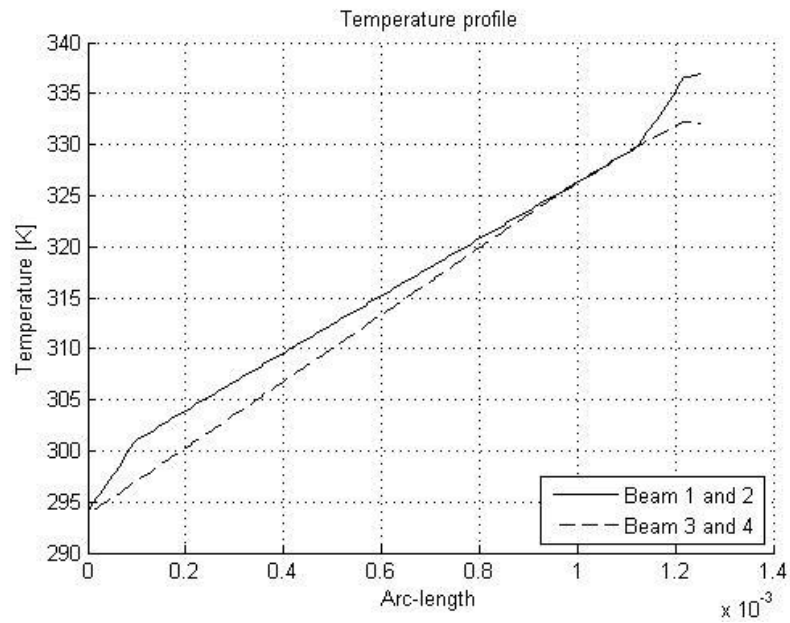


Figure 3.7: Thermal profile across the sensing beams when the gripper temperature is 450 K.

### 3.3.2 Piezoresistor temperature dependency

#### Piezoresistive coefficient ( $\pi_{l,110}$ )

A change in the piezoresistive coefficient ( $\pi_{l,110}$ ) directly influences the piezoresistivity change according to Equation (2.4). From Table 2.4 it can be seen that  $\pi_{44}$  dominates the piezoresistive coefficient in this case. In [33] the temperature dependence of  $\pi_{44}$  is investigated and it is found that the piezoresistive coefficient changes in the range from  $2.6 - 4.9e^{-13} \text{ Pa}^{-1} \cdot ^\circ\text{C}^{-1}$ . This means a piezoresistive coefficient ( $\pi_{l,110}$ ) changes 0.04% per degree and that the output voltage changes with 0.04% per degree as well. This can in most cases be neglected.

#### Resistivity change due to the temperature coefficient of resistance

The temperature coefficient of resistance (TCR) changes the resistivity of the piezoresistor. This relation is given by Equation (3.10), where  $\alpha_{Si}$  is the TCR of silicon.

$$R = R_{ref} \cdot (1 + \alpha_{Si} \cdot (T - T_{ref}))$$

$$\frac{\Delta R}{R} = \alpha_{Si} \cdot \Delta T_{res} \quad (3.10)$$

The resistance of the piezoresistor changes 0.13% per degree, which is significant considering that resistivity changes up to 10% are linear (see section 2.3.3).

By placing the piezoresistors in a Wheatstone-bridge, the temperature influence can be reduced (see Appendix A.1). However, it is essential to place all the piezoresistors (including the reference piezoresistors) close to each other to eliminate temperature differences between the piezoresistors. The position of the reference piezoresistors can be seen in Figure 3.2.

The temperature influence is compensated in the Wheatstone-bridges in measuring most of the forces. However, the influence of the temperature on the voltage output affects the  $F_z$  and  $M_x$  measurement. This is caused by the (minor) temperature differences between the sensing piezoresistors and reference piezoresistors. The temperature dependency of a Wheatstone bridge is given by Equation (3.11), where  $\Delta T_1$  and  $\Delta T_2$  are the temperature differences (between the piezoresistor and the environment) of respectively the sensing piezoresistors and the reference piezoresistors.

$$U_{out, WB} = \frac{1}{4}(\alpha_{Si} \cdot (2\Delta T_1 - 2\Delta T_2)) \cdot U_{cc} \quad (3.11)$$

If a gripper temperature is 450 K, the difference between the sensing piezoresistors and the reference piezoresistors is 3 K. This results in a voltage output of 1.95 mV for a single Wheatstone-bridge. Considering that for measuring  $F_z$  and  $M_x$  four half-active Wheatstone-bridges are needed with uncompensated temperature dependency, this results in a total voltage output of 7.8 mV due to the increasing temperature. The same voltage output is reached when the interaction force sensor is loaded with 150  $\mu\text{N}$  and 325  $\mu\text{Nmm}$ .

To reduce this influence, the temperature difference should be minimized. This could be done by positioning the piezoresistors closer together or to reduce the temperature of the interaction

force sensor in general such that the temperature difference is decreased (several solutions are proposed in section 3.3.3).

### 3.3.3 Thermal-structural interaction

The increasing temperature in the interaction force sensor also results in a deflection of the mechanical structure of the device. Consequently, stresses are introduced in the piezoresistors of the interaction force sensor. With a gripper that has a temperature of 450 K, the expansion of beams 5, 6 and 7 is  $0.35\text{ }\mu\text{m}$ , while the expansion of beams 1 – 4 is around  $0.07\text{ }\mu\text{m}$ .

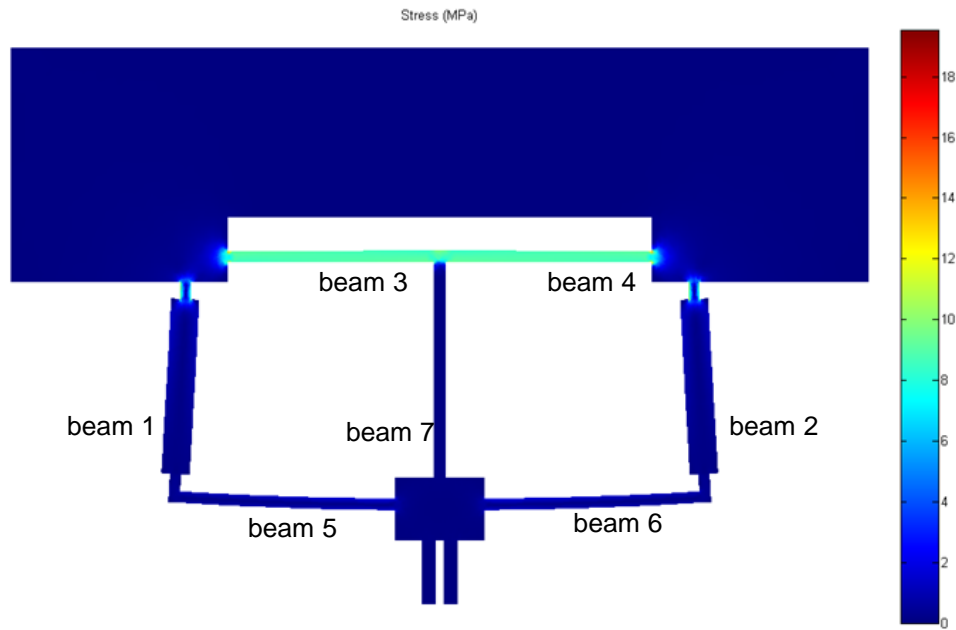


Figure 3.8: Stresses in the interaction force sensor caused by the heating of the gripper (including beam number). The expansion of the device can be seen as well.

FEM simulations with COMSOL® confirm these values. In Figure 3.8 the stresses in the interaction force device, due to the thermal expansion can be seen. Since these stresses are not uniformly distributed through the interaction force sensor, they introduce additional stresses in the piezoresistors which influences the performance of the sensor. The influence of the thermal expansion on the performance of the interaction force sensor depends on the temperature of the sensor. In Appendix B, the force-temperature-voltage relation can be seen.

Heating of the sensor results in a voltage output. This voltage must be overcome to measure a force and therefore the resolution increases. The influence on the resolution is investigated by analyzing a gripper with a temperature of 450 K. The output voltage, belonging to this temperature, is shown in Table 3.7, as well as the resolution belonging to this output voltage.

The crosstalk is influenced by the temperature as well, since the Wheatstone-bridges are affected by the stresses caused by the thermal expansion. Since the stress distribution is not

uniform across the interaction force sensor, the Wheatstone-bridges do not cancel out the other stress components anymore. Therefore a high crosstalk is present within the interaction force sensor when heated.

	$F_x$	$F_y$	$F_z$	$M_x$	$M_y$	$M_z$
<b>V<sub>out</sub> (mV)</b>	-0.198	7.916	2.226	6.780	0.006	-0.086
<b>Resolution (<math>\mu</math>N and <math>\mu</math>Nmm)</b>	17	800	44	275	0.2	14
<b>Crosstalk (%)</b>	130.8	450.5	607.3	366.8	2.9	98.9

Table 3.7: Voltage output belonging to the force at gripper temperature is 450K.

Decreasing the temperature in the interaction force sensor decreases the effects on the performance. Therefore, several options need to be examined in order to reduce these thermal influences. Possible solutions for reducing the problem due to thermal heating are:

- **Use of another gripper.** The gripper that is taken in consideration in this thesis is based on thermal actuation. By inserting a gripper which uses another actuation principle, the temperature influence can be reduced, since the temperature in such a gripper is significantly lower.
- **Inserting heat fins or heat sinks.** By additional large volumes (plates) or inserting fins, the heat dissipation is increased. However, this only applies when a micro-gripper without thermal actuation is considered. In thermal micro-grippers the temperature in the gripper has to remain the same for closing the gripper. If more heat is dissipated, more power has to be added to the gripper to reach this temperature.
- **Thermal insulation.** By adding thermal insulations such as a small part of SU-8 between the test plate and the beams, the gripper can be isolated from the interaction force sensor. However, this decreases the stiffness of the interaction force sensor, resulting in high displacements of the gripper tip when a force is applied. These large displacements have a negative impact on the position accuracy and the force range of the sensor.
- **Change the piezoresistor connections.** By rearranging the piezoresistor connections the influence of the thermal expansion can be reduced. However, this results in a higher crosstalk and a lower resolution when unheated.
- **Actively compensate for the temperature.** As shown in Equation (3.10), the temperature influences the resistivity of the piezoresistors. By measuring the piezoresistor change with the piezoresistors used for the grasping force measurement, the temperature profile is known through the sensor (since the temperature distribution through the interaction force sensor is always the same). Compensation for these thermal influences can be done using software compensation.

None of the solutions described before solves this problem completely. However, a combination of the proposed solutions reduces the influence of the thermal expansion.



---

## CHAPTER 4

# Fabrication

The fabrication techniques used for the production of the interaction force sensor, are described in this chapter. In particular the fabrication issues and the fabrication flowchart are analyzed.

### 4.1 Fabrication issues

The interaction force sensor is fabricated with silicon based technologies. These techniques allow the production of multiple devices on a single wafer. Since the standard dimensions of a die are  $15 \times 15 \text{ mm}^2$ , and the interaction force sensor is only  $7.5 \times 5 \text{ mm}^2$  (global outside dimensions, including bondpads), other structures are inserted in the wafer. These structures can be seen in Appendix C.

#### **Interaction force sensor structure**

In the design of the masks for the fabrication of the interaction force sensor, many design considerations are taken into account. The characteristics of the fabrication process adds extra design constraints to those considered in section 2.3.1 (wiring width for instance). All of these design limitations are included in the final mask design shown in Appendix C.

During fabrication heat is generated during the Deep Reactive Ion Etching process (DRIE, see section 4.2). The generated heat needs to be removed in order to prevent the interaction force sensor from overheating (and therefore damaging). To dissipate the heat during fabrication, two heat sinks are included in the design of the interaction force sensor (see Figure 4.1).

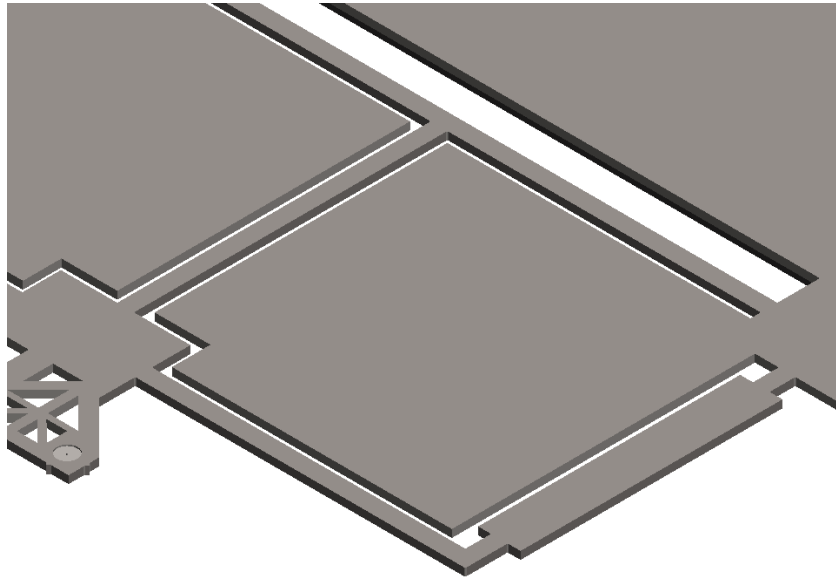


*Figure 4.1: Heat sinks are included in the design of the interaction force sensor to improve the heat dissipation during DRIE etching.*

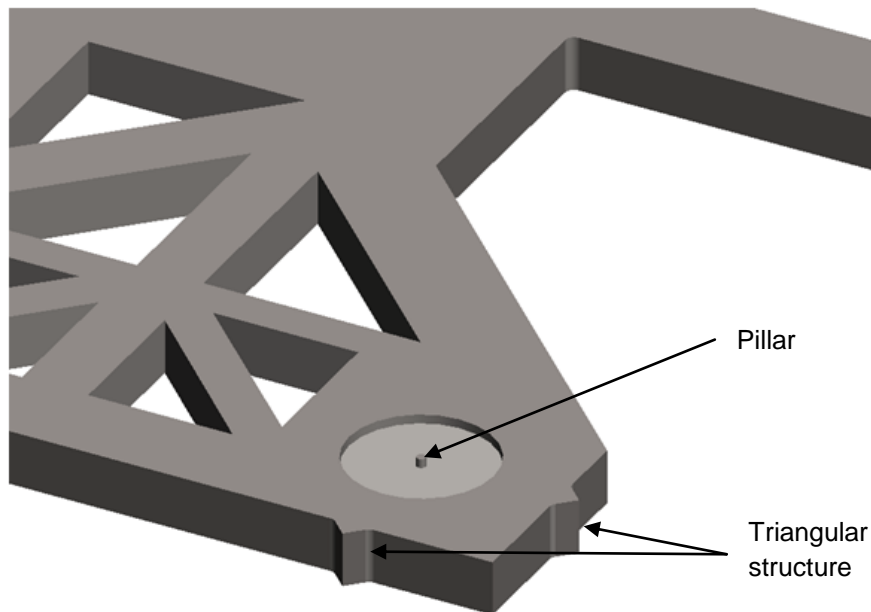


*Figure 4.2: Part of the test plate with some solutions to minimize the contact area between the force probe and the test plate.*

These heat sinks do not influence the performance of the interaction force sensor, since they are not in contact with the sensor beams. Actually, they could act as mechanical stops to prevent overloading of the interaction force sensor.

Avoiding long dicing lines is another constraint to take into account to reduce the risk of wafer breaking. Actually, after the KOH etching (see section 4.2) the wafer becomes very fragile due to the large the opening windows of the interaction force sensor (see Appendix C). The wafer tends to break along the dicing lines (fabricated with DRIE etching) due to the crystal structure of silicon. Thus, by interrupting long dicing lines the risk of losing and damaging the interaction force sensor is reduced.

### Test plate

As discussed in section 3.1.1, the forces applied by the force probe need to occur in a defined position. In order to ensure that this position is accurately defined, two mechanical solutions are included in the fabrication process:

- On the side of the test plate, five triangle structures are included (in Figure 4.2, two of them are shown). This ensures that the applied force is exactly on that line. However, the position of the applied force in the vertical direction cannot be specified and therefore the applied force can be maximum 15  $\mu\text{m}$  off.
- On the top, a pillar is included by etching some of the surrounding silicon, to ensure the force is applied on this area (see Figure 4.2). Since the contact point is on this pillar, the position uncertainty is 2.5  $\mu\text{m}$  maximum (the diameter of the pillar is actually 5  $\mu\text{m}$ ).

## 4.2 Fabrication process

The fabrication of the interaction force sensor consists of two parts: the surface micro-machining and the bulk micro-machining. The flowchart of the fabrication process is shown in Figure 4.3.

### Surface micromachining

The interaction force sensor is fabricated on a (100), p-type silicon wafer one which p-type silicon piezoresistors are integrated (on the (100) plane in the [110] direction).

The 525  $\mu\text{m}$  thick silicon substrate is provided with an n-type epitaxy layer of 1  $\mu\text{m}$ . The piezoresistors are formed using a second epitaxy layer, which is a 500 nm thick, boron doped layer with a doping concentration of  $1.0\text{e}^{18}$  ions/ $\text{cm}^3$ . By using epitaxial growth, a uniformly doped layer is formed, resulting in resistors with a high dimensional accuracy. Plasma etching is then used to define the dimensions of the piezoresistors (Figure 4.3a).

The piezoresistors are isolated from the substrate by the 1  $\mu\text{m}$  thick, n-type epitaxy layer. Isolation rings formed with ion-implantation (using boron with a dose of  $5.0\text{e}^{15}$  ions/ $\text{cm}^2$ , 180 keV), isolates the piezoresistors from each other (Figure 4.3b).

The contact pads for the substrate are realized by ion-implantation of phosphor (n-implantation with a dose of  $5.0\text{e}^{15}$  ions/ $\text{cm}^2$ , 180 keV), while the contact pads for the resistors is done using boron implantation with a dose of  $3.0\text{e}^{15}$  ions/ $\text{cm}^2$  with an energy of 15 keV.

Next a silicon nitride layer is deposited and patterned on both the front and the back side (Figure 4.3c). This acts as an electrical insulation layer for the piezoresistors and is at the same time the opening window for the KOH etching (on the back side). After opening of the contact holes, a 675 nm aluminum layer is sputtered and patterned for the interconnections.

### Bulk micro-machining

After opening the bondpads, the bulk machining of the interaction force sensor (and the micro-gripper) can be started. To form the structure the first process is a wet etching process on the back side of the wafer, which is used to define the thickness of the interaction force sensor (Figure 4.3d). The anisotropic etchant KOH, is used, so that a thickness of 30  $\mu\text{m}$  can be easily defined by the (111) crystal plane of silicon. From now on the wafer is fragile since the bulk silicon is removed in many places.

To support the formed structures, an aluminum layer is sputtered on the back. After this, the structure of the interaction force sensor is defined by deep reactive ion etching (DRIE), which takes place from the front side of the wafer (Figure 4.3e). By adding a DRIE step to fabricate the pillar for the test plate (5  $\mu\text{m}$  deep) the proposed structure is finished (Figure 4.3f). The final step is the removal of the aluminum layer on the back; after that the interaction force sensor is ready to test.

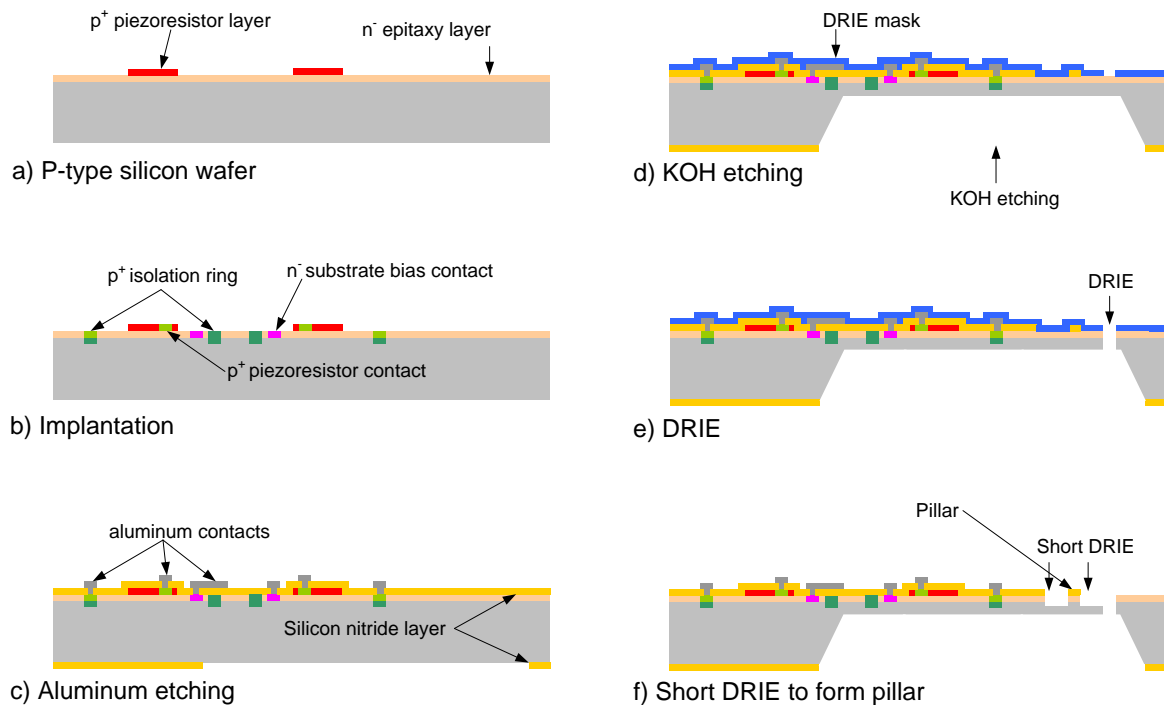


Figure 4.3: Flowchart of the fabrication process of the interaction force sensor.

# Experimental validation

In this chapter the experimental setup and the approach for the experimental validation of the interaction force sensor are described.

## 5.1 Experimental setup

In this section, the experimental setup is discussed. It is split up into two parts: the mechanical layout of the experimental setup and the electrical connections used for data acquisition.

### 5.1.1 Experimental layout

The experimental setup is shown in Figure 5.1. The measurement setup is placed on a vibration isolation table, to prevent disturbances from the floor movement.

On top of this table, a three DOF micro-positioning stage is placed. The micro-positioning stage is used for coarse positioning of the interaction force sensor. The range of this coarse positioning stage is 20 mm with a resolution of 5  $\mu\text{m}$ . On top of the positioning stage, a printed circuit board (PCB) is placed, which is connected to the interaction force sensor.

The applied force is controlled with a force probe, placed on another (fine) micro-positioner (with a range of 20  $\mu\text{m}$  and a resolution of 50 nm). The force probe is capable of applying forces with a resolution of 0.4  $\mu\text{N}$  at a frequency of 30 Hz (or 2  $\mu\text{N}$  at a frequency of 1000 Hz). Due the large tip surface of the force probe (50 x 50  $\mu\text{m}$ ), it is necessary to tilt the force probe to ensure there is a point contact between the force probe and the test plate (see section 3.1.1). Therefore, a

goniometer (an angular stage) is used, which introduces an angle of a few degrees. The accuracy of the goniometer is relatively low. However, if the force probe is tilted with an angle of  $1^\circ$ , the error of the applied force is 0.02%.

The force probe is brought into contact with the test plate using at first the course positioning stage and later on a fine positioning stage for applying a well calibrated force. An optical microscope is used for monitoring this operation. The mechanical structures as described in section 4.1 are introduced for fine definition of the force application point.

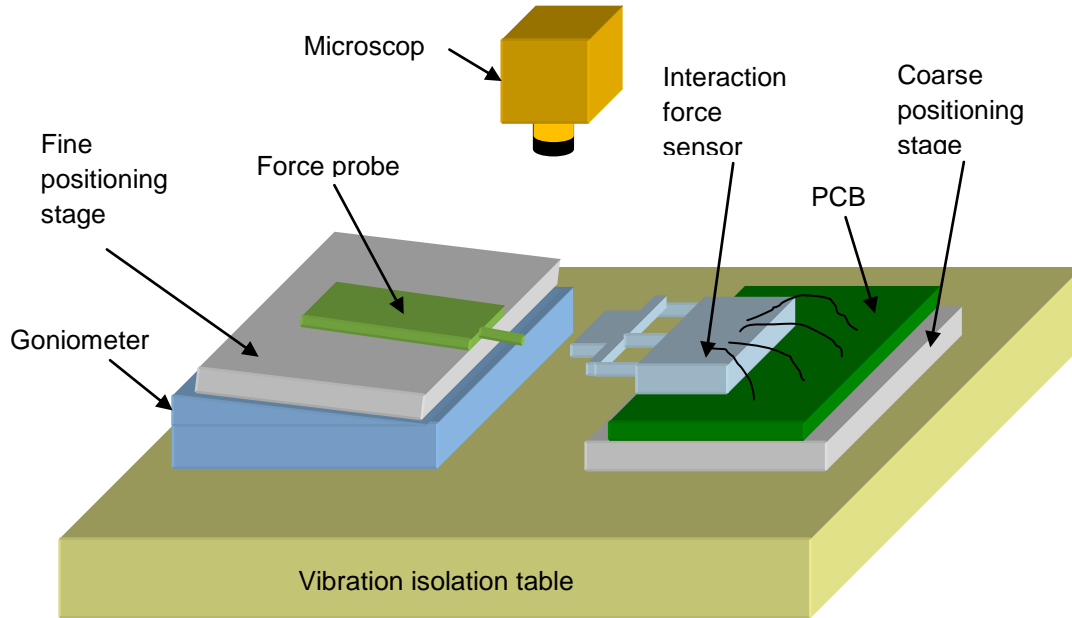


Figure 5.1: Experimental layout.

### 5.1.2 Data acquisition

The output of the Wheatstone-bridges must be conditioned, filtered and amplified, therefore a Lock-In Amplifier (LIA) is used. In Figure 5.2a the readout circuit of a single Wheatstone-bridge can be seen, which is connected to the LIA.

In the case of the interaction force sensor (as explained in section 3.2), each piezoresistor needs to be used in different positions of different Wheatstone-bridges, for the measurement of each force/torque. Moreover, each of these bridges requires to be amplified by a LIA, which is expensive. Thus, a Crosspoint Switch Array (CSA) is used in order to dynamically reconfigure the piezoresistors into a single Wheatstone-bridge, which is read out by the LIA (each bridges independently). This principle is shown in Figure 5.2b.

The CSA is an array which connects multiple wires together by means of field effect transistors (an electric field controlling the conductivity of a channel). Multiple, simultaneous connections are possible, however, only one Wheatstone-bridge at a time can be measured since this is the limit for the LIA.

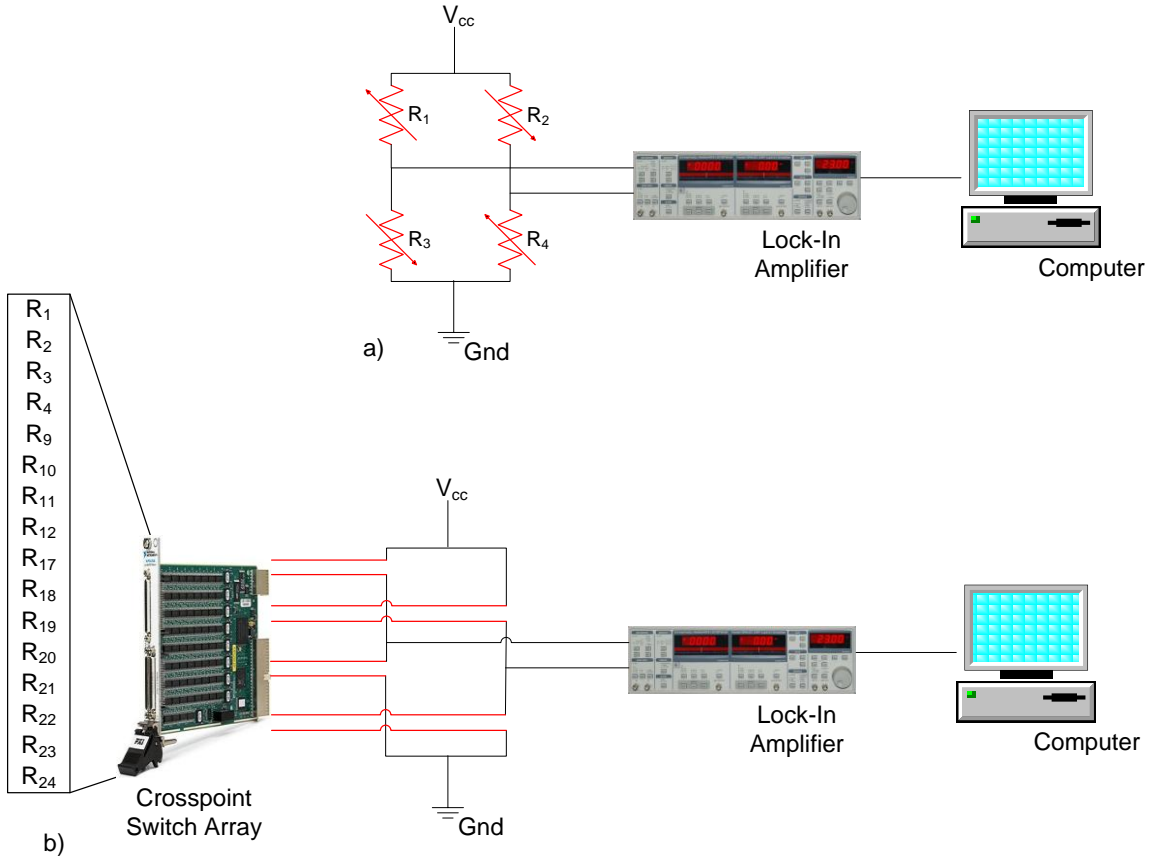


Figure 5.2: Wheatstone-bridge measuring a single bridge (a) or multiple bridges using a Crosspoint Switch Array (b).

The interaction force sensor can be read out using the circuit as shown in Figure 5.3. To connect the interaction force sensor to the acquisition boards and the computer, it needs to be connected to a printed circuit board (PCB). This connection is done by hand, using wire-bonding.

The PCB is then connected to several different devices. On the PCB the connections are split into two parts: the wires for the piezoresistors (for measuring of the interaction force and the grasping force) and the wires for the actuation of the gripper, the power supply and the grounding. This distinction is made since the wires for measuring the forces need to be connected to the CSA, while the other wires are connected to the computer immediately.

The CSA is then connected to the Lock-In Amplifier and the computer. The computer controls the CSA, specifying the active switches. It is also used for the actuation of the gripper and for signal readout of the Wheatstone-bridges.

The measuring frequency depends on the switching of the CSA, the number of Wheatstone-bridges and the settling time of the LIA. The CSA is capable of switching with a frequency of 50 kHz. With 22 different Wheatstone-bridges to be measured and a settling time of 10 msec, a measuring frequency of 20 Hz is achieved.

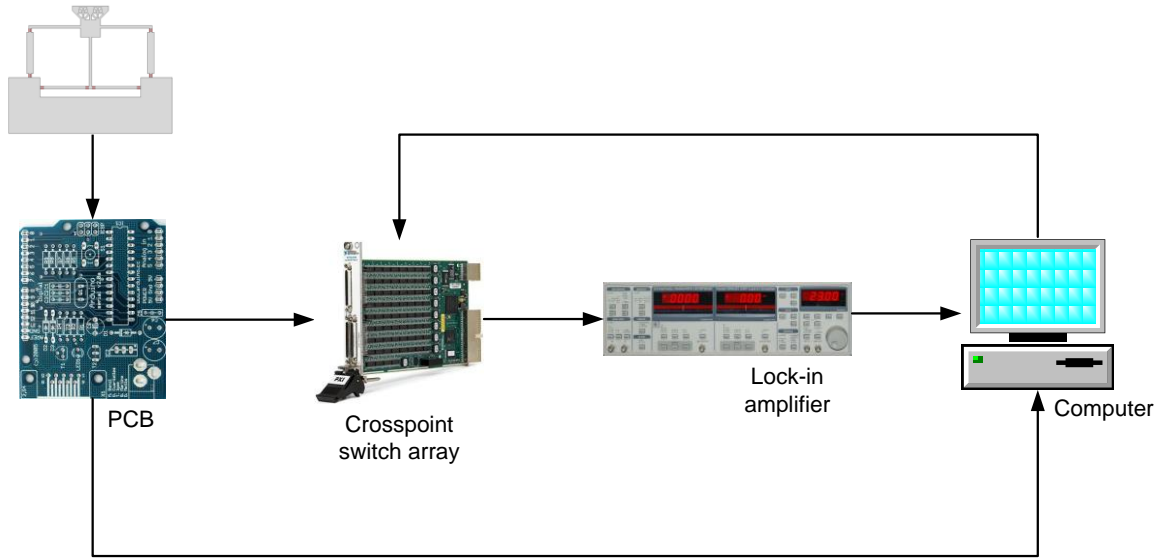


Figure 5.3: Electrical connection of the measurement setup.

## 5.2 Experimental approach

The experiments that need to be carried out, include testing with several different structures. Basic piezoresistors, the interaction force sensor with test plate and the interaction force sensor with integrated gripper need to be tested. The experiments can be divided into several different parts: First the basic mechanical and electric properties of the system must be tested. These parameters are then used to adjust the model of the sensor. Then the following set of experiments is carried out in order to validate its low frequency performance in terms of sensitivity, noise, resolution, range, temperature dependency, etc. As a next step some dynamic parameters of the sensor are tested. Finally, the functional test of the interaction force sensor with integrated gripper is carried out.

The main goal of the experiments is to test the capability of the interaction force sensor to detect the six DOF independently and validate the theoretical performance. The experiments that need to be carried out:

### 1. Basic performance of the piezoresistors.

- *Piezoresistive coefficient:* The piezoresistive coefficient is used for the theoretical performance estimation and therefore verification of the assumed piezoresistive coefficient is needed. For measuring the piezoresistive coefficient, a simple beam structure is used. This structure is easily modelled and therefore the piezoresistive coefficients are easily determined.
- *Zero-stress resistance:* The zero-stress resistances are measured directly on the piezoresistors on the simple beam structure under zero load.

## 2. Validation of the performance of the interaction force sensor.

- *Resonant frequency/stiffness measurement:* By specifying a displacement of the interaction force sensor (with the fine positioning stage) and measuring the force with the force probe, the stiffness of the sensor can be determined. Other stiffnesses of the measurement setup should be considered as well. The stiffness can be used for finding the resonant frequency of the interaction force sensor.
- *Measuring the output voltages when unloaded.* The output voltage needs to be measured when no force is applied in order to determine the pre-stress in the interaction force sensor. During the actual measurement this pre-stress can be compensated.
- *Sensitivity matrix:* By applying the six different forces ( $F_1 - F_6$ , see section 3.1.1), the output voltage is measured. After transforming the applied force to the 'centre point' force, the sensitivity matrix is retrieved. From this matrix the sensitivity and the crosstalk can be calculated (see section 3.2.2).
- *Minimum detectable force:* The minimum detectable stress (which is related to the minimum detectable force) is defined by the voltage noise, the piezoresistive coefficient and the input voltage (see section 2.3.3). The performance in terms of resolution is verified in this way.
- *Force – voltage dependency:* Although the sensitivity matrix is an (indirect) indication for the sensitivity of the interaction force sensor, it need to be verified by applying a range of forces. The output voltage belonging to the applied force, gives the force – voltage relation.
- *Sensor linearity:* The piezoresistor sensor linearity defines the force and torque range of the interaction force sensor (see Section 2.3.3). Resistivity changes up to 16% are known to be linear within 7% of the force range.
- *Temperature dependency of the interaction force sensor:* As described in section 3.3 the temperature increase due to the actuation of the gripper, influences the performance of the interaction force sensor. It must be investigated what the influence on the performance (in terms of resolution and crosstalk) is, due to an increasing temperature.
- *Reliability analysis:* The lifetime of the interaction force sensor can be investigated by repeatable cycles of applying forces, after which the performance is evaluated.

## 3. Testing of the dynamic parameters of the interaction force sensor.

- *Transfer function:* To know the way the interaction force sensor reacts when a force is applied, it is necessary to obtain the transfer function. The transfer function of the interaction force sensor defines the cut-off frequency. This indicates the operational bandwidth of the sensor. For measuring the transfer function, the force probe is used for a frequency sweep after which the voltage gain is measured.
- *Damping:* By applying a step response to the interaction force sensor, the damping can be estimated. This defines the settling time of the interaction force sensor (the time required for the response to reach and stay within 2% of its final value).

4. **Functional tests of the interaction force sensor.**

- *Force on object analysis:* By applying a force to a grasped object, the forces present in the interaction force sensor can be measured. Measurements are carried out to verify if the applied force is the same as the measured force.
- *Micro-assembly:* As a final experiment, several benchmark tests are carried out. By inserting pegs in holes, rings on pillars or aligning parts, the forces during these tasks are investigated.

# Conclusions and recommendations

## 6.1 Conclusions

In this work a novel interaction force sensor is designed and developed, in which a micro-gripper can be easily integrated. The device can be used for applications in micro-manipulation, cell handling and minimally invasive surgery.

The mechanical and electrical layout of the sensor is obtained by using a design process to improve the performance of the interaction force sensor. The influence of the investigated parameters is analyzed and, based on these results, the different concepts are evaluated and compared.

The final design of the interaction force sensor is fabricated by means of integrated circuit (IC) technology and has a dimension of  $3 \times 1.5 \times 0.03 \text{ mm}^3$ . The device is capable of measuring six DOF independently, using 16 silicon integrated piezoresistors arranged in different Wheatstone-bridges.

The performance of the interaction force sensor fulfils the requirements for assembly and manipulation tasks within the micro-handling domain. Finite element models (FEM) show that sensor should be able to reach resolutions between  $1.5 - 8.5 \text{ }\mu\text{N}$  and  $2 - 10.5 \text{ }\mu\text{Nmm}$ , for respectively force and torque measurement. The range of the interaction force sensor is from 0 up to 30 mN and 37 mNmm. The crosstalk between the different forces/torques does not exceed 4.7% and sensitivities between  $8 - 51.8 \text{ V/N}$  and  $5.9 - 31.8 \text{ V/Nmm}$  could be reached. The modelled sensor has a stiffness of 59.6 N/m, resulting in a first resonant frequency of 4456.5 Hz.

The integration of a micro-gripper (realized with IC processes) in the interaction force sensor can be easily done. However, the heat generation of the gripper influences the performance of the interaction force sensor in terms of crosstalk and resolution.

## **6.2 Recommendations for further work**

In future research, some aspects of the interaction force sensor have to be further addressed. The theoretical performance of the interaction force sensor needs to be experimentally validated and optimized.

Heat generation of the integrated micro-gripper influences the performance of the interaction force sensor. These temperature influences need to be examined carefully. Rearrangement of the piezoresistors and active compensation for the heating expansion might be a good solution to reduce the thermal influence on the performance of the interaction force sensor device. Micro-grippers based on other actuation principles (such as the electrostatic, the piezoelectric or the capacitive principle) should be considered to reduce the thermal effect.

## Piezoresistor connection

### A.1 Wheatstone-bridge

To arrange the piezoresistors in a Wheatstone-bridge there are two possibilities. A full-active or a half-active Wheatstone-bridge can be used (see Figure A.1). Depending on the type of bridge, two or four piezoresistors are needed. Only piezoresistors with the same stress (positive or negative) can be used, which means that they must be placed symmetrically.

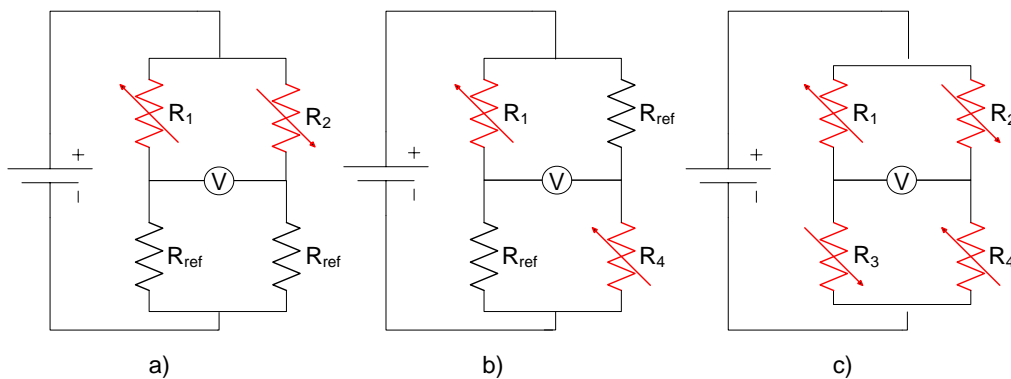


Figure A.1: Possible Wheatstone-bridges where a) and b) are half-active and c) is a full active Wheatstone-bridge.

#### Stresses

Figure A.1a) and b) are both half-active Wheatstone-bridges. In Figure A.1a the stresses are opposite in sign (one is a compressive stress and the other one is a tensile stress), while in Figure A.1b the stresses are similar (both compressive or both tensile stresses). Therefore, it is essential

that  $R_1$  and  $R_2$  (or  $R_1$  and  $R_4$  in Figure A.1b) are symmetrically placed, such that the stresses in these resistors are similar in size (but may be opposite in sign). In that case Equation (A.1) applies.

Two reference piezoresistors ( $R_{ref}$ ) are needed to complete the bridge. These reference resistors are placed as close as possible to the sensing piezoresistors to minimize temperature differences.

$$\begin{aligned} U_{out} &= \frac{1}{4} \left( \frac{\Delta R_1}{R_1} - \frac{\Delta R_{ref}}{R_{ref}} + \frac{\Delta R_{ref}}{R_{ref}} - \frac{\Delta R_2}{R_2} \right) U_{cc} \approx \frac{1}{2} \frac{\Delta R}{R} U_{cc} \\ U_{out} &= \frac{1}{4} \left( \frac{\Delta R_1}{R_1} - \frac{\Delta R_{ref}}{R_{ref}} + \frac{\Delta R_4}{R_4} - \frac{\Delta R_{ref}}{R_{ref}} \right) U_{cc} \approx \frac{1}{2} \frac{\Delta R}{R} U_{cc} \end{aligned} \quad (A.1)$$

When four piezoresistors are placed in a Wheatstone-bridge,  $R_1 - R_4$  are all sensing piezoresistors. These four piezoresistor should all be placed in such a way that the stresses are symmetrical and negative (so  $R_1 = R_4 = -R_2 = -R_3$ ). The voltage output is then given by Equation (A.2) [34].

$$U_{out} = \frac{1}{4} \left( \frac{\Delta R_1}{R_1} - \frac{\Delta R_3}{R_3} + \frac{\Delta R_4}{R_4} - \frac{\Delta R_2}{R_2} \right) U_{cc} \approx \frac{\Delta R}{R} U_{cc} \quad (A.2)$$

When  $R_1 - R_4$  all change in the exact same way (size and sign), it is not possible to place them in Wheatstone-bridges.

### Temperature dependency

To decrease the temperature dependency of a Wheatstone-bridge due to the temperature coefficient of resistance (TCR), it is necessary that the piezoresistors are placed in similar temperature regions. The temperature of the four piezoresistors is not always the identical, but usually the temperature of each logical, symmetrically placed pair is the same (with a different temperature between the two pairs). If the Wheatstone-bridge in Figure A.1c is considered, there are two possibilities to ensure that the Wheatstone-bridge is temperature independent. The first possibility is that  $R_1$  and  $R_2$  change with temperature  $\Delta T_1$ , while  $R_3$  and  $R_4$  change with temperature  $\Delta T_2$ . The second possibility to ensure that the Wheatstone-bridge is temperature independent, is if  $R_1$  and  $R_3$  change with temperature  $\Delta T_1$ , while  $R_2$  and  $R_4$  change with temperature  $\Delta T_2$ . In those cases the voltage output will be according to Equation (A.3).

$$\begin{aligned} U_{out} &= \frac{1}{4} \left( \frac{\Delta R_{T1}}{R_1} - \frac{\Delta R_{T2}}{R_3} + \frac{\Delta R_{T2}}{R_4} - \frac{\Delta R_{T1}}{R_2} \right) U_{cc} \approx 0 \\ U_{out} &= \frac{1}{4} \left( \frac{\Delta R_{T1}}{R_1} - \frac{\Delta R_{T1}}{R_3} + \frac{\Delta R_{T2}}{R_4} - \frac{\Delta R_{T2}}{R_2} \right) U_{cc} \approx 0 \end{aligned} \quad (A.3)$$

However, if piezoresistors  $R_1$  and  $R_4$  change with temperature  $\Delta T_1$  and  $R_2$  and  $R_3$  with temperature  $\Delta T_2$ , then the temperature is not compensated (see Equation (A.4)).

$$U_{out, WB} = \frac{1}{4} \left( \frac{\Delta R_{T1}}{R_1} - \frac{\Delta R_{T2}}{R_3} + \frac{\Delta R_{T1}}{R_4} - \frac{\Delta R_{T2}}{R_2} \right) U_{cc} \approx \frac{\Delta R}{R} U_{cc} \quad (A.4)$$

When the resistivity changes according to Equation (A.5), then the output voltage as a function of temperature is given by Equation (A.6).

$$R = R_{ref} \cdot (1 + \alpha_{Si} \cdot (T - T_{ref})) \quad (A.5)$$

$$\begin{aligned} U_{out, WB} &= \frac{1}{4}(\alpha_{Si} \cdot \Delta T_1 - \alpha_{Si} \cdot \Delta T_2 + \alpha_{Si} \cdot \Delta T_2 - \alpha_{Si} \cdot \Delta T_1)U_{cc} \\ U_{out, WB} &= \frac{1}{4}(\alpha_{Si} \cdot (2\Delta T_1 - 2\Delta T_2))U_{cc} \end{aligned} \quad (A.6)$$

## A.2 Crosspoint Switch Array

The Crosspoint Switch Array (CSA) used for this research is a switch array from National Instruments<sup>2</sup>. The CSA dynamically arranges the piezoresistors in a single Wheatstone-bridge, which is filtered and amplified using a Lock-In Amplifier (LIA). The connections of the piezoresistors in a single Wheatstone-bridge is given in Figure A.2. Each dot represents an electrical connection, which is depending on the piezoresistor arrangement (controlled by a computer).

In theory, two Wheatstone-bridges can be measured simultaneously, however, the LIA is the limiting factor in this case. The sampling time for each Wheatstone-bridge is identical by measuring two bridges at a time, does not improve the sampling frequency.

All the piezoresistors ( $R_1 - R_{24}$  and  $R_{ref,1} - R_{ref,8}$ ) are connected to the CSA, which are 48 connections in total. The arrangement of the piezoresistors in the Wheatstone-bridges for the interaction force sensor is given in Appendix B.

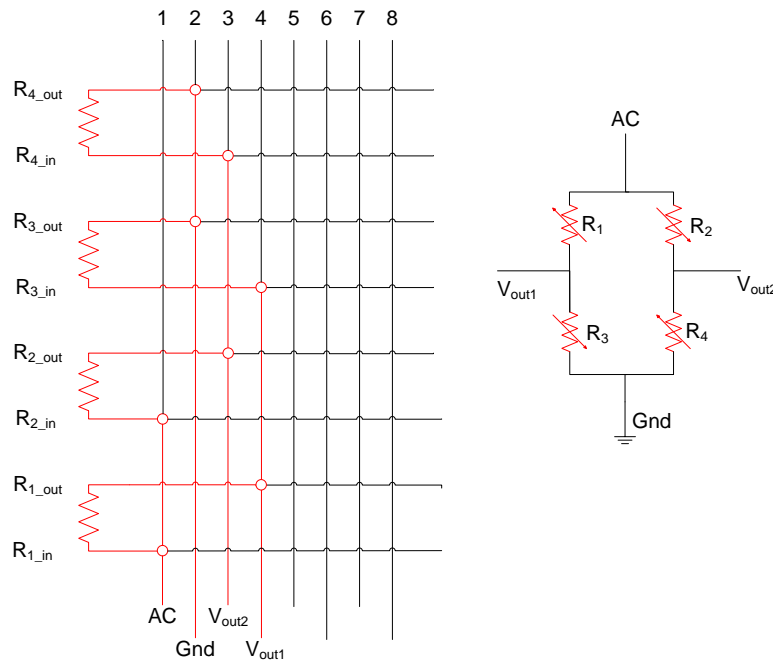


Figure A.2: The connection of a full-active Wheatstone-bridge in the CSA. In reality all the piezoresistors are connected to the CSA.

<sup>2</sup> <http://sine.ni.com/nips/cds/view/p/lang/en/nid/204243>



---

## APPENDIX B

# Force measurement analysis

In this appendix the detection of each different force is explained. The discussion of the force or torque detection can be split up into four different parts:

- **Global stress analysis with piezoresistors:** The global stress distribution through the interaction force sensor can be seen. The force is applied at the 'black dot' location of the interaction force sensor, because this is an easy way to separate the forces from each other. It is the centre point of the three beams and therefore symmetrical in multiple directions.
- **Stress distribution along the sensing beams 1 and 3:** Each line in the figure represents the stresses along an edge of the beam (on the line  $R_1 - R_3$ ,  $R_2 - R_4$  and  $R_{17} - R_{19}$ ,  $R_{18} - R_{20}$ ), when a force of 100  $\mu\text{N}$  or a torque of 100  $\mu\text{Nmm}$  is applied. Only half of the sensor is considered, since the stresses in the other beam are the same due to symmetry.
- **Wheatstone-bridges used for detection of the force/torque:** The Wheatstone-bridges are shown with colours matching the Wheatstone-bridges as suggested in Table 3.4.
- **Force and temperature dependency:** The force-temperature-voltage relation is shown. Heating of the sensor, results in a voltage output, due to the temperature coefficient of resistance (TCR) and the thermal expansion of the sensor. This voltage output corresponds to a force input (when unheated). Moreover, moving over a horizontal line from temperature to the force (so with constant voltage output), gives the loss of resolution due to the thermal heating.

## B.1 $F_x$ Measurement

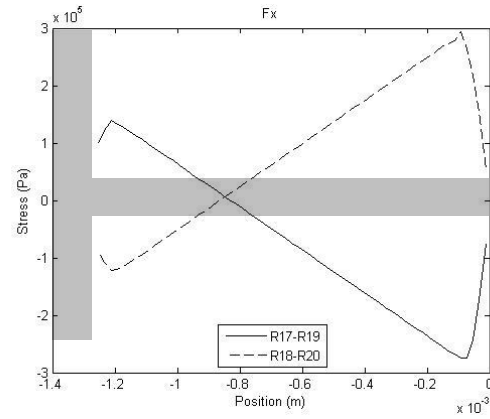
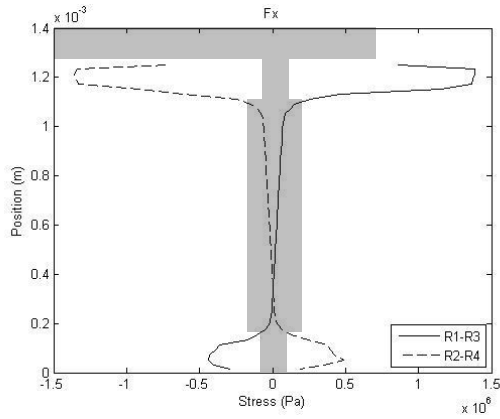
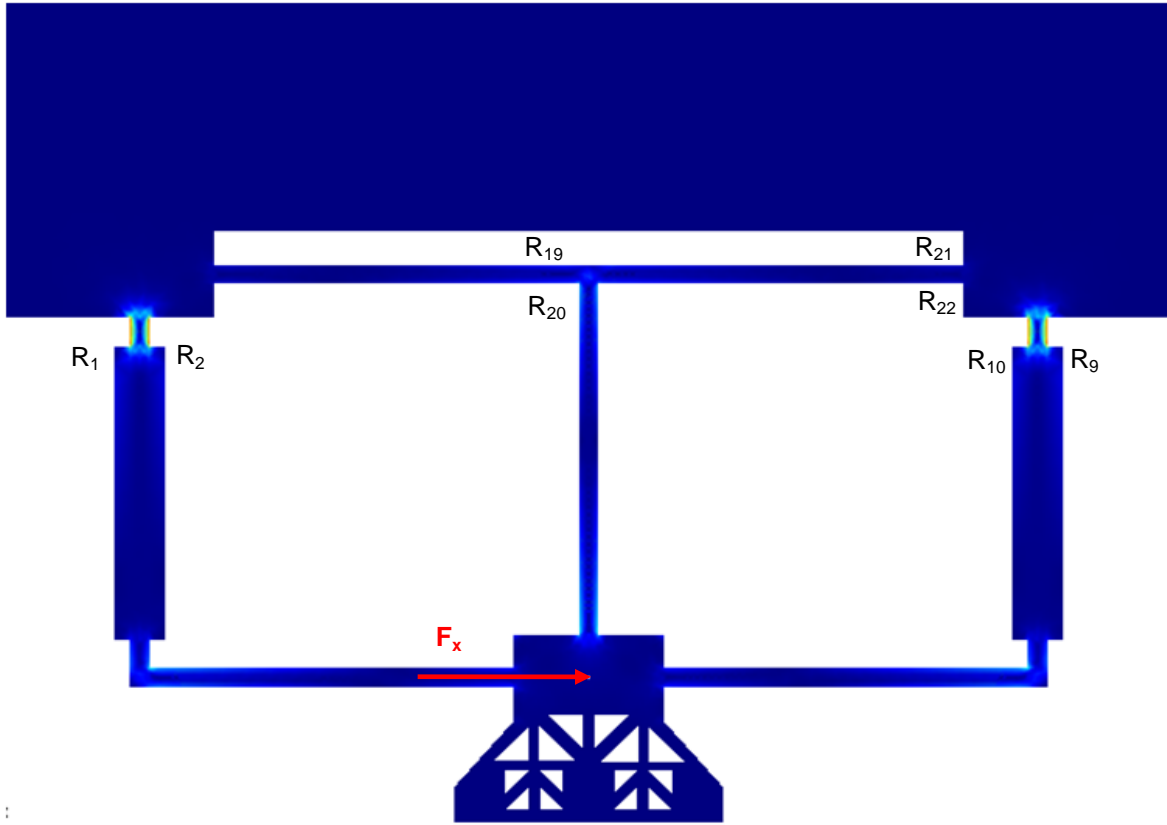


Figure B.1: Stress distribution through the interaction force sensor when force  $F_x$  is applied, with the location of the piezoresistor used for measuring  $F_x$ . On the top the global stress distribution can be seen, while at the bottom the stress distribution through the sensing beam 1 and 3.

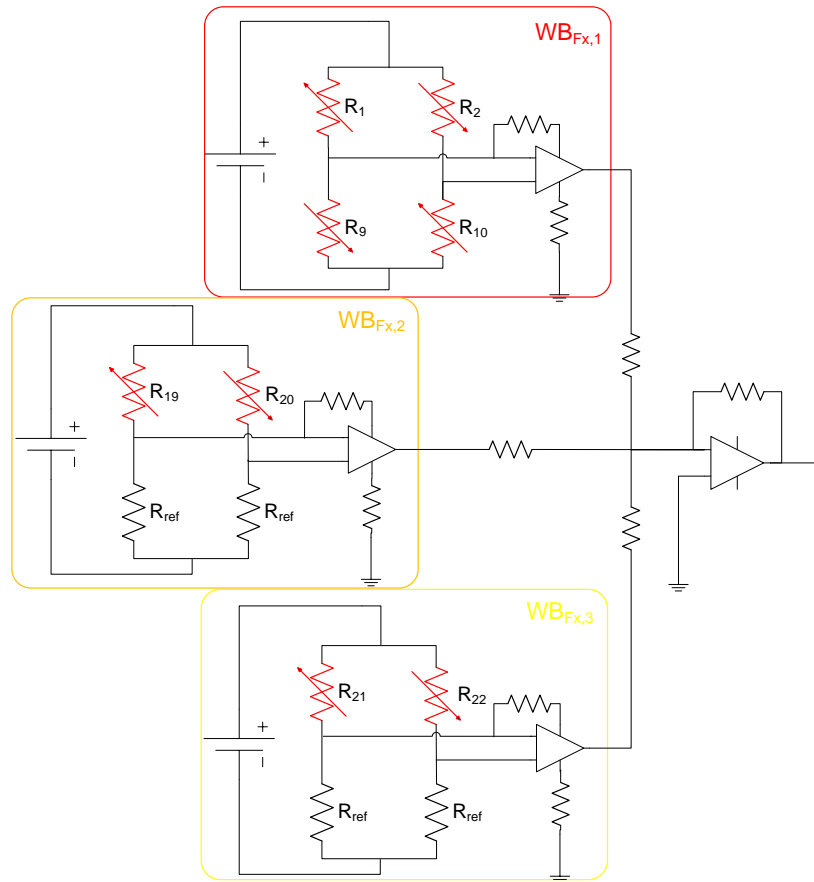


Figure B.2: Wheatstone-bridge layout for measuring  $F_x$ .

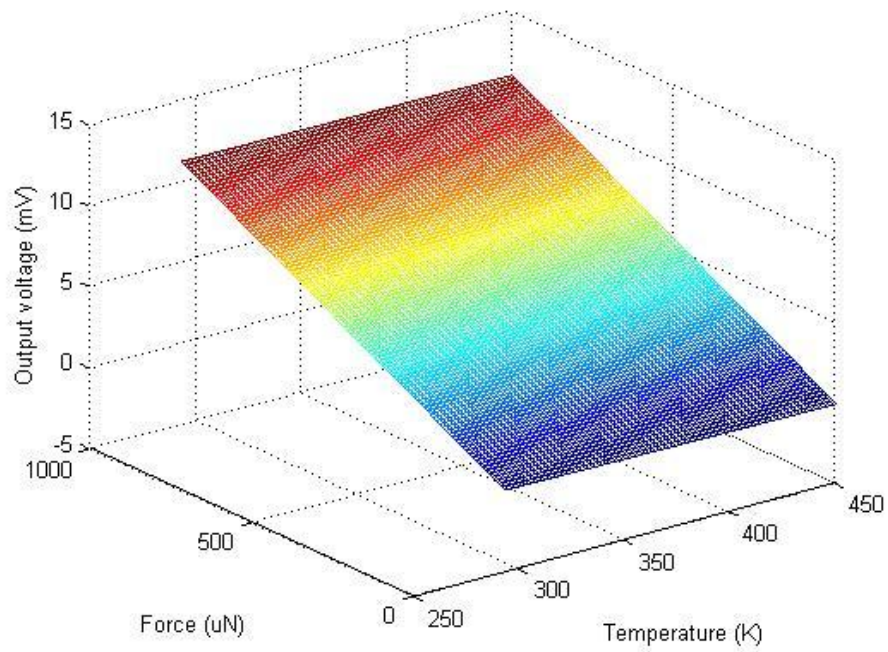


Figure B.3: Force-Temperature-Voltage relation for measuring  $F_x$ .

## B.2 $F_y$ Measurement

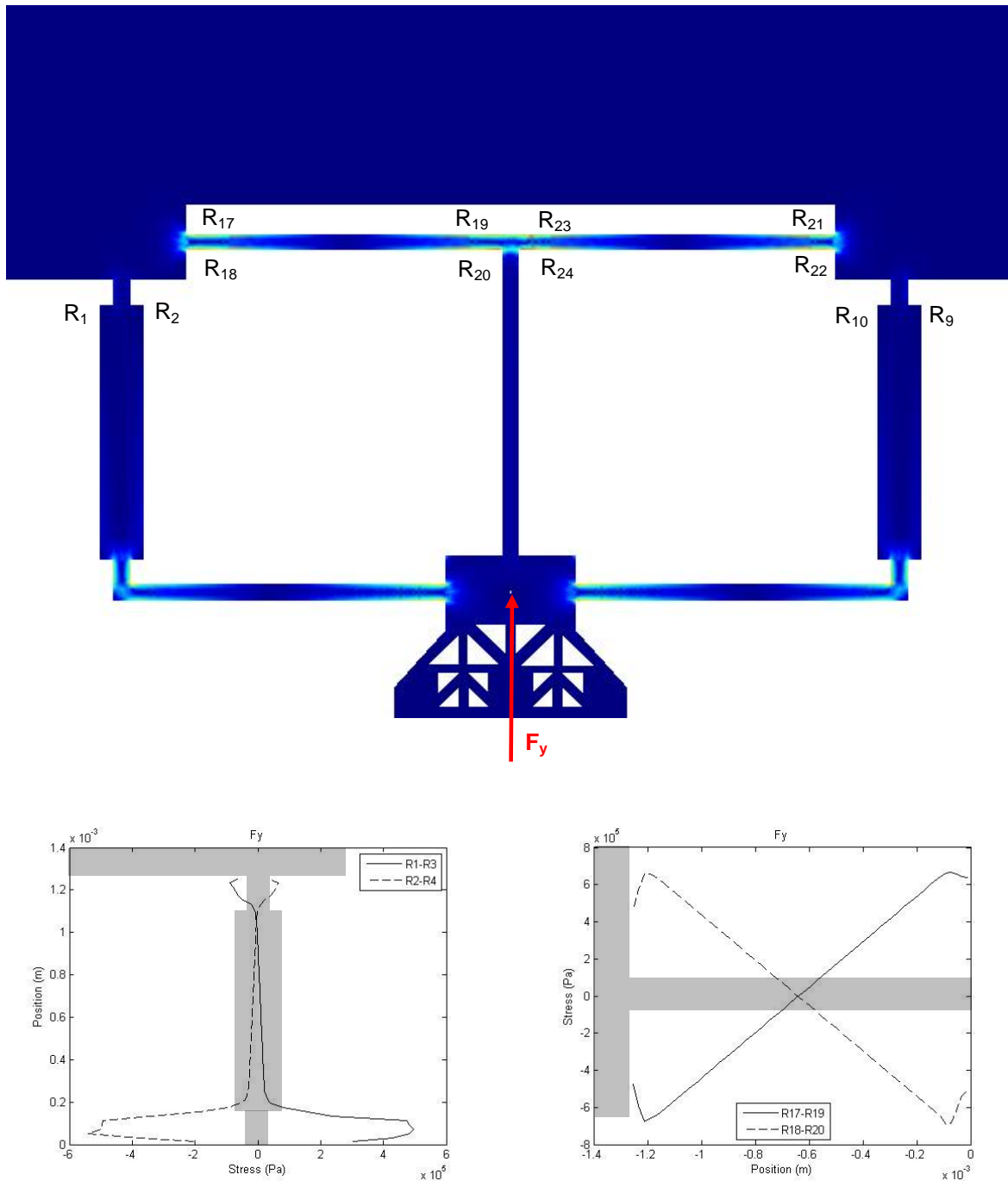


Figure B.4: Stress distribution through the interaction force sensor when force  $F_y$  is applied, with the location of the piezoresistor used for measuring  $F_y$ . On the top the global stress distribution can be seen, while at the bottom the stress distribution through the sensing beam 1 and 3.

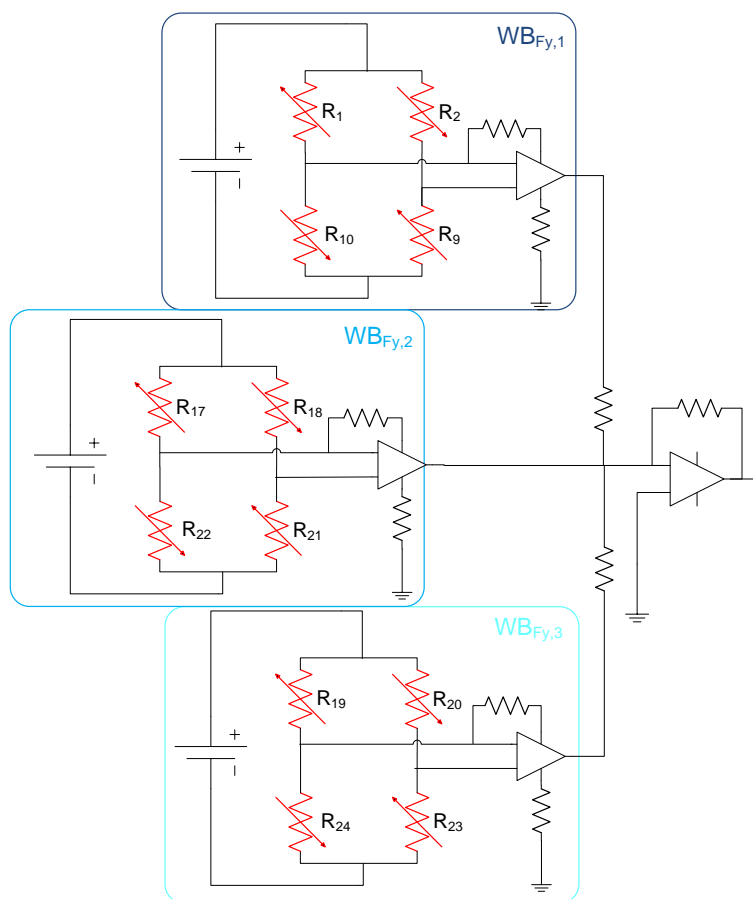


Figure B.5: Wheatstone-bridge layout for measuring  $F_y$ .

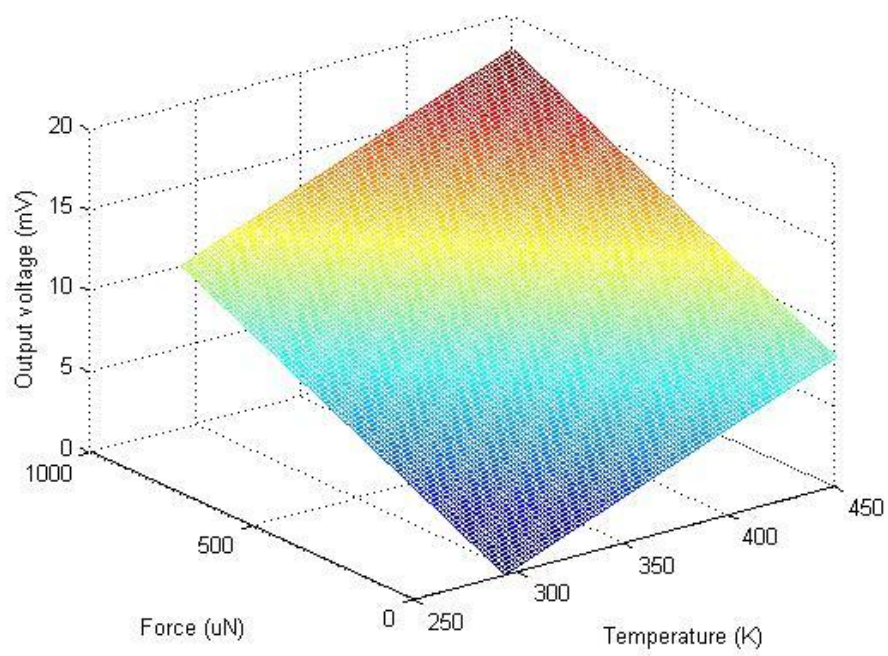


Figure B.6: Force-Temperature-Voltage relation for measuring  $F_y$ .

### B.3 $F_z$ Measurement

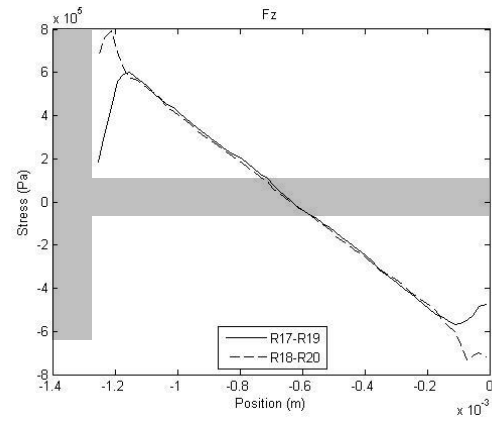
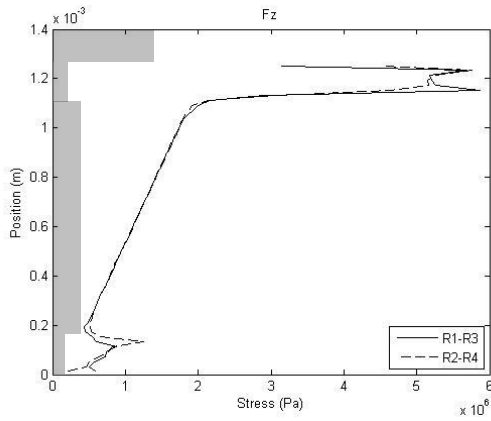
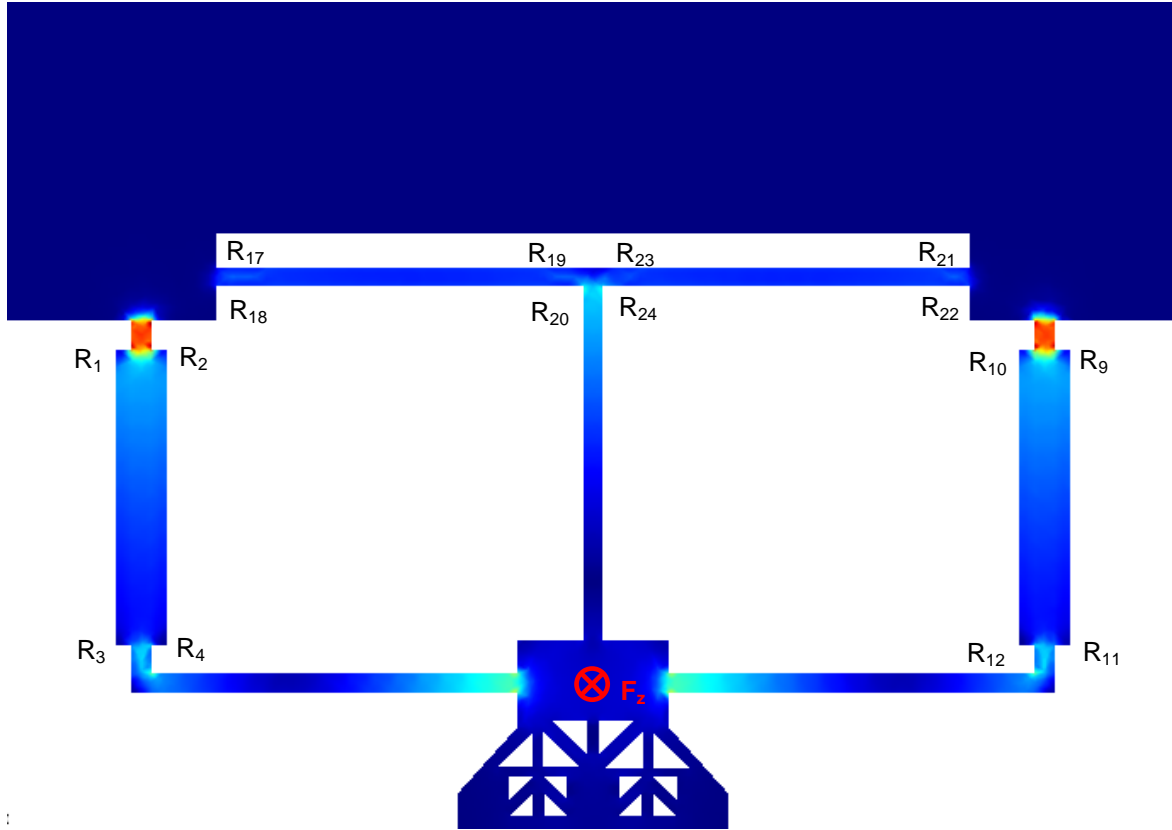


Figure B.7: Stress distribution through the interaction force sensor when force  $F_z$  is applied, with the location of the piezoresistor used for measuring  $F_z$ . On the top the global stress distribution can be seen, while at the bottom the stress distribution through the sensing beam 1 and 3.

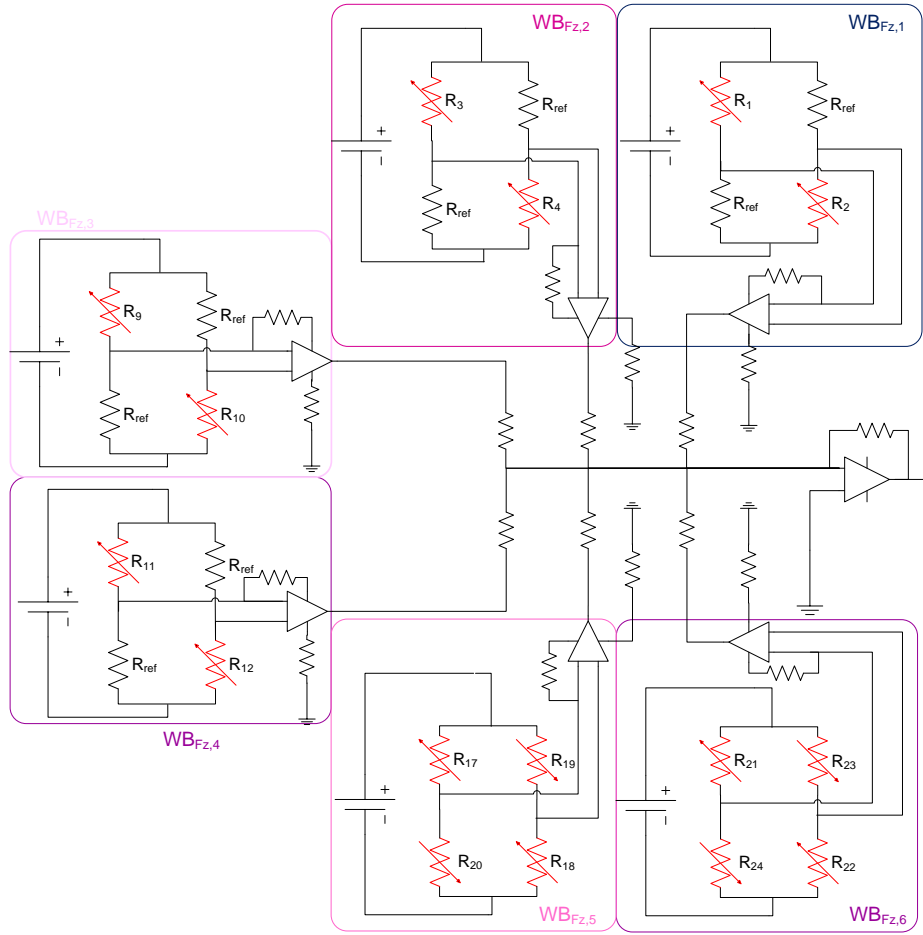


Figure B.8: Wheatstone-bridge layout for measuring  $F_z$ .

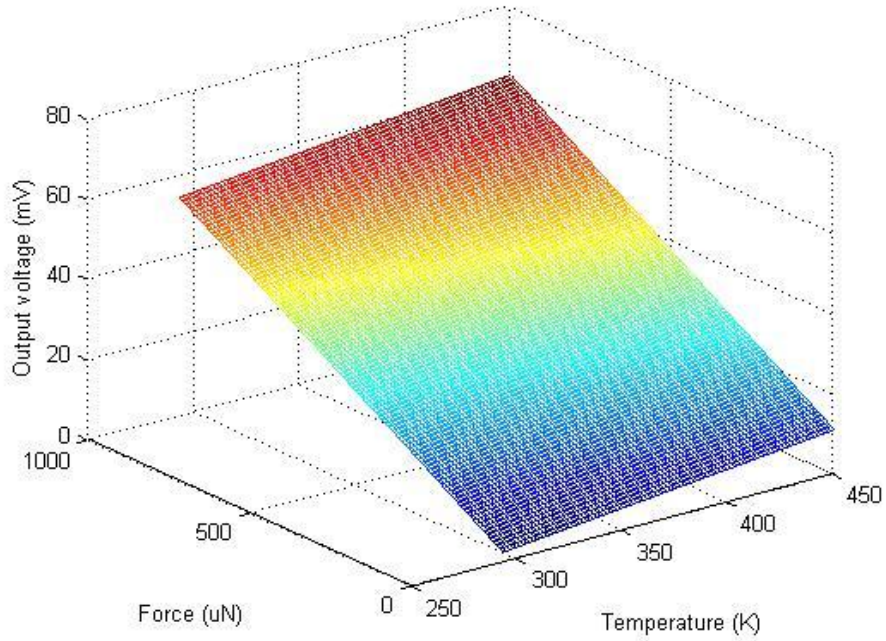


Figure B.9: Force-Temperature-Voltage relation for measuring  $F_z$ .

## B.4 $M_x$ Measurement

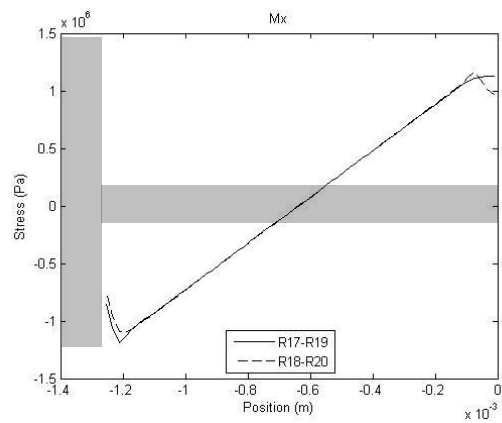
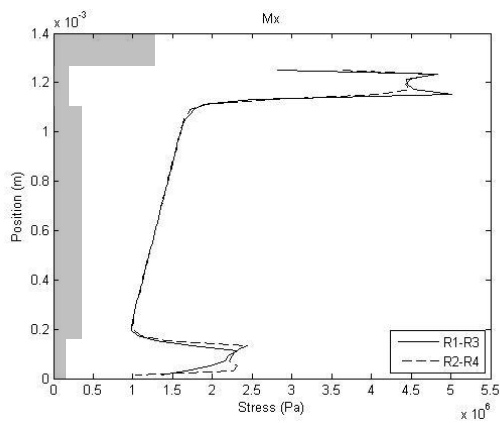
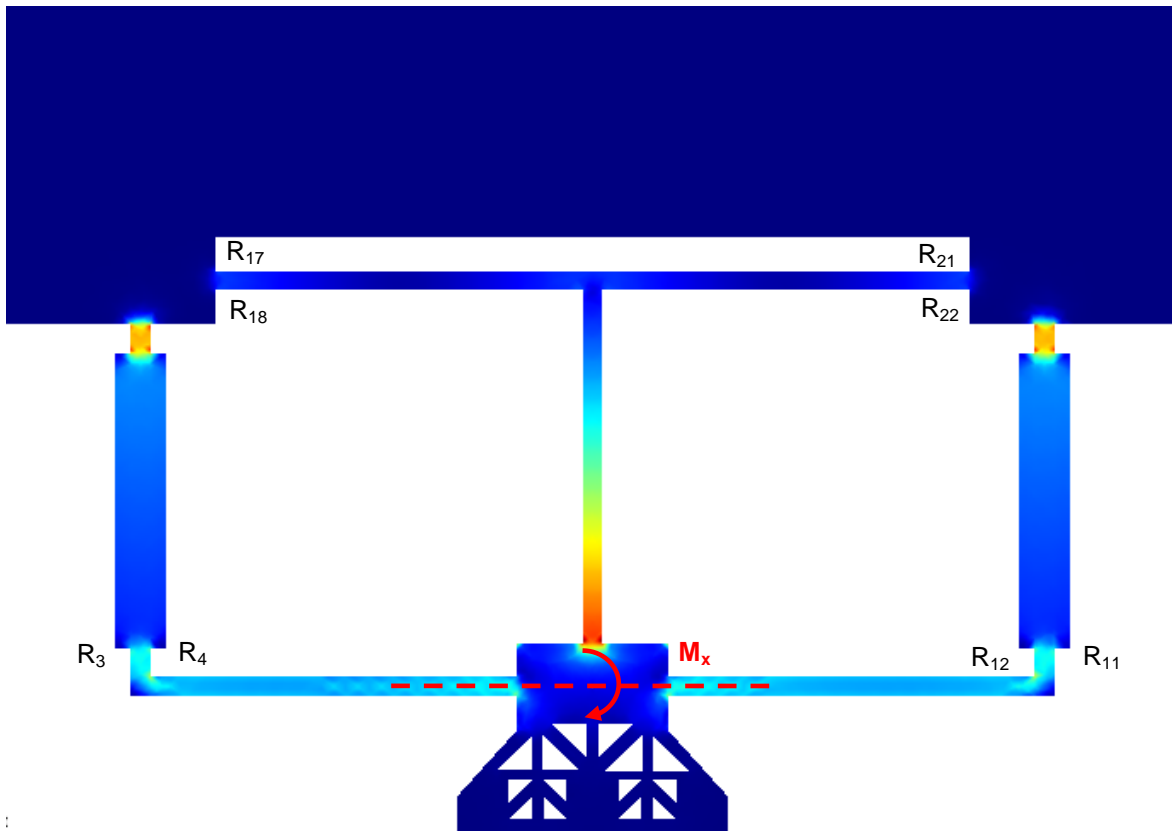


Figure B.10: Stress distribution through the interaction force sensor when force  $M_x$  is applied, with the location of the piezoresistor used for measuring  $M_x$ . On the top the global stress distribution can be seen

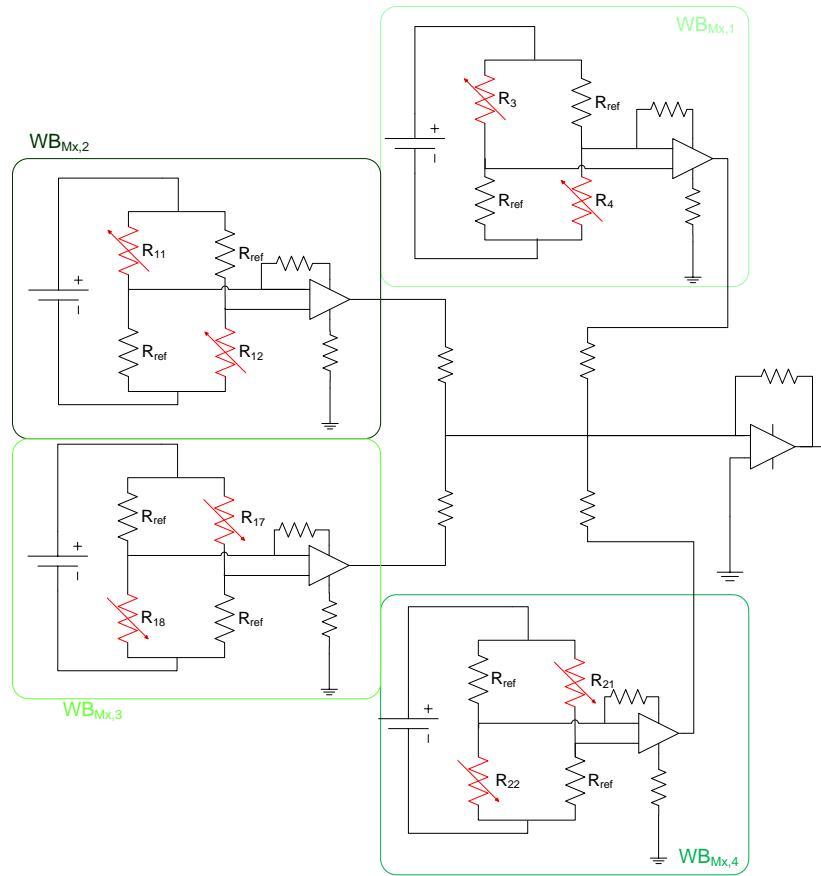


Figure B.11: Wheatstone-bridge layout for measuring  $M_x$ .

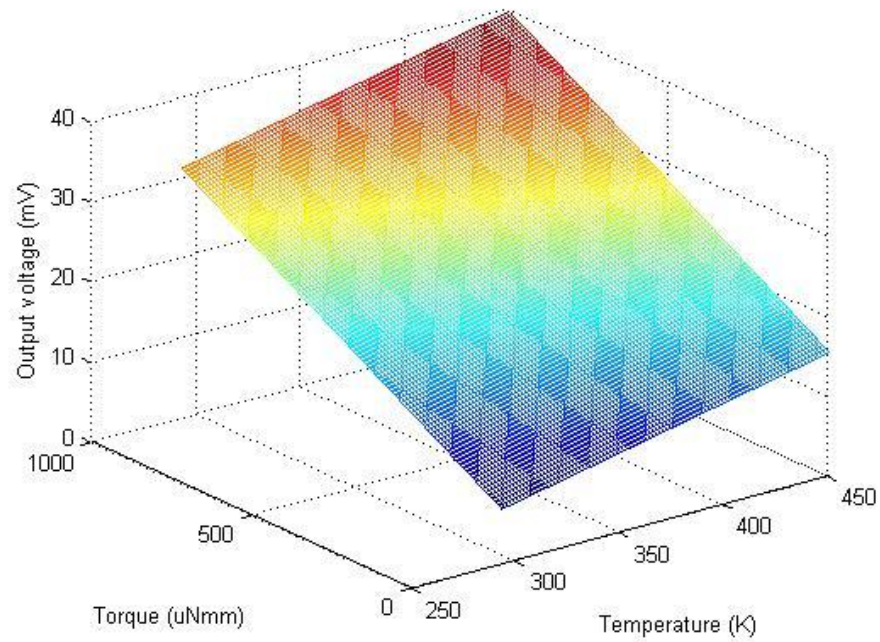


Figure B.12: Force-Temperature-Voltage relation for measuring  $M_x$ .

## B.5 $M_y$ Measurement

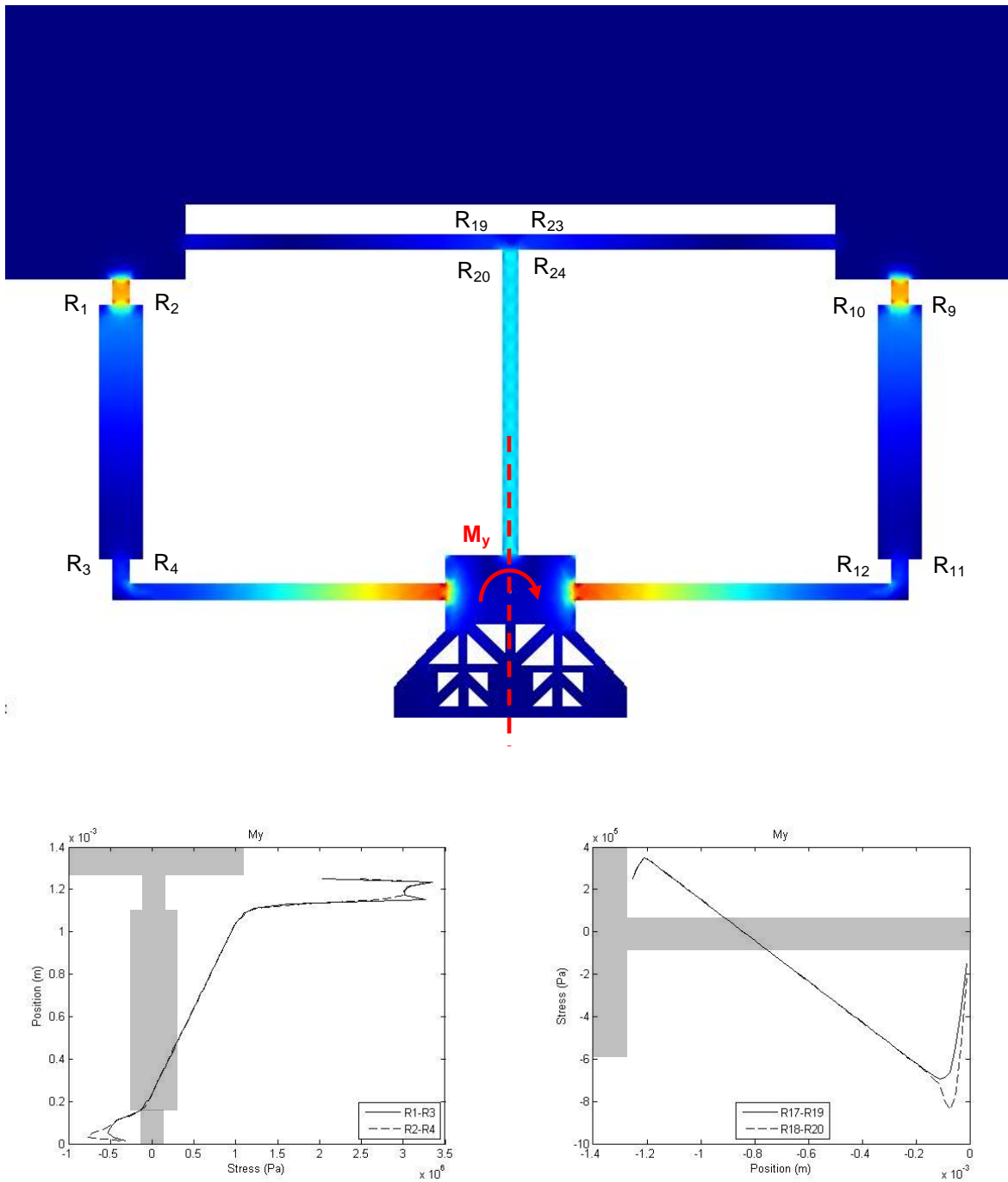


Figure B.13: Stress distribution through the interaction force sensor when force  $M_y$  is applied, with the location of the piezoresistor used for measuring  $M_y$ . On the top the global stress distribution can be seen

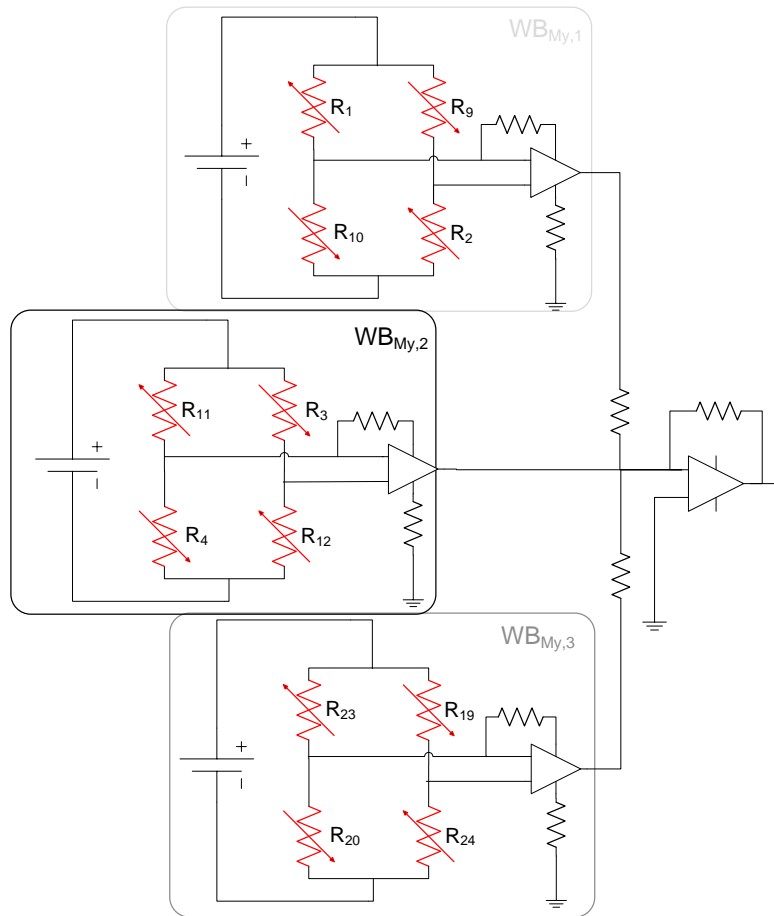


Figure B.14: Wheatstone-bridge layout for measuring  $M_y$ .

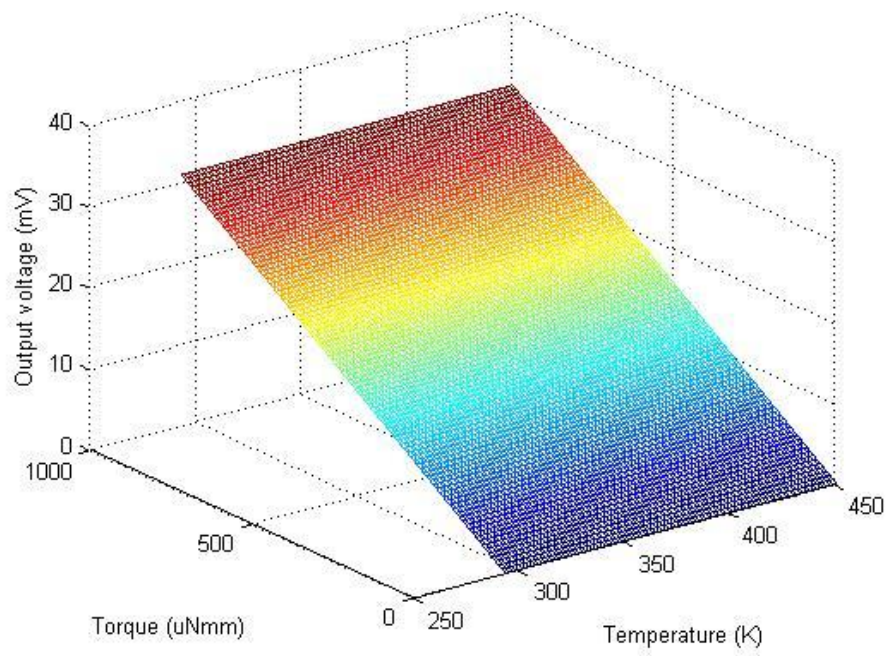


Figure B.15: Force-Temperature-Voltage relation for measuring  $M_y$ .

## B.6 $M_z$ Measurement

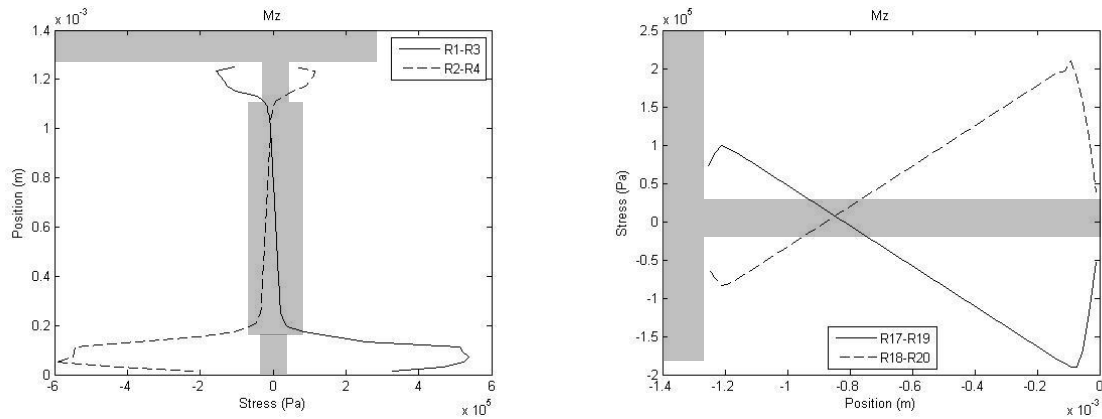
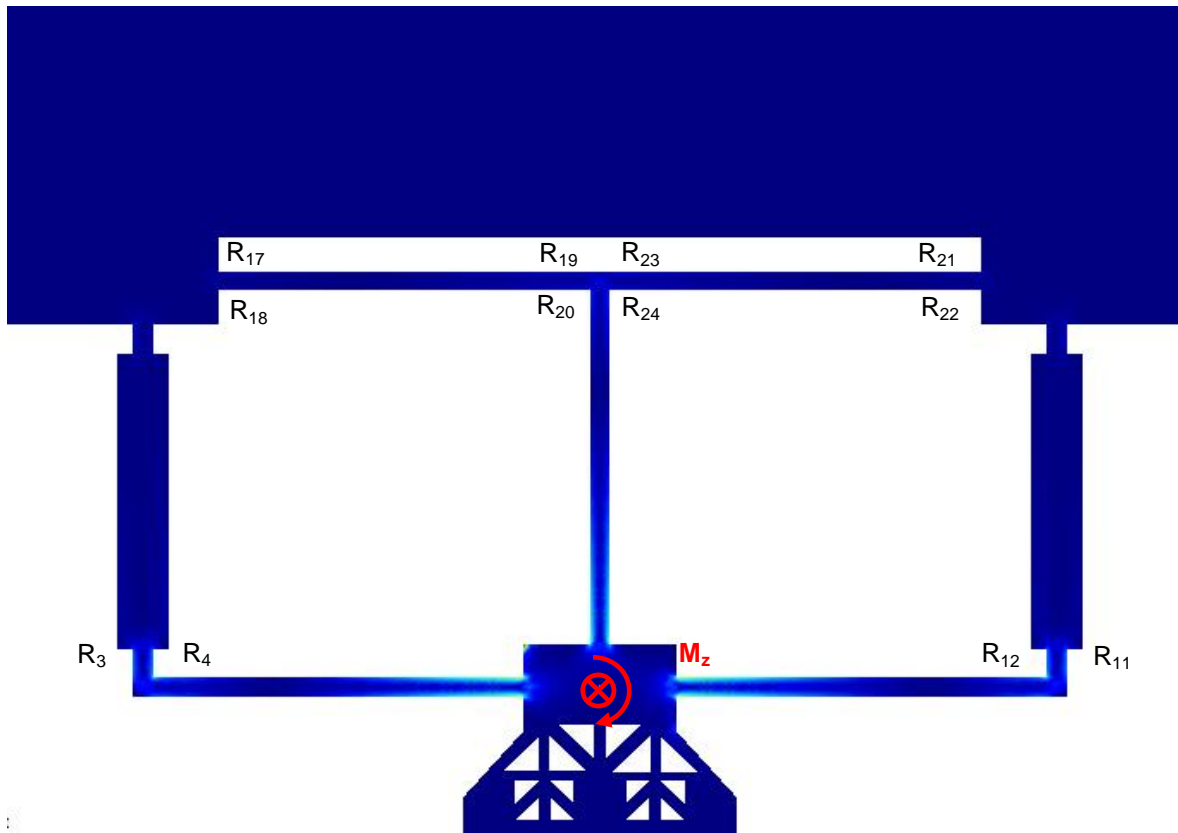


Figure B.16: Stress distribution through the interaction force sensor when force  $M_z$  is applied, with the location of the piezoresistor used for measuring  $M_z$ . On the top the global stress distribution can be seen

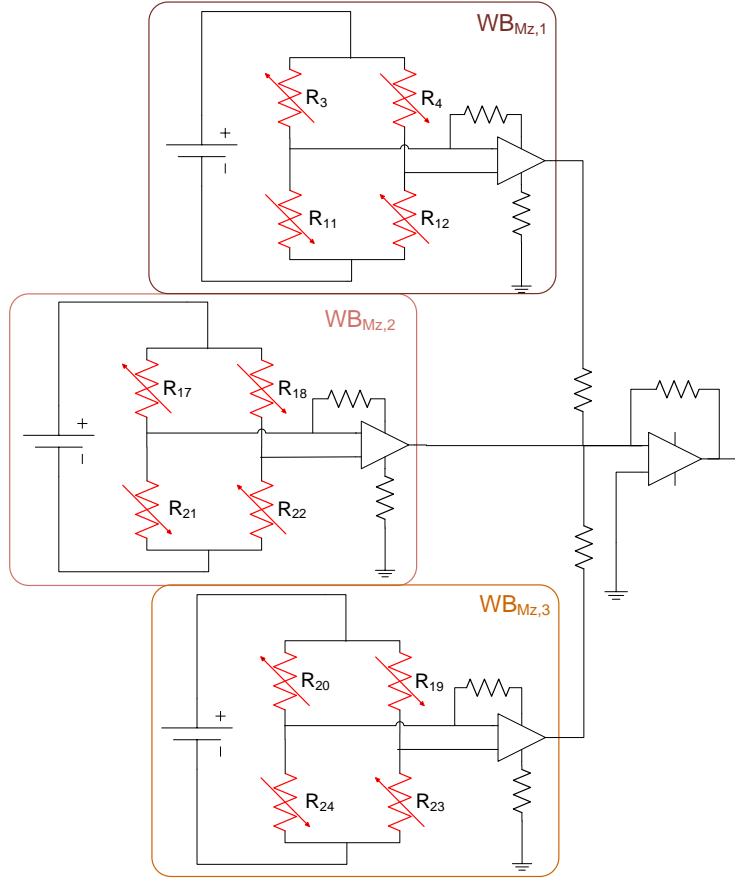


Figure B.17: Wheatstone-bridge layout for measuring  $M_z$ .

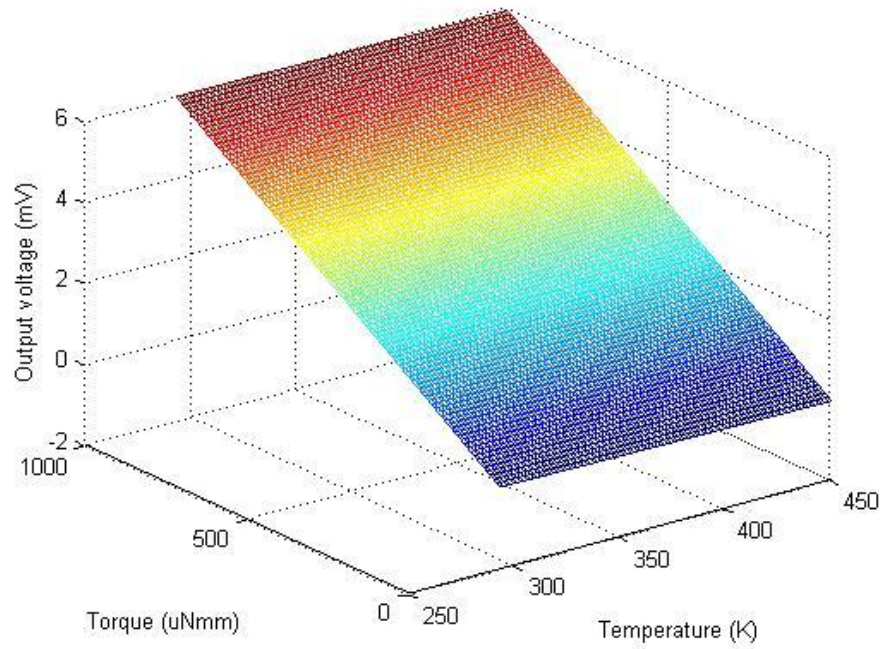


Figure B.18: Force-Temperature-Voltage relation for measuring  $M_z$ .



---

## APPENDIX C

### Wafer design

On one single die, multiple devices are fabricated. Since the standard dimensions of a die are  $15 \times 15 \text{ mm}^2$ , and the interaction force sensor is only  $7.5 \times 5 \text{ mm}^2$  (global outside dimensions, including bondpads), other structures are inserted in the die. The global overview of the fabricated devices can be seen in Figure C.1 and its specifications in Table C.1. Next the details of the interaction force sensor with test plate and the micro-gripper are given. Different colours represent different layers (and thus different masks) for the fabrication of the device.

Section	Device
A	Interaction force sensor with test plate as proposed in this thesis.
B	Interaction force sensor with integrated micro-gripper (developed by [12]).
C	Some basic test structures for determining the piezoresistive behaviour.
D	Different micro-grippers with opening ranges from $40 - 100 \text{ }\mu\text{m}$ . Including micro-grippers with a “two-stage” tip (tip opening of $40/80 \text{ }\mu\text{m}$ and $60/100 \text{ }\mu\text{m}$ ).
E	Basic structures for micro-assembly tests.
F	Gripper with position detection capability (position detection as proposed by [4]).
X	Several other structures (outside the scope of this thesis).

*Table C.1: Devices on the wafer.*

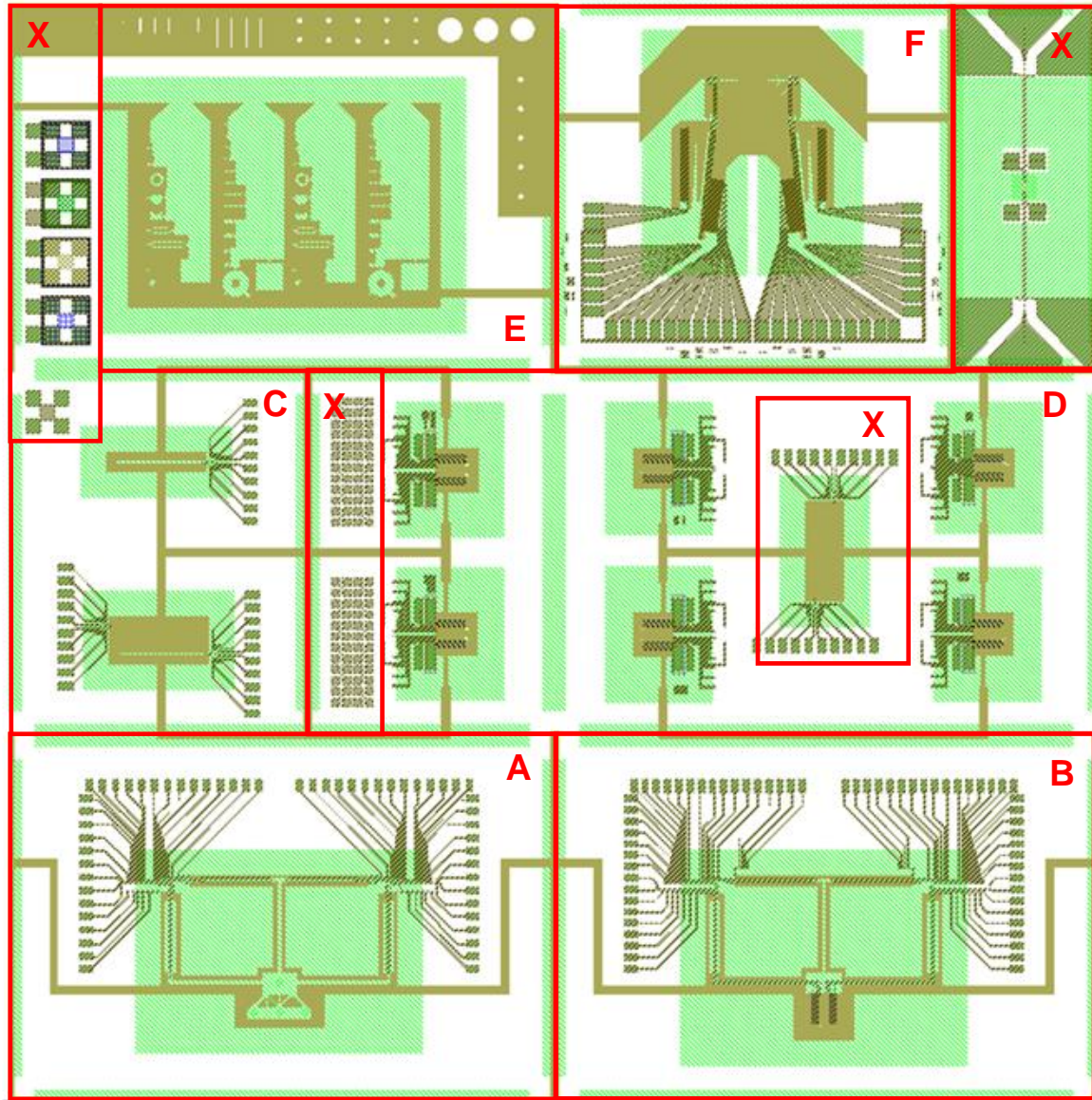


Figure C.1: Layout of the die fabricated at DIMES.

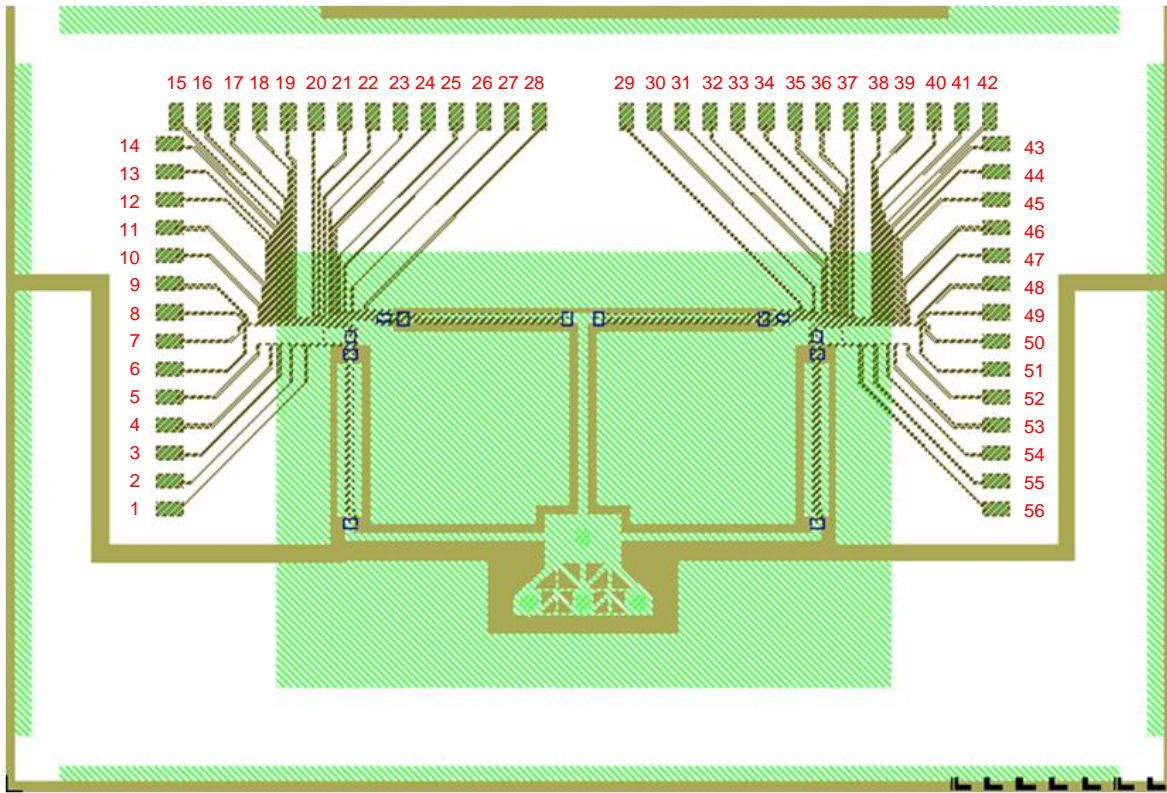


Figure C.2: Detail of the L-edit draft (A) of the interaction force sensor, including connections.

1	R <sub>1_out</sub>	20	R <sub>ref_out</sub>	39	R <sub>24_in</sub>
2	R <sub>1_in</sub>	21	V <sub>cc</sub>	40	R <sub>24_out</sub>
3	R <sub>3_out</sub>	22	R <sub>ref_in</sub>	41	R <sub>22_in</sub>
4	R <sub>3_in</sub>	23	R <sub>ref_out</sub>	42	R <sub>22_out</sub>
5	V <sub>cc</sub>	24	Gnd	43	R <sub>10_out</sub>
6	R <sub>ref_out</sub>	25	R <sub>19_in</sub>	44	R <sub>10_in</sub>
7	R <sub>ref_in</sub>	26	R <sub>19_out</sub>	45	R <sub>12_out</sub>
8	Gnd	27	R <sub>17_in</sub>	46	R <sub>12_in</sub>
9	R <sub>ref_out</sub>	28	R <sub>17_out</sub>	47	R <sub>ref_in</sub>
10	R <sub>ref_in</sub>	29	R <sub>21_in</sub>	48	R <sub>ref_out</sub>
11	R <sub>4_out</sub>	30	R <sub>21_out</sub>	49	Gnd
12	R <sub>4_in</sub>	31	R <sub>23_in</sub>	50	R <sub>ref_in</sub>
13	R <sub>2_out</sub>	32	R <sub>23_out</sub>	51	R <sub>ref_out</sub>
14	R <sub>2_in</sub>	33	Gnd	52	V <sub>cc</sub>
15	R <sub>18_in</sub>	34	R <sub>ref_in</sub>	53	R <sub>11_out</sub>
16	R <sub>18_out</sub>	35	R <sub>ref_out</sub>	54	R <sub>11_in</sub>
17	R <sub>20_in</sub>	36	V <sub>cc</sub>	55	R <sub>9_out</sub>
18	R <sub>20_out</sub>	37	R <sub>ref_in</sub>	56	R <sub>9_in</sub>
19	R <sub>ref_in</sub>	38	R <sub>ref_out</sub>		

Table C.2: Connections of the interaction force sensor with test plate.

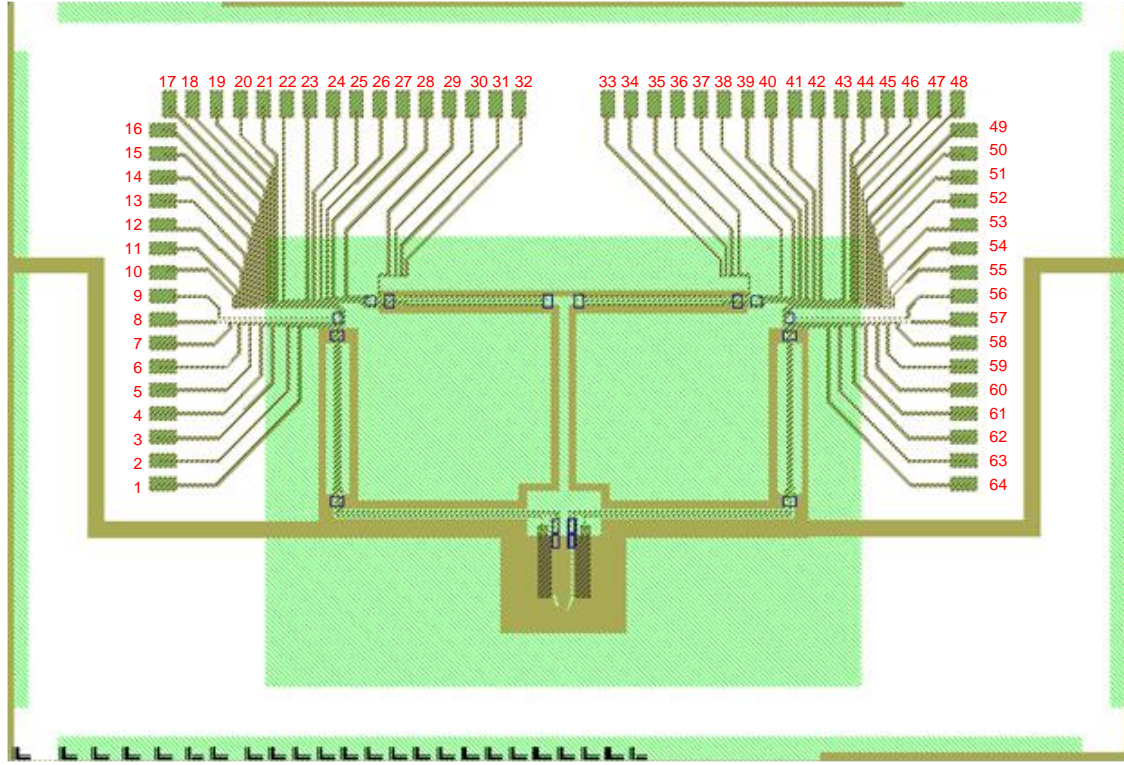


Figure C.3: Detail of the L-edit draft (A) of the interaction force sensor, including connections.

1	R <sub>1_out</sub>	23	R <sub>ref_in</sub>	45	R <sub>22_in</sub>
2	R <sub>1_in</sub>	24	R <sub>ref_out</sub>	46	R <sub>22_out</sub>
3	R <sub>3_out</sub>	25	V <sub>cc</sub>	47	R <sub>10_out</sub>
4	R <sub>3_in</sub>	26	R <sub>ref_in</sub>	48	R <sub>10_in</sub>
5	V <sub>cc-act</sub>	27	R <sub>ref_out</sub>	49	R <sub>12_out</sub>
6	Gnd <sub>act</sub>	28	Gnd	50	R <sub>12_in</sub>
7	V <sub>cc</sub>	29	R <sub>19_in</sub>	51	R <sub>ref_in</sub>
8	Out <sub>2</sub>	30	R <sub>19_out</sub>	52	R <sub>ref_out</sub>
9	Out <sub>1</sub>	31	R <sub>17_in</sub>	53	Gnd
10	R <sub>ref_out</sub>	32	R <sub>17_out</sub>	54	R <sub>ref_in</sub>
11	R <sub>ref_in</sub>	33	R <sub>21_in</sub>	55	R <sub>ref_out</sub>
12	Gnd	34	R <sub>21_out</sub>	56	Out <sub>1</sub>
13	R <sub>ref_out</sub>	35	R <sub>23_in</sub>	57	Out <sub>2</sub>
14	R <sub>ref_in</sub>	36	R <sub>23_out</sub>	58	V <sub>cc</sub>
15	R <sub>4_out</sub>	37	Gnd	59	Gnd <sub>act</sub>
16	R <sub>4_in</sub>	38	R <sub>ref_in</sub>	60	V <sub>cc-act</sub>
17	R <sub>2_in</sub>	39	R <sub>ref_out</sub>	61	R <sub>11_out</sub>
18	R <sub>2_out</sub>	40	V <sub>cc</sub>	62	R <sub>11_in</sub>
19	R <sub>18_in</sub>	41	R <sub>ref_in</sub>	63	R <sub>9_out</sub>
20	R <sub>18_out</sub>	42	R <sub>ref_out</sub>	64	R <sub>9_in</sub>
21	R <sub>20_in</sub>	43	R <sub>24_in</sub>		
22	R <sub>20_out</sub>	44	R <sub>24_out</sub>		

Table C.3: Connections of the interaction force sensor with integrated micro-gripper.

---

## APPENDIX D

### Fabrication flowchart

#### Frontside process

1. Substrate: p-type, (100), Si wafer, thickness =  $525 \pm 5 \mu\text{m}$
2. Lithography and Oxidation: ASM wafer stepper; define the stepper alignment marks
3. Epitaxy:  $1 \mu\text{m}$  thick n-type (Arsenic doping  $1\text{e}16 \text{ atoms/cm}^3$ ) layer and 500 nm thick p-type (Boron doping  $1\text{e}18 \text{ atoms/cm}^3$ ) layer on top
4. Lithography: ASM wafer stepper; define the piezoresistors
5. Silicon plasma etching: Drytek 384T plasma etcher
6. Cleaning: Oxygen plasma and  $\text{HNO}_3$  based wet cleaning
7. Oxidation: Wet oxidation; thickness = 30 nm
8. Lithography: ASM wafer stepper; define the DP windows
9. Implantation: Boron ions,  $E = 180 \text{ keV}$ , Dose =  $5\text{e}15 \text{ ions/cm}^2$
10. Cleaning: Oxygen plasma and  $\text{HNO}_3$  based wet cleaning
11. Lithography: ASM wafer stepper; define the DN windows
12. Implantation: Phosphorus ions,  $E = 180 \text{ keV}$ , Dose =  $5\text{e}15 \text{ ions/cm}^2$
13. Cleaning: Oxygen plasma and  $\text{HNO}_3$  based wet cleaning
14. Lithography: ASM wafer stepper; define the LP windows
15. Implantation: Boron ions,  $E = 15 \text{ keV}$ , Dose =  $3\text{e}15 \text{ ions/cm}^2$
16. Cleaning: Oxygen plasma and  $\text{HNO}_3$  based wet cleaning
17. Silicon nitride deposition: thickness = 300 nm
18. Annealing: in Ar,  $T = 950 \text{ }^\circ\text{C}$ ,  $t = 20 \text{ minutes}$

#### Backside process

19. Lithography: EV 240 contact aligner; define the KOH windows
20. Silicon nitride plasma etching: Drytek 384T plasma etcher
21. Cleaning: Oxygen plasma and  $\text{HNO}_3$  based wet cleaning

### **Frontside process**

22. Lithography: ASM wafer stepper; define the CO windows
23. Silicon nitride plasma etching: Drytek 384T plasma etcher
24. Cleaning: Oxygen plasma and HNO<sub>3</sub> based wet cleaning
25. DIP Etching: HF (0.55 %), t = 4 minutes, rinse in demineralized water 3 minutes, dry
26. Metallization: Trikon Sigma, sputtering of Al/Si, thickness = 675 nm, T = 350 °C
27. Lithography: ASM wafer stepper; define the IC wire connections
28. Aluminum plasma etching: Trikon Omega 201 plasma etcher, T = 25 °C
29. Cleaning: Oxygen plasma and HNO<sub>3</sub> based wet cleaning
30. Lithography: EV 240 contact aligner; define the pad opening
31. Silicon nitride plasma etching: Drytek 384T plasma etcher
32. Cleaning: Oxygen plasma and HNO<sub>3</sub> based wet cleaning
33. Alloying
34. Lithography: ASM wafer stepper; define the interaction force sensor (DRIE mask)
35. Cleaning: HNO<sub>3</sub> based wet cleaning

### **Backside process**

36. Silicon KOH etching: KOH (33 %), T = 85 °C, protect the wafer front side by Silicet vacuum holder; etching depth = 495 µm (etch rate = 0.8 µm/minute)
37. Cleaning: HNO<sub>3</sub> based wet cleaning
38. Metallization: Trikon Sigma, Al/Si sputtering, thickness = 675 nm, T = 50 °C

### **Frontside process**

39. Silicon plasma etching (long): Adixen ASM100 plasma etcher
40. Silicon oxide plasma etching (short): Drytek 384T plasma etcher
41. Silicon plasma etching (short): Adixen ASM100 plasma etcher
42. Aluminum wet etching: T = 35 °C
43. Cleaning: Oxygen plasma and HNO<sub>3</sub> based wet cleaning

# Acknowledgement

The field of micro and nano engineering is very challenging and I couldn't have succeeded this thesis without the help of many other people. Therefore I enlisted the people to whom I owe my gratitude.

First of all, I would like to explain my gratitude to my direct supervisor Marcello Porta. I would like to thank you for your guidance during the thesis and sharing your knowledge about the force sensing in micro-handling. You provided me with the necessary feedback and took the lead during the times it didn't go so smoothly.

Furthermore, I want to thank Pablo Estevez and Jia Wei for their view and input during my thesis. During the times I was stuck you really helped me out by coming up with new and innovative ideas, which made this project a success.

I thank Marcel Tichem and Urs Staufer for their supervision of my thesis. With your sharp and analytical insight you pointed out the possible pitfalls and guided me during this thesis.

Graduating is a challenging and sometimes lonely task in which I was lucky to be supported by other (PME) students. My special gratitude goes out to Erik and Wijnand for their pleasant company. Thank you for the great times on the innovation platform!

Finally, I would like to thank my parents, family and friends for their interest and for (pretending to) understand what I was doing. You were always there during the occasional hard and frustrating times and supported me with the necessary comforting words, which provided me with the perseverance to finish this thesis.



# Bibliography

- [1] F. Arai, et al., "Micro manipulation based on micro physics-strategy based on attractive force reduction and stress measurement." 1995. Int. Conf. on Intelligent Robots and Systems. Vol. 2, pp. 236-241.
- [2] G. Reinhart, et al., "Telepresence as a Solution to Manual Micro-Assembly." Institute for Machine Tools and Industrial Management.
- [3] Y. Xie, et al., "A Force Control Based Cell Injection Approach in a Bio-Robotics System." 2009.
- [4] J. Wei, et al., "A Contact Position Detection and Interaction Force Monitoring Sensor for Micro-Assembly Applications." 2009. Transducers.
- [5] K. Deng and W.H. Ko., "A study of static friction silicon and silicon compounds." Journal of Micromechanics and Microengineering, 1991, Issue 14, Vol. 2.
- [6] J.J. Gorman and N.G. Dagalakis., "Probe-base micro-scale manipulation and assembly using force feedback." 2006. 1st Joint Emer. Prep. & Response/Robotic & Remote Sys. Top. Mtg.
- [7] D.H. Kim, et al., "Development of a Piezoelectric Polymer-based Sensorized Microgripper for Microassembly and Micromanipulation." Microsystem Technologies, 2003, Vol. 10, pp. 275–280. Springer-Verlag.
- [8] Y. Shen, N. Xi and W.J. Li., "Force-guided assembly of micro-mirrors." Las Vegas : IEEE, 2003. Int. Conf. on Intelligent Robots and Systems.
- [9] X. Liu, et al., "Nano-Newton Force Sensing and Control in Microrobotic Cell Manipulation." Toronto : Advanced Micro and Nanosystems Laboratory.
- [10] A. Sieber, et al., "A novel haptic platform for real time bilateral biomanipulation with a MEMS sensor for triaxial force feedback." Sensors and Actuators, 2007, Vol. 142, pp. 19 - 27.
- [11] D.H. Kim, et al., "A Superelastic Alloy Microgripper with Embedded Electromagnetic Actuators and Piezoelectric Force Sensors: A Numerical and Experimental Study." Smart Materials and Structures, 2005, Issue 6, Vol. 14, pp. 1265 - 1272.
- [12] T. Chu Duc., *Sensing Microgripper for Microparticle Handling*. DIMES, Delft University of Technology. 2007. p. 153.

- [13] F. Beyeler, et al., "Monolithically Fabricated Microgripper with Integrated Force Sensor for Manipulating Microobjects and Biological Cells Aligned in an Ultrasonic Field." New York : Institute of Electrical and Electronics Engineers, 2007, Issue 1, Vol. 16, pp. 7 - 15.
- [14] Y. Zhou and B.J. Nelson., "The Effect of Material Properties and Gripping Force on Micrograsping." San Francisco : IEEE, 2000. Int. Conf. on Robotics and Automation.
- [15] K. Kim, et al., "Micronewton Force-Controlled Manipulation of Biomaterials Using a Monolithic MEMS Micro-Gripper with Two-Axis Force Feedback." Pasadena : IEEE, 2008. Int. Conf. on Robotics and Automation. pp. 19 - 23.
- [16] B. Kuebler, U. Seibold and G. Hirzinger., "Development of Actuated and Sensor Integrated Forceps for Minimally Invasive Robotic Surgery." Int. Journal of Medical Robotics and Computer Assisted Surgery, 2005, pp. 96 - 107.
- [17] P. Valdastri, et al., "Integration of a Miniaturised triaxial Force Sensor in a Minimally Invasive Surgical Tool." Transactions on Biomedical Engineering, 2006, Issue 11, Vol. 53.
- [18] L.J. Love., "Force-Reflecting Micro Tele-Operation with Haptic Feedback." Transactions on Robotics and Automation, 2003.
- [19] Y. Shen, et al., "A Novel PVDF Microforce/Force Rate Sensor for Practical Applications in Micromanipulation." Sensor Review, 2004, Issue 3, Vol. 24, pp. 274 - 283.
- [20] D.V. Dao, et al., "Silicon Piezo-Resistive Six-Degree of Freedom Micro-Force Moment Sensor." 2003.
- [21] W.L. Jin and C.D. Mote., "Development and Calibration of a Sub-Millimeter Three-Component Force Sensor." Sensors and Actuators, 1997, Vol. 65, pp. 89 - 94.
- [22] G.A. Roman, et al., "Design of a Piezoresistive Surface Micromachined Three-Axis Force Transducer for Microassembly." 2005. Int. Conf. on Mechanical Engineering and Exposition.
- [23] F. Beyeler, S. Muntwyler and B.J. Nelson., "Design and Calibration of a Microfabricated 6-Axis Force-Torque Sensor for Microrobotic Applications." 2008.
- [24] T.L. Brooks., "Telerobotic Response Requirements." 1990.
- [25] T. Chen, et al., "A Sidewall Piezoresistive Force Sensor Used in a MEMS." ICIRA 2008, Part II, 2008, pp. 207 - 216.
- [26] S.D. Senturia., *Microsystem Design*. Boston : Kluwer Academic Publishers, 2001/2002. p. 689.
- [27] S. Middelhoek, S.A. Audet and P.J. French., *Silicon Sensors*. Delft : TU Delft, 2000. p. 441.

- [28] Y. Kanda., "A Graphical Representation of the Piezoresistance Coefficients in Silicon." Transactions on Electron Devices, 1982, Vol. 29.
- [29] K.E. Petersen., "Silicon as a Mechanical Material." 1982. Proc. on the IEEE. Vol. 70.
- [30] J.A. Harley and T.W. Kenny., "1/f Noise Considerations for the Design and Process Optimization of Piezoresistive Cantilevers." Journal of Microelectromechanical Systems, 2000, Issue 2, Vol. 9.
- [31] L.K.J. Vandamme and S. Oosterhoff., "Annealing of Ion-Implanted Resistors Reduces the 1/f Noise." Journal of Applied Physics, 1985, Issue 9, Vol. 59.
- [32] N.D. Mankame and G.K. Ananthasuresh., "Comprehensive Thermal Modeling and Characterization of an Electro-Thermal-Compliant Microactuator." Journal of Micromechanics and Microengineering, 2001, Issue 5, Vol. 11, pp. 452 - 462.
- [33] R.C. Jaeger and J.C. Suhling., "Off-Axis Sensor Rosettes for Measurement of the Piezoresistive Coefficient of Silicon." Transactions on Components, Hybrids and Manufacturing Technology, 1993, Issue 8, Vol. 16.
- [34] Bentley, J.P., "Principles of Measurement Systems." s.l. : Pearson Education Ltd., 2005. p. 528.

